

# The Role of *Ab Initio* Beta-Decay Calculations in Light Nuclei for Probes of Physics Beyond the Standard Model

Grigor H. Sargsyan<sup>a,\*</sup>, Garrett B. King<sup>b</sup>, Ayala Glick-Magid<sup>c</sup>, Chien-Yeah Seng<sup>d</sup>

<sup>a</sup>*Facility for Rare Isotope Beams, Michigan State University, East Lansing, Michigan 48824, USA.*

<sup>b</sup>*Theoretical Division, Los Alamos National Laboratory, Los Alamos, NM 87545, USA*

<sup>c</sup>*Tel Aviv University, Tel Aviv 69978, Israel*

<sup>d</sup>*Department of Physics and Astronomy, University of Tennessee, Knoxville, TN 37996*

## Abstract

Precision beta decay experiments serve as powerful probes of physics beyond the Standard Model, enabling stringent tests of fundamental symmetries of nature. In particular, these experiments primarily focus on precise determinations of the Cabibbo-Kobayashi-Maskawa matrix element  $V_{ud}$  and the search for exotic weak currents, both of which depend critically on theoretical calculations of radiative, recoil-order, and isospin-breaking corrections with quantified uncertainties. In recent years, *ab initio* nuclear many-body methods—grounded in realistic nucleon-nucleon interactions and systematically improvable approximations—have advanced considerably in their ability to compute these higher-order corrections for various nuclei. This review provides a comprehensive overview of state-of-the-art *ab initio* calculations of beta-decay corrections, encompassing both radiative corrections and recoil-order terms, and examines their significance for precision tests of the Standard Model. We discuss the theoretical formalisms employed, including the integration of effective field theory frameworks with many-body approaches. Particular attention is given to recent results for superallowed Fermi decays (e.g.,  $^{10}\text{C} \rightarrow ^{10}\text{B}$  and  $^{14}\text{O} \rightarrow ^{14}\text{C}$ ) and allowed Gamow-Teller transitions (e.g.,  $^6\text{He} \rightarrow ^6\text{Li}$ ,  $^8\text{Li} \rightarrow ^8\text{Be}$ ,  $^8\text{B} \rightarrow ^8\text{Be}$ ), where *ab initio* calculations have achieved unprecedented precision. We also highlight emerging calculations for unique forbidden decays, which offer complementary sensitivity to BSM physics. Finally, we outline future directions aimed at extending the reach of *ab initio* calculations to heavier nuclei and additional decay modes, thereby strengthening the synergy between theory and experiment in the ongoing search for new physics.

**Keywords:** Beta decay, Beyond the Standard Model, Ab initio methods, Electroweak interactions in nuclear physics, Radiative corrections, Recoil-order corrections

---

\*Corresponding author

Email address: [sargsyan@frib.msu.edu](mailto:sargsyan@frib.msu.edu) (Grigor H. Sargsyan)

# Contents

<b>1</b>	<b>Introduction</b>	<b>3</b>
<b>2</b>	<b>Many-body methods</b>	<b>4</b>
2.1	No-core configuration interaction approaches . . . . .	5
2.1.1	No-core shell model . . . . .	5
2.1.2	Symmetry-adapted no-core shell model . . . . .	6
2.2	Quantum Monte Carlo approaches . . . . .	7
2.2.1	Variational Monte Carlo . . . . .	9
2.2.2	Green's function Monte Carlo . . . . .	9
2.2.3	Auxiliary field diffusion Monte Carlo . . . . .	10
2.2.4	Mixed Estimates for off-diagonal transitions . . . . .	11
<b>3</b>	<b>Radiative Corrections to superallowed nuclear beta decays</b>	<b>11</b>
3.1	Background . . . . .	11
3.2	Theory framework . . . . .	12
3.2.1	Current algebra formalism . . . . .	13
3.2.2	Effective field theory formalism . . . . .	14
3.2.3	Connection between the two approaches . . . . .	17
3.3	$^{10}\text{C} \rightarrow {}^{10}\text{B}$ with No-Core Shell Model . . . . .	18
3.4	$^{10}\text{C} \rightarrow {}^{10}\text{B}$ and $^{14}\text{O} \rightarrow {}^{14}\text{N}$ with Quantum Monte Carlo . . . . .	20
<b>4</b>	<b>Recoil-order corrections to allowed beta decays</b>	<b>22</b>
4.1	$^6\text{He} \rightarrow {}^6\text{Li}$ beta decay corrections with NCSM . . . . .	22
4.2	$^6\text{He} \rightarrow {}^6\text{Li}$ beta decay spectrum with QMC . . . . .	25
4.3	$^8\text{Li} \rightarrow {}^8\text{Be}$ and $^8\text{B} \rightarrow {}^8\text{Be}$ beta decays corrections with SA-NCSM . . . . .	29
<b>5</b>	<b>Summary and outlook</b>	<b>32</b>
<b>A</b>	<b>Appendices, if necessary</b>	<b>51</b>

# 1. Introduction

The search for beyond the Standard Model (BSM) physics is one of the most pressing open questions in modern particle physics. This area of research is vital for our understanding of the universe, from the origin of matter and the universe’s matter-antimatter asymmetry to the properties of dark matter and the behavior of fundamental forces at high energies. Searches of BSM physics have been central topics for some of the largest high-energy particle accelerators in the world, such as the Large Hadron Collider (LHC). On the other hand, low-energy nuclear beta decays have emerged as a powerful and complementary probe of BSM physics that can rival the sensitivity of large-scale particle accelerator experiments. The precise measurements of beta decay spectra and transition rates, often obtained with high accuracy in experiments involving radioactive nuclei, have already produced some of the most stringent constraints on BSM physics, and hold promise for further advances in our understanding of the universe’s fundamental laws.

Within the broader landscape of precision physics programs [1, 2, 3, 4, 5], the study of beta decay processes stands out as a particularly vibrant and significant area. In the Standard Model (SM), these decays are fundamentally driven by the exchange of a W boson, connecting light quark and lepton currents. Crucially, the strength of the interaction between the W boson and quarks within the SM is governed by the Cabibbo-Kobayashi-Maskawa (CKM) matrix [6, 7]. Consequently, beta decays offer a unique opportunity to precisely extract  $V_{ud}$ , the upper left element of this fundamental matrix. Indeed, this method currently represents the most precise means of determining  $V_{ud}$ , by a substantial margin [8]. Deviations from the unitarity of the CKM matrix would indicate the existence of BSM physics, and a renewed interest in this topic has followed the recent suggestion of a CKM unitarity violation at  $\sim 3\sigma$  [9], which favors non-zero right-handed quark couplings (see, e.g. [10] and references therein).

Furthermore, searches for BSM physics in beta decay test the left-handed vector minus axial-vector ( $V - A$ ) structure of the weak interaction by looking for minuscule admixtures of non-SM currents. In an effective low-energy description, possible contributions from right-handed vector, scalar, and tensor currents—potentially arising from new heavy mediators—would modify decay observables relative to SM expectations. Precision measurements of beta-decay correlation coefficients (for example, electron–antineutrino correlations and angular/momentum correlations) and the beta-spectrum shape provide sensitivity to these exotic couplings [3, 4, 11, 12]. Together with radiative and recoil-order corrections, the results place stringent constraints on new physics scenarios such as exotic scalar or tensor interactions.

The extraction of fundamental parameters from precision beta-decay data depends on theoretical inputs for radiative corrections, isospin-breaking effects, and recoil-order terms. Given the precision that current measurements achieve, it is vital to have an accurate description of these higher-order corrections with quantified uncertainties to be able to distinguish between new physics and conventional nuclear physics effects. Nuclear *ab initio* methods—based on realistic nucleon-nucleon interactions—have made substantial progress in computing corrections to the beta decay for an expanding set of nuclei [13, 14, 15, 16, 17, 18, 19, 20]. *Ab initio* models are able to provide first-principles descriptions of nuclei and beta decay corrections with quantified uncertainties. The calculations from *ab initio* methods are systematically improvable as the nucleon-nucleon interactions and many-body truncations are refined [21, 22]. These advances strengthen the reliability of beta-decay observables used to test the SM and constrain BSM physics.

This review gives an overview of recent *ab initio* calculations of beta decay radiative and recoil-order corrections and discusses their significance to the precision measurements that probe physics beyond the Standard Model. In the following sections, we detail the many-body methods that have been employed to perform *ab initio* calculations of these corrections and briefly discuss their application span for future studies. Moreover, we outline the formalism essential for deriving

radiative corrections necessary for the precise extraction of the  $V_{ud}$  matrix element of the CKM matrix, highlighting some of the most recent results. Furthermore, we examine advancements in computing nuclear recoil-order corrections to beta decays that need to be accounted for in high-precision experiments that probe BSM physics. We conclude with a summary and an outlook to future studies hence aiming to illuminate the path toward more accurate tests of fundamental theories.

## 2. Many-body methods

The landscape of *ab initio* nuclear theory [21], which has increasingly come to define many-body calculations that describe nuclei at the finest resolution scale possible and are systematically improvable [22], has grown steadily over the last decade. While the fundamental theory of the strong interaction is QCD, and there has been progress in describing nuclei with lattice approaches [23], the finest degrees of freedom to describe most few-body nuclei are protons and neutrons (collectively, nucleons). While there are a number of *ab initio* approaches in the literature, we will limit the scope of this section to methods based on the no-core configuration interaction (NCCI) and quantum Monte Carlo (QMC) approaches as they are the ones relevant for our subsequent discussion.

Generically, one would like to solve the  $A$ -body Schrödinger equation with a nuclear Hamiltonian that can be schematically represented as,

$$H = \sum_i T_i + V_{\text{Coul}} + \sum_{i < j} v_{ij} + \sum_{i < j < k} V_{ijk} + \dots, \quad (2.1)$$

where  $T_i$  are the kinetic energies of the nucleons,  $V_{\text{Coul}}$  is the Coulomb interaction between the protons, and  $v_{ij}$  and  $V_{ijk}$  are two- and three-nucleon interactions, respectively. In principle, there could be four-nucleon and other many-nucleon forces; however, the studies reviewed in this work retain at most three-nucleon contributions. The interaction between nucleons is not fundamental, and thus one must model these potentials. Historically, the community adopted phenomenological interactions to model the nuclear interaction—such as, for instance, the Argonne  $v_{18}$  (AV18) [24] and CD-Bonn potentials [25]—which proved reasonably successful to understand a variety of phenomena. These approaches, despite their strong predictive capabilities, are not systematically improvable. In more recent years, approaches based on chiral effective field theory ( $\chi$ EFT) have come to the forefront. It is beyond the scope of this review to cover the full details of this approach, and interested readers are directed to the reviews of Refs. [26, 27, 28, 29]. The salient feature of  $\chi$ EFT is that the separation of scales between low-energy QCD ( $Q \approx m_\pi$ ) and the scale of heavy meson ( $\Lambda_\chi \approx 1$  GeV) allows one to derive a nuclear interaction that can be expanded in powers of  $Q/\Lambda_\chi$ . While similarly successful as the phenomenological approach, it is worth mentioning that one must adopt a particular power counting scheme for the  $\chi$ EFT expansion. Determining the appropriate power counting remains an open question in low-energy nuclear theory [30, 31]. Thus, the  $\chi$ EFT approach is *in principle* systematically improvable and the works reviewed here comprise the best effort of the community toward *ab initio* modeling of  $\beta$  decays. Ongoing research in low-energy nuclear interactions aims at advancing the field toward a truly systematically improvable approach that builds upon the efforts that we detail in this article.

Finally, once a model for  $H$  is adopted, one needs solve the Schrödinger Equation,

$$H |\Psi(J^\pi; T, T_z)\rangle = E |\Psi(J^\pi; T, T_z)\rangle, \quad (2.2)$$

to obtain the nuclear wave function  $\Psi$  with the appropriate spin-parity  $J^\pi$ , isospin  $T$ , and isospin projection  $T_z$  corresponding to an energy  $E$ . Using these wave functions, one is interested in evaluating transitions mediated by weak charge

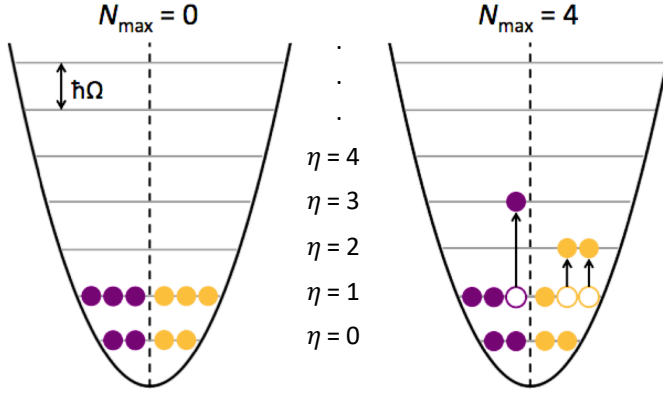


Figure 2.1:  $N_{\max}=0$  and  $N_{\max}=4$  configurations in  $^{10}\text{B}$  in a standard particle-based NCSM (a single configuration is shown in each case).

( $\rho$ ) and current ( $\mathbf{j}$ ) operators which are schematically given as,

$$\rho = \sum_i \rho_i + \sum_{ij} \rho_{ij} + \dots, \quad (2.3)$$

$$\mathbf{j} = \sum_i \mathbf{j}_i + \sum_{ij} \mathbf{j}_{ij} + \dots, \quad (2.4)$$

where the one-body terms represent an impulse approximation picture of single nucleon coupling to an external field, while two-body contributions represent two correlated nucleons coupling simultaneously to each other and to an external field.

## 2.1. No-core configuration interaction approaches

### 2.1.1. No-core shell model

*Ab initio* configuration-interaction models, such as the no-core shell model (NCSM) and the symmetry-adapted no-core shell model (SA-NCSM) adopt a complete orthonormal basis  $\psi_i$ , such that the expansion of  $\Psi(J^\pi; T, T_z)$  in terms of unknown coefficients  $d_k$ ,  $\Psi(J^\pi; T, T_z) = \sum_k d_k \psi_k(\vec{r}_1, \vec{r}_2, \dots, \vec{r}_A)$ , renders Eq. (2.2) into a matrix eigenvalue equation,

$$\sum_{k'} H_{kk'} d_{k'} = E d_k, \quad (2.5)$$

where the many-body Hamiltonian matrix elements are  $H_{kk'} = \langle \psi_k | H | \psi_{k'} \rangle$  and are calculated for the given interaction (2.1). The many-body basis is a finite set of antisymmetrized products of single-particle states (Slater determinants), referred to as a ‘‘model space’’. Typically, the single-particle states of a three-dimensional spherical HO are used:  $\phi_{\eta(\ell\frac{1}{2})j}(\mathbf{r}; b) = R_{\eta\ell}(r; b) \mathcal{Y}_{(\ell\frac{1}{2})j}(\hat{r}) = \sum_{m\sigma} C_{\ell m \frac{1}{2}\sigma}^{j m_j} R_{\eta\ell}(r; b) Y_{\ell m}(\hat{r}) \chi_{\frac{1}{2}\sigma}$ , with radial wavefunctions  $R_{\eta\ell}(r; b)$  and spin functions  $\chi_{\frac{1}{2}\sigma}$ , where  $\eta = 2n_r + \ell$  is the HO shell number,  $\ell$  is coupled with spin-1/2 to  $j$ , and the oscillator length  $b = \sqrt{\frac{\hbar\Omega}{m\Omega}}$  with oscillator frequency  $\hbar\Omega$  (an additional quantum number  $t_z$  is added to distinguish between protons and neutrons).

In calculations, the model space is finite and is provided for given  $N_{\max}$ , which is the total HO excitations above the nuclear configuration of the lowest HO energy allowed by the Pauli principle (Fig. 2.1). The minimal model space for each nucleus corresponds to  $N_{\max}=0$ , and it increases in steps of 2 for states sharing the same parity. Odd  $N_{\max}$  values encompass states with the opposite parity. It is important that in the conventional NCSM with complete model spaces truncated by  $N_{\max}$  (see the review [32]) the center-of-mass (c.m.) wavefunction can be factored out exactly since the c.m. operator ( $\hat{N}_{\text{c.m.}}$ ) does not mix c.m. states with different HO excitations [33]. Such a model space allows for

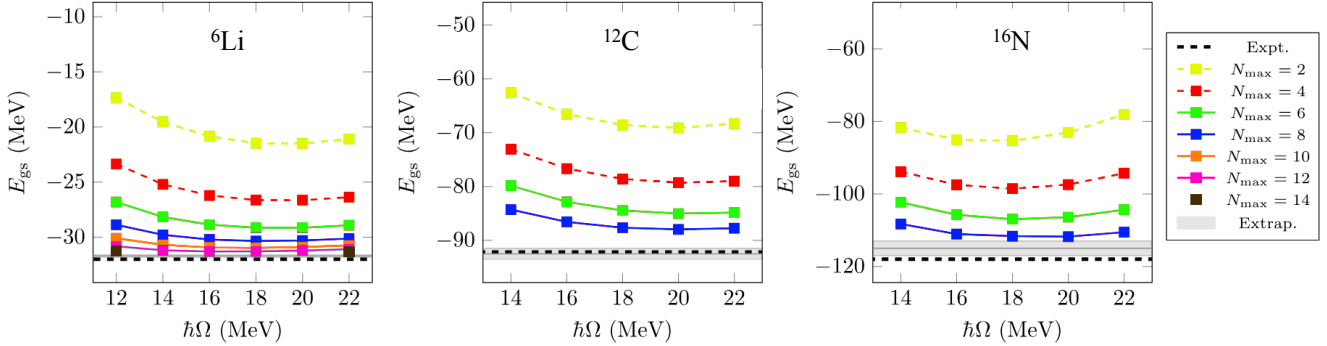


Figure 2.2: Ground-state energies of  $^6\text{Li}$ ,  $^{12}\text{C}$ , and  $^{16}\text{N}$  obtained with the NN-N4LO +  $3\text{N}_{\text{Inl}}^*$  interaction [34] with different HO frequencies. Data for the figure is taken from Ref. [35].

preservation of translational invariance of the nuclear self-bound system and provides solutions in terms of single-particle HO wavefunctions that are analytically known.

With larger model spaces utilized in the no-core shell-model theory, the eigensolutions converge to the exact values, and the corresponding observables become independent from the  $\hbar\Omega$  basis parameter. Examples of ground state energy (eigenvalue) convergence with increasing  $N_{\text{max}}$  are presented in Fig. 2.2. The eigenvectors obtained by solving Eq. (2.5) are then used to calculate various nuclear observables, such as radii, electromagnetic transition strengths and beta decay strengths. Several methods have been used for extrapolating observables calculated in finite model spaces and specific  $\hbar\Omega$  values to the infinite model space value [36, 37, 38, 39, 40]. As  $N_{\text{max}}$  increases, the number of configurations in the model space grows combinatorially. Consequently, the computational cost rises rapidly, typically limiting NCSM calculations to light nuclei or to relatively small model spaces.

### 2.1.2. Symmetry-adapted no-core shell model

The NCSM many-body basis can be arranged into  $\text{SU}(3)$  subspaces of given deformation, and these can further be grouped into  $\text{Sp}(3, \mathbb{R}) \supset \text{SU}(3)$  subspaces of given nuclear shape, referred to as symmetry-adapted (SA) bases. The symmetries of interest are  $\text{SU}(3)$  and  $\text{Sp}(3, \mathbb{R})$ . The  $\text{SU}(3)$  group is the exact symmetry of the three-dimensional spherical HO, while the  $\text{Sp}(3, \mathbb{R})$  (symplectic) symmetry represents the dynamical symmetry of the three-dimensional spherical HO. Such near symmetries were first recognized by Bohr & Mottelson (1975 Physics Nobel Prize) [41], followed by Elliott's seminal work [42, 43, 44] and the microscopic no-core formulation by Rowe & Rosensteel [45, 46].

The SA-NCSM basis states are labeled schematically as

$$|\vec{\gamma}, N(\lambda \mu) \kappa L; (S_p S_n) S; J \rangle \quad (2.6)$$

where  $S_p$ ,  $S_n$ , and  $S$  denote the proton, neutron, and total intrinsic spins, respectively, and  $(\lambda \mu)$  indicates a set of quantum numbers that label an  $\text{SU}(3)$  irreducible representation (or "irrep"). This means that each basis state is labeled according to  $\text{SU}(3)_{(\lambda \mu)} \times \text{SU}(2)_S$  by  $S$  and  $(\lambda \mu)$  quantum numbers with  $\lambda = N_z - N_x$  and  $\mu = N_x - N_y$ , where  $N_x + N_y + N_z = N$  is the total number of the HO quanta distributed in the  $x$ ,  $y$ , and  $z$  direction (in addition to other quantum numbers that are needed for complete labeling). The label  $\kappa$  distinguishes multiple instances of the same orbital angular momentum  $L$  within the parent irrep  $(\lambda \mu)$ . The angular momentum  $L$  is coupled with the intrinsic spin  $S$  to form the total angular momentum  $J$ . The symbol  $\vec{\gamma}$  schematically denotes the additional quantum numbers required to specify the distribution of nucleons across the major HO shells, including their single-shell and inter-shell quantum numbers. The  $\text{SU}(3)$  labels

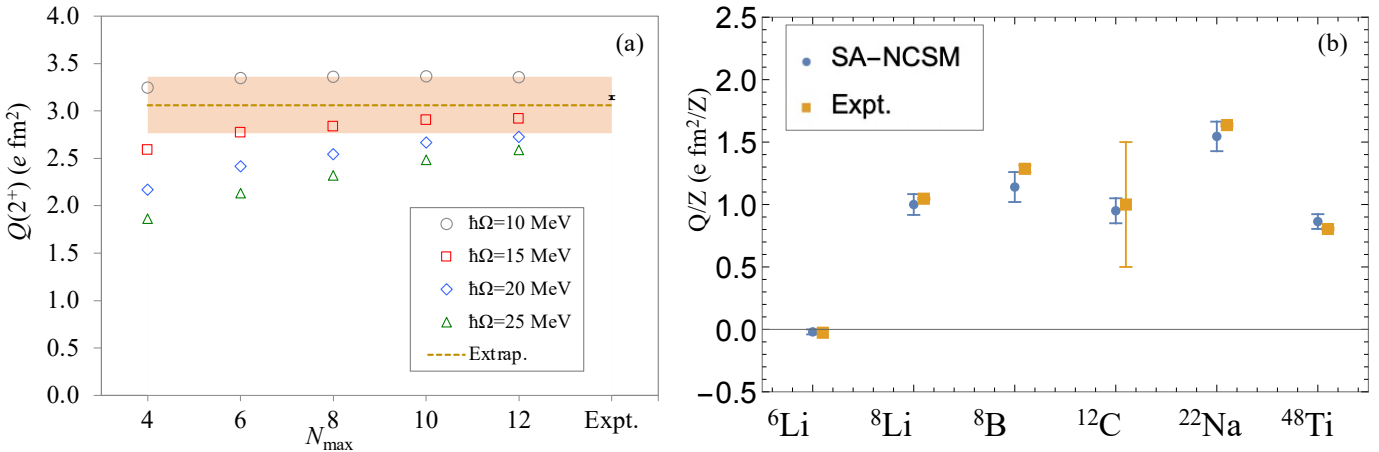


Figure 2.3: (a) Convergence of the  $^8\text{Li}$  ground state quadrupole moment vs.  $N_{\max}$  calculated using SA-NCSM with different HO parameters ( $\hbar\Omega$ ) and compared to the experimental value from [54]. The dashed horizontal line with a band shows the infinite-space extrapolated value. Figure adapted from Ref. [14] with permission. (b) Quadrupole moments of various nuclei divided by their proton numbers calculated using SA-NCSM and compared to the experimental values from Ref. [55]. Uncertainties of some of the experimental values are smaller than the size of the marker.

$(\lambda \mu)$  bring forward important information about nuclear shapes and deformation, according to an established mapping [47, 45, 48]. For example,  $(0 0)$ ,  $(0 \mu)$  and  $(\lambda 0)$  describe spherical, oblate and prolate deformation, respectively. This basis organization allows traditional and complete model spaces to be augmented for large  $N$  by a subset of the SA basis states (referred to ‘‘SA model spaces’’). Since small complete model spaces (up to a small  $N$  value) are often sufficient to describe less deformed shapes, the additional SA basis states in high  $N$  subspaces are exactly those needed for the full description of spatially expanded (very deformed or clustered) configurations [49, 50].

Similarly to NCSM, in SA-NCSM (see the review [49]), the c.m. wavefunction can be factored out exactly since c.m. states are SU(3) scalar, and do not mix SU(3) subspaces of the SA-NCSM [33, 51, 52]. It should be noted that while the SA basis is complete and related to the NCSM basis by a unitary transformation, the SA basis states are not constructed by this transformation; rather, they are generated via an efficient group-theoretical algorithm [53].

The outstanding feature of SA-NCSM is its ability to express solutions in a physically meaningful basis that captures the collective behavior and symmetries underlying nuclear dynamics. Large model spaces are needed to represent essential collective modes and to connect to continuum degrees of freedom within the interaction range. Beyond this range, SA-NCSM uses exact Coulomb eigenfunctions. The aim is to attain unprecedented accuracy across systems heavier than the lightest nuclei, while supplying nuclear-structure and reaction information for theory and experiment. Hence, SA-NCSM enables *ab initio* calculations for spherical and deformed nuclei up to the Titanium region [50, 56, 57, 58, 59, 60, 61, 62] (Fig. 2.3), incorporating crucial correlations in the wavefunction, such as collective and clustering effects that are notoriously difficult to tackle in polynomial-scaling methods [63, 60, 64].

## 2.2. Quantum Monte Carlo approaches

In this section, we outline QMC approaches to solving the many-body Schrödinger Equation for strongly-correlated nucleons. These methods comprise a suite of stochastic approaches to solve the many-body problem non-perturbatively, retaining the full complexity of interparticle correlations generated by the the nuclear interaction. In the literature, there are reviews of both QMC approaches to study nuclei [66, 67], and more recently their application to the study

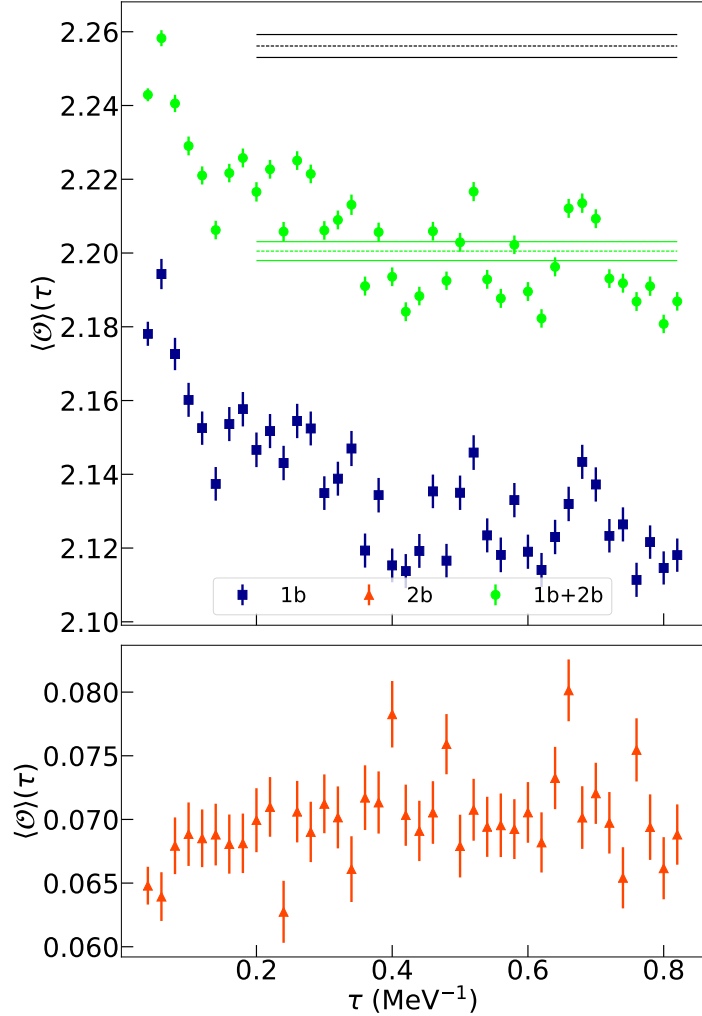


Figure 2.4: GFMC propagation of the  ${}^6\text{He} \rightarrow {}^6\text{Li}$  Gamow-Teller  $\beta$  decay transition matrix element for the NV2+3-Ia nuclear Hamiltonian. The one-body matrix element is shown in blue in the top panel, and is compared with the matrix element retaining one- and two-body transition operators shown in green. The two-body contribution is isolated in the bottom panel and plotted in orange. The average GFMC estimate is shown by the green dotted line, with statistical uncertainty represented by the solid green lines. The average is compared to a variational monte carlo calculation with central value represented by the dashed black line, and statistical uncertainties shown with the solid black lines. Figure reprint with permission from Ref. [65].

of electroweak processes in light nuclei [68]. Here, we aim to cover the salient features of the methods so that QMC results may be understood in the broader context of *ab initio* modeling of  $\beta$  decays, and direct interested readers to the aforementioned reviews for detailed discussion.

### 2.2.1. Variational Monte Carlo

The QMC approach in nuclei begins with variational Monte Carlo (VMC) [69], which requires an ansatz for the form of the trial wave function  $|\Psi_T\rangle$  that will be optimized. The most generic form of a trial wave function factorizes the system into a model wave function  $|\Phi\rangle$  that encodes the quantum numbers and long range structure of the system, and a correlation operator  $\hat{F}$  that reflects the impact of the nuclear interaction at short distances; *i.e.*,

$$|\Psi_T\rangle = \hat{F} |\Phi\rangle . \quad (2.7)$$

The precise form of  $\hat{F}$  and  $|\Phi\rangle$  depend on which diffusion Monte Carlo approach is used to improve upon the VMC calculations, and will be discussed in the following two sections. Here, it is worth noting simply that the variational wave function is optimized by minimizing the energy expectation value,

$$E_T = \frac{\langle \Psi_T | H | \Psi_T \rangle}{\langle \Psi_T | \Psi_T \rangle} \leq E_0 , \quad (2.8)$$

where  $E_0$  is the true energy of the ground state. This integral can be evaluated with Metropolis Monte Carlo techniques. In the following sections, we will refer to the optimized variational state as  $|\Psi_V\rangle$ .

### 2.2.2. Green's function Monte Carlo

Green's function Monte Carlo is a diffusion Monte Carlo technique that improves upon the result from VMC. Generally, diffusion approaches work by solving the time-dependent Schrödinger Equation,

$$i \frac{\partial}{\partial t} |\Psi(t)\rangle = (H - E_T) |\Psi(t)\rangle , \quad (2.9)$$

making a change of variable to imaginary time  $\tau = it$ , where  $E_T$  is an arbitrary energy offset. Eq. 2.9 is now a diffusion equation in  $\tau$ , the solution of which is an exponential,

$$|\Psi(\tau)\rangle = e^{-(H - E_T)\tau} |\Psi(0)\rangle . \quad (2.10)$$

Taking our initial state to be  $|\Psi(0)\rangle = |\Psi_V\rangle$ , and noting that any state can be expanded in the exact eigenstates  $|\psi_i\rangle$  of  $H$  as,

$$|\Psi_V\rangle = \sum_{i=0}^{\infty} c_i |\psi_i\rangle , \quad (2.11)$$

with complex coefficients  $c_i$ , we can obtain the true ground state  $|\psi_0\rangle$  by choosing  $E_T = E_0$  taking the limit,

$$\lim_{\tau \rightarrow \infty} e^{-(H - E_0)\tau} |\Psi_T\rangle \propto c_0 \psi_0 . \quad (2.12)$$

In practice, this is achieved by acting on the state in several small imaginary time steps  $\Delta\tau$ ,

$$|\Psi(\tau)\rangle = \left[ e^{-(H - E_0)\Delta\tau} \right]^n |\Psi_V\rangle . \quad (2.13)$$

When performing a GFMC calculation, one must consider the evolution of several sets of configurations  $\mathbf{R}$ , where  $\mathbf{R}$  is used as short-hand to denote the set of  $3A$  spatial coordinates and  $2^A A!/(N!Z!)$  spin-isospin degrees of freedom. Projecting

Eq. 2.10 for a short imaginary time onto configuration space, and using a completeness of the states  $|\mathbf{R}'\rangle$ , we obtain,

$$\Psi(\mathbf{R}, \tau + \Delta\tau) = \int d\mathbf{R}' \langle \mathbf{R} | e^{-(H-E_0)\Delta\tau} |\mathbf{R}'\rangle \Psi(\mathbf{R}', \tau) \quad (2.14)$$

$$= \int d\mathbf{R}' G(\mathbf{R}, \mathbf{R}', \Delta\tau) \Psi(\mathbf{R}', \tau), \quad (2.15)$$

where we define the short-time propagator  $G(\mathbf{R}, \mathbf{R}', \Delta\tau) = \langle \mathbf{R} | e^{-(H-E_0)\Delta\tau} |\mathbf{R}'\rangle$ , and denote the matrix element  $\langle \mathbf{R} | \Psi(\tau) \rangle$  as  $\Psi(\mathbf{R}, \tau)$ . The propagation in imaginary time can thus be performed by sampling  $G(\mathbf{R}, \mathbf{R}', \Delta\tau)$  with Monte Carlo techniques to evolve the configurations to the next time step. Expectation values of operators must also be computed as a function of imaginary time, and averaged once convergence is reached. Figure 2.4 shows this for the  ${}^6\text{He}$  Gamow-Teller  $\beta$  decay matrix element computed in Ref. [65] with GFMC using the NV2+3-Ia chiral interaction [70, 71].

The form of the VMC trial wave function used in nuclear structure calculations has the form [72]

$$|\Psi_T\rangle = \mathcal{S} \prod_{i < j}^A \left[ 1 + U_{ij} + \sum_{k \neq i, j}^A U_{ijk} \right] |\Psi_J\rangle, \quad (2.16)$$

with  $U_{ij}$  and  $U_{ijk}$  being two- and three-body correlation operators designed to reflect the impact of the nuclear interaction at short distances, and  $\mathcal{S}$  being symmetrization operator. The component  $\Psi_J$  serves the role of the unperturbed model wave function and contains information about the symmetries and quantum numbers of the system. Details of the specific form of  $\Psi_J$  are discussed in the review of Ref. [66]. The correlation operators  $U_{ij}$  are spin and isospin dependent, and have a radial dependence that comes from solutions to a set of coupled screened two-body Schrödinger equations for different spin-isospin ( $ST$ ) channels of the  $NN$  system. Instead,  $U_{ijk}$  comes directly from the three-body force operators, and has variational parameters governing the strength of each term, as well as re-scaling the interparticle separations. Specific forms of the correlation operators can be found in Ref. [73].

### 2.2.3. Auxiliary field diffusion Monte Carlo

The spin-isospin basis of configuration space for the GFMC wave function grows exponentially with  $A$ , thus limiting its application to light nuclei. The auxiliary field diffusion Monte Carlo (AFDMC) approach [66, 74, 75] was developed to circumvent this limitation. Like GFMC, one solves a diffusion equation in imaginary time. Now, however, one assumes a wave function with single particle representation, whose projection onto a spin state  $S$  is given by [75],

$$\langle S | \Psi \rangle \propto \xi_{\alpha_1}(s_1) \xi_{\alpha_2}(s_2) \dots \xi_{\alpha_A}(s_A), \quad (2.17)$$

This wave function has the advantage that it scales polynomially in  $A$ , allowing for the computation of nuclei that are too large to access with GFMC. An important consideration is how operators quadratic in spin act on the wave function. Consider the example,

$$\begin{aligned} \langle S | \boldsymbol{\sigma}_1 \cdot \boldsymbol{\sigma}_2 | \Psi \rangle &\propto 2\xi_{\alpha_1}(s_2) \xi_{\alpha_2}(s_1) \dots \xi_{\alpha_A}(s_A) - \xi_{\alpha_1}(s_1) \xi_{\alpha_2}(s_2) \dots \xi_{\alpha_A}(s_A) \\ &= 2\langle S' | \Psi \rangle - \langle S | \Psi \rangle, \end{aligned} \quad (2.18)$$

which demonstrates that the basis is not closed to the action of quadratic operations. Linear operations only involve rotations of spins or isospins of single nucleons. Thus, to maintain the computational advantage of the single particle basis, one can linearize quadratic spin and isospin operators with the Hubbard-Stratonovich transformation,

$$e^{-\frac{\lambda}{2}\mathcal{O}^2} = \frac{1}{\sqrt{2\pi}} \int dx e^{-\frac{x^2}{2}} e^{x\sqrt{-\lambda}\mathcal{O}}, \quad (2.19)$$

where the  $x$  are called auxiliary fields, and the integral can be performed via Monte Carlo sampling drawing from the probability distribution  $P(x) = \exp[-x^2/2]$ . Details of the linearization of the operators can be found in Ref. [67], and this transformation allows for the imaginary time propagation of up to quadratic spin-isospin operators in imaginary time when using the AFDMC basis.

#### 2.2.4. Mixed Estimates for off-diagonal transitions

Ideally, for off-diagonal matrix elements of some operator  $\mathcal{O}$  between some initial state  $i$  and final state  $f$ , one would compute,

$$\langle \mathcal{O}(\tau) \rangle = \frac{\langle \Psi^f(\tau) | \mathcal{O} | \Psi^i(\tau) \rangle}{\sqrt{\langle \Psi^f(\tau) | \Psi^f(\tau) \rangle} \sqrt{\langle \Psi^i(\tau) | \Psi^i(\tau) \rangle}}; \quad (2.20)$$

however, such a calculation would make analyzing a variety of matrix elements numerically quite costly, as each expectation value would require its own GFMC or AFDMC propagation. Because of this, the standard approach for off-diagonal matrix elements in diffusion Monte Carlo is to compute a mixed estimate, which is a suitable approximation given the quality of the VMC wave functions used in nuclear calculations. One assumes the GFMC state at each  $\tau$  is a perturbation on top of the VMC wave function; *i.e.*,  $\Psi(\tau) = \Psi_V + \delta\Psi$ . Working to first order in  $\delta\Psi$ , we have that [76],

$$\begin{aligned} \langle \mathcal{O}(\tau) \rangle \approx & \sqrt{\frac{\langle \Psi_V^f | \Psi^f(\tau) \rangle}{\langle \Psi_V^i | \Psi_V^i \rangle}} \frac{\langle \Psi^f(\tau) | \mathcal{O} | \Psi_V^i \rangle}{\langle \Psi^f(\tau) | \Psi_V^f \rangle} + \sqrt{\frac{\langle \Psi_V^i | \Psi^i(\tau) \rangle}{\langle \Psi_V^f | \Psi_V^f \rangle}} \frac{\langle \Psi^i(\tau) | \mathcal{O}^\dagger | \Psi_V^f \rangle}{\langle \Psi^i(\tau) | \Psi_V^i \rangle} \\ & - \frac{1}{2} \left[ \sqrt{\frac{\langle \Psi_V^f | \Psi_V^f \rangle}{\langle \Psi_V^i | \Psi_V^i \rangle}} \frac{\langle \Psi_V^f | \mathcal{O} | \Psi_V^i \rangle}{\langle \Psi_V^f | \Psi_V^f \rangle} + \sqrt{\frac{\langle \Psi_V^i | \Psi_V^i \rangle}{\langle \Psi_V^f | \Psi_V^f \rangle}} \frac{\langle \Psi^i | \mathcal{O}^\dagger | \Psi^f \rangle}{\langle \Psi_V^i | \Psi_V^i \rangle} \right]. \end{aligned} \quad (2.21)$$

The quantities  $\langle \Psi_f(\tau) | \mathcal{O} | \Psi_V^i \rangle / \langle \Psi_f(\tau) | \Psi_V^f \rangle$  and  $\langle \Psi_i(\tau) | \mathcal{O}^\dagger | \Psi_V^f \rangle / \langle \Psi_i(\tau) | \Psi_V^i \rangle$  are obtained from the GFMC walk, and the term in brackets is the VMC matrix element for the off diagonal transition averaged over the VMC walks for both the initial and final state to improve the statistical uncertainty of the calculation. A further approximation typically made in the literature is as follows,

$$\begin{aligned} \langle \mathcal{O}(\tau) \rangle \approx & \sqrt{\frac{\langle \Psi_V^f | \Psi_V^f \rangle}{\langle \Psi_V^i | \Psi_V^i \rangle}} \frac{\langle \Psi^f(\tau) | \mathcal{O} | \Psi_V^i \rangle}{\langle \Psi^f(\tau) | \Psi_V^f \rangle} + \sqrt{\frac{\langle \Psi_V^i | \Psi_V^i \rangle}{\langle \Psi_V^f | \Psi_V^f \rangle}} \frac{\langle \Psi^i(\tau) | \mathcal{O}^\dagger | \Psi_V^f \rangle}{\langle \Psi^i(\tau) | \Psi_V^i \rangle} \\ & - \frac{1}{2} \left[ \sqrt{\frac{\langle \Psi_V^f | \Psi_V^f \rangle}{\langle \Psi_V^i | \Psi_V^i \rangle}} \frac{\langle \Psi_V^f | \mathcal{O} | \Psi_V^i \rangle}{\langle \Psi_V^f | \Psi_V^f \rangle} + \sqrt{\frac{\langle \Psi_V^i | \Psi_V^i \rangle}{\langle \Psi_V^f | \Psi_V^f \rangle}} \frac{\langle \Psi^i | \mathcal{O}^\dagger | \Psi^f \rangle}{\langle \Psi_V^i | \Psi_V^i \rangle} \right]. \end{aligned} \quad (2.22)$$

## 3. Radiative Corrections to superallowed nuclear beta decays

### 3.1. Background

Beta decays provide a perfect avenue to test predictions of SM at low energies [5]. As a most straightforward application, by measuring the decay lifetime one can access the parameter  $V_{ud}$ , which is the upper-left element of the Cabibbo-Kobayashi-Maskawa (CKM) matrix [6, 7]. This allows us to test a major SM prediction, the so-called “first-row CKM unitarity”:

$$|V_{ud}|^2 + |V_{us}|^2 + |V_{ub}|^2 = 1. \quad (3.1)$$

A precision level of  $10^{-4}$  in such a test will constrain new physics at multi-TeV scale, which is competitive to high-energy experiments at colliders.

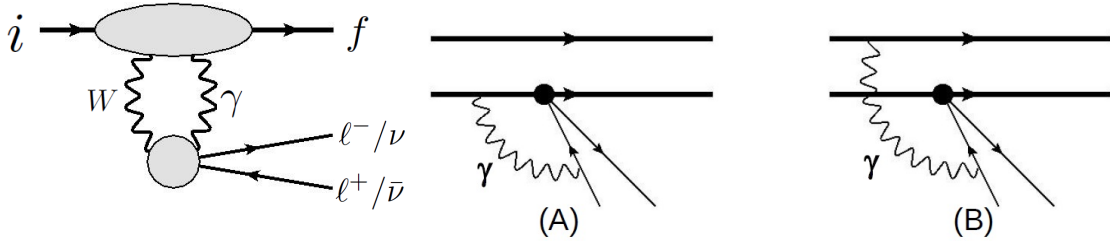


Figure 3.1: First diagram: A generic  $\gamma W$ -box diagram for  $\beta^\pm$ -decay. Second and third diagram: the “traditional” picture for  $\delta_{\text{NS}}$ .

$V_{ud}$  can be extracted from beta decays of pion, free neutron, and nuclei. For pion which is theoretically the cleanest with recent lattice calculations of the electromagnetic radiative corrections (RC) [77, 78], the bottleneck is the large experimental uncertainty in the  $\pi_{e3}$  branching ratio [79], although improvements are anticipated through the future PIONEER experiment [80]. For free neutron decay, recent years have seen tremendous improvements in the study of RC [81, 82, 83, 84, 85, 86, 87, 88, 89, 90, 91] based on dispersion relation, lattice QCD and effective field theory, but again the bottlenecks are from the experimental side, including discrepancies in the neutron lifetime (see, e.g. Ref.[92] and references therein) and axial coupling [93, 94, 95] measurements.

At the present, superallowed  $0^+ \rightarrow 0^+$  beta decays of  $T = 1$  nuclei provide the best avenue to extract  $V_{ud}$ . There are two major benefits in this channel: (1) It is a pure Fermi transition, so the decay amplitude is largely fixed by isospin symmetry modulo small corrections (which is the aim of our study); (2) At the present, there are 23 measured transitions, 15 of which have partial half-life precision better than 0.23% [96], thus averaging over different transitions largely reduces the experimental uncertainty. As a consequence, the error of  $V_{ud}$  determined from this decay mode is dominated by theory uncertainties instead of experiment, and *ab initio* calculations play a key role in reducing such uncertainties.

### 3.2. Theory framework

$V_{ud}$  can be extracted from the superallowed decay half life  $t$  through the following master formula:

$$|V_{ud}|_{0^+}^2 = \frac{2984.431(3) \text{ s}}{\mathcal{F}t(1 + \Delta_R^V)}, \quad (3.2)$$

where  $\Delta_R^V$  is a nucleus-independent RC which is also present in the free neutron decay. All the SM theory inputs that depend on the decaying nuclear system reside in the following quantity:

$$\mathcal{F} \equiv f(1 + \delta'_r)(1 + \delta_{\text{NS}} - \delta_C), \quad (3.3)$$

where  $f$  is the “statistical rate function” that comes from the phase space integral of the tree-level squared amplitude corrected by various leading SM effects (e.g. Fermi function and the nuclear weak form factor),  $\delta'_r$  is an “outer” RC which is largely independent of the detailed nuclear structure,  $\delta_C$  is the isospin-symmetry-breaking correction to the Fermi matrix element, and  $\delta_{\text{NS}}$  is the nuclear structure (NS)-dependent RC. It is interesting to note that, since  $V_{ud}$  is a nucleus-independent quantity, the product  $\mathcal{F}t$  should also be nucleus-independent if SM is correct, despite that  $\mathcal{F}$  and  $t$  are separately nucleus-dependent.

$\delta_{\text{NS}}$  arises from the nucleus-dependent part of the so-called “nuclear  $\gamma W$ -box diagram”, given by the first diagram in Fig. 3.1. To be more specific, it is contributed by the “axial” box diagram, where the  $W$ -boson is coupled to the axial

component of the nuclear weak current. The “traditional” picture to understand the origin of  $\delta_{\text{NS}}$ , is that it comes from the second and third diagrams in Fig. 3.1:

- Type A: Both the weak and the electromagnetic (EM) vertices are acting on the same nucleon, but it is a bound nucleon instead of a free nucleon, so the weak and EM couplings are shifted from the “free” values to the “quenched” values, that are numerically smaller.
- Type B: The weak and EM vertices can act on two different nucleons, so this is intrinsically a nucleus-dependent contribution.

Within this picture, one can write:

$$\delta_{\text{NS}} = \delta_{\text{NS,A}} + \delta_{\text{NS,B}} , \quad (3.4)$$

and both terms were calculated using shell model [97, 98, 99, 100].

The recent dispersive representation of the nuclear  $\gamma W$ -box diagram [82] showed that the traditional picture above is an incomplete description. In the dispersive approach, the integrand of the  $\gamma W$  box diagram depends on the absorption spectrum of the target, and therefore  $\delta_{\text{NS}}$  arises essentially from the difference between the nuclear and the nucleon absorption spectrum. Take the type-A contribution as an example: Since the quenched couplings are derived from low-energy nuclear excitations, the replacement of “free” coupling by “quenched” couplings essentially accounts for the contribution to  $\delta_{\text{NS}}$  from low-lying nuclear excited states. It misses, however, more important nuclear effects such as the quasi-elastic absorption peak, which comes not from a highly off-shell nucleon, but from an almost on-shell nucleon loosely bounded to the nucleus. This means, the traditional shell model estimation of  $\delta_{\text{NS}}$  contains a large theory systematics which was not included in their error budget. Ref. [82] estimated this systematic effect using a crude Fermi gas model, which results in an overall shift of  $\delta_{\text{NS}}$  to more negative values, accompanied by an inflated total uncertainty. In the most recent critical survey of  $V_{ud}$  from superallowed decays [96],

$$|V_{ud}|_{0+}^2 = 0.94815(9)_{\text{exp}}(18)_{\Delta_R^V(53)}_{\delta_{\text{NS}}(11)}_{\delta'_r(8)}_{\delta_C} , \quad (3.5)$$

we see that  $\delta_{\text{NS}}$  is the dominant source of uncertainty in  $V_{ud}$  at face value. Therefore, an urgent task in this field is to systematically reduce the theory uncertainty of  $\delta_{\text{NS}}$  by a factor of  $\sim 2$  or more for all important superallowed transitions.

### 3.2.1. Current algebra formalism

Refs. [82, 101, 102] lay out the rigorous theory framework that allows an *ab initio* calculation of  $\delta_{\text{NS}}$ , based on the current algebra approach formulated by Sirlin [103]. It consists of writing the nuclear axial  $\gamma W$ -box diagram amplitude as follows:

$$\square(E_e) = \frac{e^2}{M_F^{(0)}} \Re \int \frac{d^4 q}{(2\pi)^4} \frac{M_W^2}{M_W^2 - q^2} \frac{\left[ Q^2 + M\nu \frac{p \cdot q m_e^2 - p_e \cdot q p \cdot p_e}{M^2 m_e^2 - (p \cdot p_e)^2} \right] T_3(\nu, Q^2)}{[(p_e - q)^2 - m_e^2 + i\varepsilon](q^2 + i\varepsilon)M\nu} , \quad (3.6)$$

where  $M_F^{(0)} = \sqrt{2}$  is the Fermi matrix element in the isospin limit,  $M$  is the mass of the decaying nucleus, and  $E_e$  is the electron energy. The quantity

$$T_3(\nu, Q^2) = -\frac{2M\nu}{|\vec{q}|} \sum_X \left[ \frac{\langle \phi_f | J_{\text{em}}^x(\vec{q}) | X \rangle \langle X | J_{W5}^{\dagger y}(-\vec{q}) | \phi_i \rangle}{\nu_X - \nu - i\varepsilon} + \frac{\langle \phi_f | J_{W5}^y(-\vec{q}) | X \rangle \langle X | J_{\text{em}}^x(\vec{q}) | \phi_i \rangle}{\nu_X + \nu - i\varepsilon} \right] \quad (3.7)$$

is the P-odd invariant amplitude of the so-called “generalized Compton tensor”, where  $X$  represents all on-shell nuclear and hadronic intermediate states. The nuclear-structure-dependent RC is then just the difference between the nuclear

and single-nucleon box diagram:

$$\delta_{\text{NS}} = 2(\langle \square_{\text{nucl}}(E_e) \rangle - \square_n) , \quad (3.8)$$

where  $\langle \dots \rangle$  denotes the average over the beta spectrum.

To facilitate the numerical integration over the loop momentum, we first perform a Wick rotation to the box diagram integral. It leads to the following separation:

$$\square = \square_{\text{Wick}} + \square_{\text{res},e} + \square_{\text{res},T_3} , \quad (3.9)$$

where the first term is the Wick-rotated term, the second is the pole contribution from the electron propagator, and the third terms is the pole contribution from  $T_3$ . The combination of the first two terms is a regular function of  $E_e$ , which can be expanded as:

$$\square_{\text{Wick}} + \square_{\text{res},e} = \Xi_0 + \Xi_1 E_e + \mathcal{O}(E_e^2) . \quad (3.10)$$

In the single-nucleon sector, the smallest energy scale is  $m_\pi$  and  $E_e/m_\pi \sim 10^{-2}$ , which renders the linear term  $\Xi_1 E_e$  irrelevant. Therefore we can express  $\delta_{\text{NS}}$  as:

$$\delta_{\text{NS}} \approx 2(\Xi_0^{\text{nucl}} - \Xi_0^n) + 2\Xi_1^{\text{nucl}} \langle E_e \rangle + \langle (\square(E_e))_{\text{res},T_3} \rangle . \quad (3.11)$$

The first two expansion coefficients are the focus of *ab initio* calculations:

$$\begin{aligned} \Xi_0 &= \int \frac{d^4 q_E}{(2\pi)^4} \frac{M_W^2}{M_W^2 + Q^2} \frac{1}{(Q^2)^2} \frac{Q^2 - \nu_E^2}{\nu_E} \frac{T_3(i\nu_E, Q^2)}{MM_F^{(0)}} \\ \Xi_1 &= -\frac{8}{3} e^2 \Re \int \frac{d^4 q_E}{(2\pi)^4} \frac{Q^2 - \nu_E^2}{(Q^2)^3} \frac{iT_3(i\nu_E, Q^2)}{MM_F^{(0)}} , \end{aligned} \quad (3.12)$$

where  $q_E = (\mathbf{q}, \nu_E)$  is the Euclidean loop momentum, and  $Q^2 = \mathbf{q}^2 + \nu_E^2$ . An alternative representation of  $\Xi_{0,1}$  can be derived through the dispersion relation of  $T_3$ . It reads:

$$\begin{aligned} \Xi_0 &= \frac{\alpha}{\pi} \int_0^\infty dQ^2 \frac{M_W^2}{M_W^2 + Q^2} \int_{\nu_0}^\infty \frac{d\nu}{\nu} \frac{\nu + 2\sqrt{\nu^2 + Q^2}}{(\nu + \sqrt{\nu^2 + Q^2})^2} \frac{F_{3,-}(\nu, Q^2)}{MM_F^{(0)}} \\ \Xi_1 &= \frac{2\alpha}{3\pi} \int_0^\infty dQ^2 \int_{\nu_0}^\infty \frac{\nu + 3\sqrt{\nu^2 + Q^2}}{(\nu + \sqrt{\nu^2 + Q^2})^3} \frac{F_{3,+}(\nu, Q^2)}{MM_F^{(0)}} , \end{aligned} \quad (3.13)$$

which is expressed in terms of the nuclear response functions:

$$F_{3,\pm}(\nu, Q^2) = -\frac{iM\nu}{2|\vec{q}|} \sum_X \delta(E_X - M - \nu) \left\{ \langle \phi_f | J_{\text{em}}^x(\vec{q}) | X \rangle \langle X | (J_{W5}^{\dagger y}(-\vec{q}) | \phi_i \rangle \mp \langle \phi_f | J_{W5}^{\dagger y}(-\vec{q}) | X \rangle \langle X | (J_{\text{em}}^x(\vec{q}) | \phi_i \rangle \right\} . \quad (3.14)$$

Therefore, one can either choose to compute  $T_3$  from Eq.(3.7) or  $F_{3,\pm}$  from Eq.(3.14) with *ab initio* methods. Both expressions involve the summation of all intermediate states  $X$ , which makes it computationally more demanding; however, with this approach one explicitly captures the full contribution to  $\delta_{\text{NS}}$  from physics at all scales.

The current algebra approach has been adopted to compute  $\delta_{\text{NS}}$  for  ${}^{10}\text{C} \rightarrow {}^{10}\text{B}$  using NCSM [17], which we will describe in Section 3.3. Follow-up studies on  ${}^{14}\text{O} \rightarrow {}^{14}\text{N}$  and  ${}^{18}\text{Ne} \rightarrow {}^{18}\text{F}$  are ongoing.

### 3.2.2. Effective field theory formalism

Refs. [19, 18] took an alternative path, namely the effective field theory (EFT) approach to describe the RC. It consists of first splitting the loop integral into different regions of the loop momentum  $q$ . Two regions are relevant to the structure-dependent RC: (1) The ‘ultrasoft’ region where  $q_0 \sim \mathbf{q} \sim 10^0$  MeV, and (2) The ‘potential’ region, where

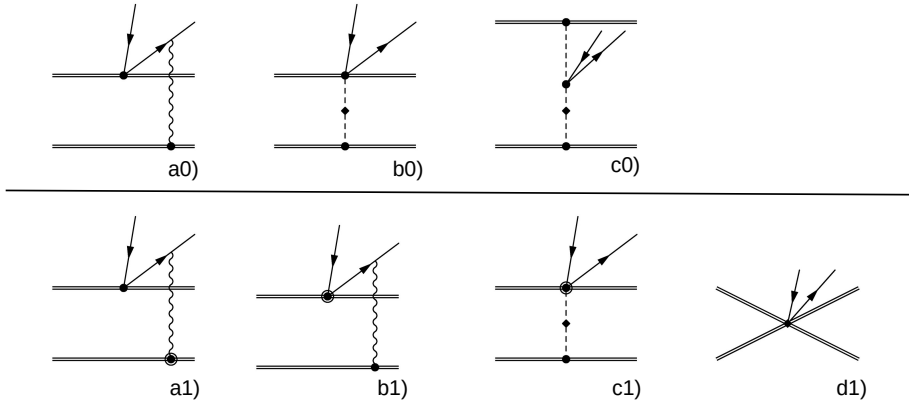


Figure 3.2: Lowest-order Feynman diagrams contributing to the effective two-body potentials. Figures courtesy of Wouter Dekens.

$q_0 \sim 10^0$  MeV  $\ll \mathbf{q} \sim 10^2$  MeV. The contribution from the ultrasoft region is sensitive to details of nuclear excited states and thus need to be evaluated explicitly. On the other hand, the contribution from the potential region turns out to be largely independent of the nuclear intermediate states. Therefore, in this region one may derive an ‘‘effective potential’’ from few-nucleon Feynman diagrams and simply evaluate its ground-state nuclear matrix element.

In the EFT framework, the weak Hamiltonian responsible for nuclear beta decays reads:

$$H_{\text{EW}} = \sqrt{2} G_F V_{ud} \bar{e}_L \gamma_\mu v_L \mathcal{J}_W^\mu , \quad (3.15)$$

where the effective weak current reads:

$$\begin{aligned} \mathcal{J}_W^\mu &= \sum_{n=1}^A (g_V \delta^{\mu 0} - g_A \delta^{\mu i} \sigma^{(n)i}) \tau^{(n)+} + (\mathcal{J}^{2b})^\mu + \dots \\ &\quad + \delta^{\mu 0} (\mathcal{V}_E^0 + E_0 \mathcal{V}_E^\pi) + \delta^{\mu i} \mathcal{V}_i + p_e^\mu \mathcal{V}_{m_e} + \dots , \end{aligned} \quad (3.16)$$

with  $E_0$  the electron end-point energy. We retain here only the one-body and two-body contributions. The one-body term in the first line consists of the vector and axial coupling  $g_V$  and  $g_A$  which are already renormalized by nucleus-independent RC [88, 104], and  $(\mathcal{J}^{2b})^\mu$  is the pure-QCD two-body current. Meanwhile, the second line consists of two-body potentials that can be obtained diagrammatically from Fig. 3.2. First, at  $\mathcal{O}(\alpha)$ , the lepton-energy-dependent potentials read:

$$\begin{aligned} \mathcal{V}_E^0 &= \frac{1}{3} \left( \frac{1}{2} + \frac{4E_e}{E_0} \right) \mathcal{V}_E + \mathcal{V}_E^\pi \\ \mathcal{V}_{m_e} &= \frac{1}{2} \mathcal{V}_E + \mathcal{V}_{m_e}^\pi , \end{aligned} \quad (3.17)$$

where  $\mathcal{V}_E$  is obtained from Fig. 3.2(a0):

$$\mathcal{V}_E(\mathbf{q}) = g_V \sum_{j < k} e^2 \frac{1}{\mathbf{q}^4} (\tau^{+(j)} P_p^{(k)} + P_p^{(j)} \tau^{+(k)}) , \quad (3.18)$$

and  $\mathcal{V}_E^\pi$  comes from the electromagnetically-induced pion mass splitting, i.e. Figs. 3.2(b0),(c0), characterized by the

coupling constant  $Z_\pi$ :

$$\begin{aligned}
\mathcal{V}_E^\pi(\mathbf{q}) &= \frac{g_A^2 Z_\pi e^2}{3} \sum_{j < k} (\tau^{+(j)} \tau_3^{(k)} + \tau_3^{(j)} \tau^{+(k)}) \frac{1}{[\mathbf{q}^2 + m_\pi^2]^2} \\
&\quad \times \left\{ \sigma^{(j)} \cdot \sigma^{(k)} \left( 1 - \frac{1}{3} \frac{\mathbf{q}^2}{\mathbf{q}^2 + m_\pi^2} - \frac{2}{3} \frac{\mathbf{q}^4}{(\mathbf{q}^2 + m_\pi^2)^2} \right) + \frac{2}{3} S^{(jk)} \left( \frac{1}{2} \frac{\mathbf{q}^2}{\mathbf{q}^2 + m_\pi^2} + \frac{\mathbf{q}^4}{(\mathbf{q}^2 + m_\pi^2)^2} \right) \right\} \\
\mathcal{V}_{m_e}^\pi(\mathbf{q}) &= -\frac{g_A^2 Z_\pi e^2}{3} \sum_{j < k} (\tau^{+(j)} \tau_3^{(k)} + \tau_3^{(j)} \tau^{+(k)}) \frac{1}{[\mathbf{q}^2 + m_\pi^2]^2} \\
&\quad \times \left\{ \sigma^{(j)} \cdot \sigma^{(k)} \left( 1 - \frac{4}{3} \frac{\mathbf{q}^2}{\mathbf{q}^2 + m_\pi^2} - \frac{2}{3} \frac{\mathbf{q}^4}{(\mathbf{q}^2 + m_\pi^2)^2} \right) + \frac{2}{3} S^{(jk)} \left( 2 \frac{\mathbf{q}^2}{\mathbf{q}^2 + m_\pi^2} + \frac{\mathbf{q}^4}{(\mathbf{q}^2 + m_\pi^2)^2} \right) \right\}. \quad (3.19)
\end{aligned}$$

Here we have defined operators in the spin and isospin space:

$$P_{p,n}^{(j)} = \frac{\mathbb{1}^{(j)} \pm \tau_3^{(j)}}{2}, \quad S^{(jk)} = \sigma^{(j)} \cdot \sigma^{(k)} - \frac{3\mathbf{q} \cdot \sigma^{(j)} \mathbf{q} \cdot \sigma^{(k)}}{\mathbf{q}^2}. \quad (3.20)$$

More interesting are the lepton-energy-independent potential  $\mathcal{V}^0$ . At  $\mathcal{O}(\alpha)$ , it consists of three terms derived from the last four diagrams in Fig. 3.2:

$$\mathcal{V}^0 = \mathcal{V}_0^{\text{mag}} + \mathcal{V}_0^{\text{rec}} + \mathcal{V}_0^{\text{CT}}. \quad (3.21)$$

First, the long-distance “magnetic” and “recoil” potential obtained from Figs. 3.2(a1)-(c1) read <sup>1</sup>:

$$\begin{aligned}
\mathcal{V}_0^{\text{mag}}(\mathbf{q}) &= \sum_{j < k} \frac{e^2}{3} \frac{g_A}{m_N} \frac{1}{\mathbf{q}^2} \left( \sigma^{(j)} \cdot \sigma^{(k)} + \frac{1}{2} S^{(jk)} \right) [(1 + \kappa_p) \tau^{+(j)} P_p^{(k)} + \kappa_n \tau^{+(j)} P_n^{(k)} + (j \leftrightarrow k)] \\
\mathcal{V}_0^{\text{rec}}(\mathbf{q}, \mathbf{P}) &= \sum_{j < k} \left[ i \frac{e^2 g_A}{2m_N} \frac{\tau^{+(j)} P_p^{(k)}}{\mathbf{q}^4} (\mathbf{P}_k \times \mathbf{q}) \cdot \sigma^{(j)} - \frac{Z_\pi e^2 g_A^2}{m_N} \frac{\tau^{+(j)} \tau_3^{(k)}}{(\mathbf{q}^2 + m_\pi^2)^2} \sigma^{(j)} \cdot \mathbf{q} \sigma^{(k)} \cdot \mathbf{P}_j + (j \leftrightarrow k) \right]. \quad (3.22)
\end{aligned}$$

For future purpose, we can split the “recoil” potential into two pieces:

$$\mathcal{V}_0^{\text{rec}} = \mathcal{V}_0^{\text{rec},1} + \mathcal{V}_0^{\text{rec},2} \quad (3.23)$$

which are linear and quadratic to  $g_A$ , respectively. There are also  $\mathcal{O}(\alpha^2)$  terms in the potential which we do not display here.

Renormalization analysis shows that the nuclear matrix element of  $\mathcal{V}_0^{\text{mag}}$  depends logarithmically on the ultraviolet (UV) cutoff. This signals sensitivity to the UV physics which must be absorbed by an extra “counterterm” potential coming from Fig. 3.2(d1):

$$\mathcal{V}_0^{\text{CT}} = e^2 (g_{V1}^{NN} O_1 + g_{V2}^{NN} O_2), \quad (3.24)$$

where

$$O_1 = \sum_{j \neq k} \tau^{+(j)} \mathbb{1}^{(k)}, \quad O_2 = \sum_{j < k} [\tau^{+(j)} \tau_3^{(k)} + (j \leftrightarrow k)]. \quad (3.25)$$

This potential introduces two new low energy constants (LECs)  $g_{V1}^{NN}$ ,  $g_{V2}^{NN}$  which values are not fixed by chiral symmetry and must be determined by other means. This is very similar to the EFT description of neutrinoless double beta decay [105, 106].

The EFT approach has been adopted to compute  $\delta_{\text{NS}}$  for  $^{14}\text{O} \rightarrow {}^{14}\text{N}$  [18, 19] and  $^{10}\text{C} \rightarrow {}^{10}\text{B}$  [20] using quantum Monte Carlo, which we will describe in Section 3.4. There is also an ongoing, parallel effort to compute  $\delta_{\text{NS}}$  in superallowed

<sup>1</sup>There was a typo in the expression of  $\mathcal{V}_0^{\text{rec}}(\mathbf{q}, \mathbf{P})$  in Ref.[19] which affected their final numerical result.

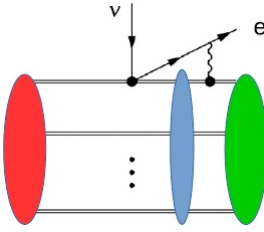


Figure 3.3: RC diagram with the weak and electromagnetic vertices acting on the same nucleon. Figure courtesy of Wouter Dekens.

decays of  $^{10}\text{C}$ ,  $^{14}\text{O}$ ,  $^{26}\text{Al}$ ,  $^{34}\text{Cl}$ ,  $^{38}\text{K}$ ,  $^{42}\text{Sc}$ ,  $^{46}\text{V}$ ,  $^{50}\text{Mn}$  and  $^{54}\text{Co}$  using coupled cluster method <sup>2</sup>. It is highly desirable to have multiple *ab initio* calculation of the same nuclei in order to better understand the method-dependence of the final result and thus better quantify the theory uncertainties.

### 3.2.3. Connection between the two approaches

The two different descriptions of  $\delta_{\text{NS}}$  must be equivalent and it is important their connections in order to properly compare different results. The current algebra approach deals explicitly with the nuclear “axial”  $\gamma W$ -box diagram, while the EFT approach represents a general treatment of all electromagnetic effects. To connect the two approaches we simply identify components in the latter that comes from the axial  $\gamma W$ -box diagram. In long-distance two-body contributions, this is represented by the two-body potentials that are linear to  $g_A$ , namely  $\mathcal{V}_0^{\text{mag}}$  and  $\mathcal{V}_0^{\text{rec},1}$ . Additionally, the counterterm potential serves to cancel the UV divergence of the nuclear matrix element of  $\mathcal{V}_0^{\text{mag}}$ , so they have to appear together. As a result, we have the following matching [107]:

$$\delta_{\text{NS}} = \frac{2}{M_F^{(0)}} \langle \mathcal{V}_0^{\text{mag}} + \mathcal{V}_0^{\text{rec},1} + \mathcal{V}_0^{\text{CT}} \rangle_{fi} . \quad (3.26)$$

This relation is useful in the following sense. On the one hand,  $\delta_{\text{NS}}$  can be computed explicitly with the current algebra approach, but it involves the summation over all nuclear intermediate states which is computationally more demanding. On the other hand, the ground-state nuclear matrix elements of effective two-body potentials are much easier to compute, but the theory precision is limited by the two unknown LECs. So, a useful way to make progress is to first choose a pair of superallowed transitions that can be easily handled in both methods. One then computes the LHS of Eq.(3.26) using the current algebra approach, and the RHS using the EFT approach. With that, we are able to extract the values of the two unknown LECs by the above matching relation. Once the LECs are known, one can proceed with the EFT approach for other transitions without being limited by their large theory uncertainties. Thus, we verify that the physics in the counterterms can indeed be obtained explicitly in the current algebra approach.

Of course, for the matching to be useful we need to be sure that the direct ab-initio calculation of  $\delta_{\text{NS}}$  through the summation of nuclear intermediate states will include the physics contained in the EFT counterterms, and indeed it does. This can be seen by investigating the type of diagrams depicted in Fig. 3.3, where the weak and electromagnetic vertices act on a single nucleon. In a full theory valid in all energy scales, this diagram involves the integration of the single-nucleon form factors convoluted with the nucleon momentum distribution in a nucleus (the so-called “Fermi smearing”, which gives rise to the quasi-elastic nucleon contribution to  $\delta_{\text{NS}}$ ); it probes the loop momentum up to a few hundred MeV, and such a contribution is explicitly included in the calculation of  $T_3$  through the summation of nuclear intermediate states. On the

---

<sup>2</sup>Private communication with Samuel Novario.

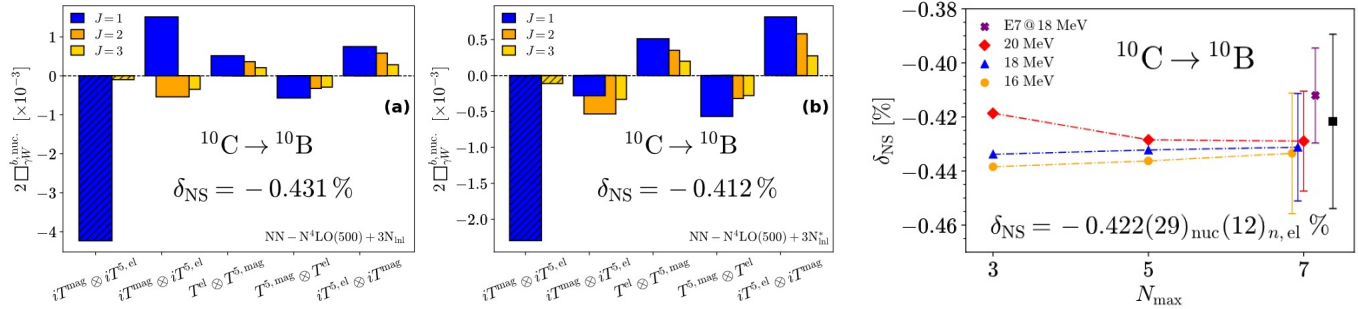


Figure 3.4: Main results of the  $\delta_{\text{NS}}$  calculation for  ${}^{10}\text{C} \rightarrow {}^{10}\text{B}$  in Ref.[17] (see the text for explanation).

other hand, as explained in Ref. [19], the same diagram in the EFT language probes only physics at the ultrasoft region, i.e.  $q \sim 10^0$  MeV. Therefore, the contribution from the quasielastic nucleons does not reside in Fig.3.3, but instead in the nuclear matrix element of the counterterm potentials.

### 3.3. ${}^{10}\text{C} \rightarrow {}^{10}\text{B}$ with No-Core Shell Model

Ref.[17] performed the first *ab initio* calculation of  $\delta_{\text{NS}}$  in the  ${}^{10}\text{C} \rightarrow {}^{10}\text{B}$  superallowed beta decay based on the current algebra approach using NCSM. Two strategies are adopted to facilitate the computation of the P-odd invariant amplitude  $T_3$ :

- The Lanczos strength method [108, 109, 110] is used to enable an efficient summation over all nuclear intermediate states  $X$ .
- The electroweak current operators are expanded in terms of multipole operator with increasing angular quantum number  $J$  [111, 112]. Matrix elements of multipole operators with respect to harmonic oscillator states are well-documented, so one can make use of results in the literature to simplify the calculation.

The main results of Ref. [17] are summarized in Fig.3.4. The first two plots show the contributions from different products of multipole operators to the nuclear box diagram, and one indeed finds that the contribution decreases rapidly with increasing  $J$ . These two diagrams are based on two different choices of three-nucleon forces [113, 34], which has a mild effect to the central value of  $\delta_{\text{NS}}$  that is taken as a measure of the uncertainty from the chiral interactions. The third diagram demonstrates the quick convergence of our result with increasing  $N_{\text{max}}$ , which becomes basically flat at  $N_{\text{max}} = 7$ , much faster than most typical NCSM calculations. The variation of the result with respect to the oscillator frequency  $\Omega$  is also shown in the same plot.

Despite these promising features, nuclear *ab initio* calculations cannot capture all nuclear physics that reside in  $\delta_{\text{NS}}$ . The reason is apparent: from the dispersive analysis, we know that  $\delta_{\text{NS}}$  is induced by the difference between the single-nucleon absorption spectrum and the nuclear spectrum spectrum, both are contributed by nucleonic and non-nucleonic DOFs. Since *ab initio* calculations are based on chiral Lagrangian that typically consists only of nucleon fields, it can only account for nuclear modifications to contribution from the nucleonic DOFs. In other words, it only covers contributions from intermediate states  $X$  in Eq.(3.7) that are just made out of nucleons, while the contributions from all other intermediate states involving non-nucleonic particles are missed. The uncertainty due to this missing effects need to be included in the error budget.

To get a more complete picture, we start from the single-nucleon box diagram, and split it into the “elastic” and “inelastic” pieces:

$$\square_n = \square_n^{\text{el}} + \square_n^{\text{inel}} , \quad (3.27)$$

where the elastic piece depends only on free nucleon form factors. This splitting is possible in the dispersive analysis [81, 85]. The nuclear modification to the first term,  $\square_n^{\text{el}}$ , is accounted for in *ab initio* calculation, which we denote as  $\square_{\text{nuc}}^{\text{ab-initio}}$ . So, we can write the full nuclear box diagram as

$$\square_{\text{nuc}} = \square_{\text{nuc}}^{\text{ab-initio}} + (\square_n^{\text{inel}} + \delta(\square_n^{\text{inel}})_{\text{shad}}) , \quad (3.28)$$

where  $\delta(\square_n^{\text{inel}})_{\text{shad}}$  denotes nuclear modification to  $\square_n^{\text{inel}}$  due primarily to the so-called “shadowing” effect at high energy [114, 115]. In Ref. [17], this term was included as an uncertainty. To estimate its size, one first splits the nucleon part into:

$$\square_n^{\text{inel}} = (\square_n^{\text{inel}})^< + (\square_n^{\text{inel}})^> , \quad (3.29)$$

where the superscripts “ $<$ ” and “ $>$ ” denote the contribution from the loop integral below and above  $Q^2 = 2 \text{ GeV}^2$ . For  $Q^2 > 2 \text{ GeV}^2$ , the integral is related to a sum rule of the parity-odd structure function  $F_3$ , similar to the well-known Gross-Llewellyn Smith (GLS) sum rule [116]; the latter is experimentally demonstrated to hold even for heavy nuclei [117, 118] after including higher-order perturbative QCD effects, so one may assume that this part is not modified. Meanwhile, the nuclear modification to  $(\square_n^{\text{inel}})^<$  can be inferred from the experimental knowledge of the ratio  $R$  between the nucleon and nuclear structure function  $F_2$ . Depending on the value of the Bjorken variable  $x_B$ ,  $R$  may deviate positively or negatively from 1 due to different physical mechanisms, such as nuclear shadowing, anti-shadowing, EMC effect and Fermi motion. For  $A \approx 10$ , the maximum deviation of  $R$  from 1 is about 20% [115]. So, one may simply multiply  $(\square_n^{\text{inel}})^<$  by 20%, and take it as a conservative estimation of the absolute size of  $\delta(\square_n^{\text{inel}})_{\text{shad}}$  which will be included as an error.

The full result of  $\delta_{\text{NS}}$  for  ${}^{10}\text{C} \rightarrow {}^{10}\text{B}$  obtained in Ref. [17] reads<sup>3</sup>:

$$\delta_{\text{NS}} = -0.422(14) \text{ PME}(4)_{\Omega}(9)_{\chi}(24)_{\text{sh}}\% , \quad (3.30)$$

where the sources of (nucleus-dependent) theoretical errors are: (i) PME: The “partial model error”, due to many-body basis truncation, multipole expansion truncation, and single-nucleon dipole form factors; (ii)  $\Omega$ : The choice of oscillator frequency; (iii)  $\chi$ : The chiral expansion truncation; and (iv) sh: The nuclear shadowing effect. It is informative to track the “evolution” of this number over time:

$$\begin{aligned} \delta_{\text{NS}}(\%) &: -0.345(35) , \text{ Shell model} \\ &\rightarrow -0.400(50) , \text{ DR + Fermi gas model} \\ &\rightarrow -0.422(29) , \text{ } Ab \text{ initio NCSM} \end{aligned} \quad (3.31)$$

The first calculation with shell model was based on the type-A/type-B picture. This was later discovered in the dispersive analysis to contain a large theory systematic, which was estimated using a crude Fermi gas model [82, 119]; this resulted in a shift to  $\delta_{\text{NS}}$  to the more negative side, accompanied by an inflated theory uncertainty. This result is then confirmed by the *ab initio* calculation in Ref. [17] but with a substantially reduced uncertainty.

---

<sup>3</sup>We do not include the uncertainty due to the subtraction of the single-nucleon box diagram which was displayed in Fig.3.4, because it goes away upon combining  $\delta_{\text{NS}}$  and  $\Delta_R^V$ .

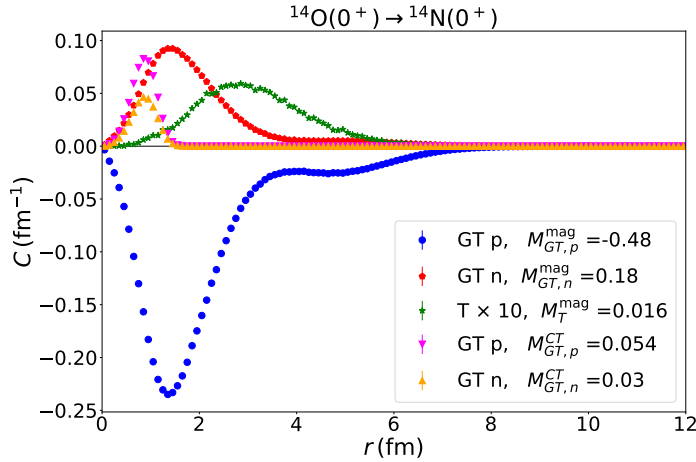


Figure 3.5: Nuclear matrix element densities of various potentials contributing to  $\overline{\delta_{\text{NS}}}$  in  $^{14}\text{O} \rightarrow ^{14}\text{N}$  computed with VMC plotted as a function of interparticle spacing  $r$ . The integrated curves correspond to the matrix elements in the legend of the plot.

Model	Method	$\delta_{\text{NS}}^{(0)}$	$\overline{\delta_{\text{NS}}^E}$
NV2+3-Ia	VMC	$-(4.03 + 0.25 \pm 0.69) \cdot 10^{-3}$	$1.01 \cdot 10^{-3}$
	GFMC	$-(4.43 + 0.21 \pm 0.77) \cdot 10^{-3}$	$0.97 \cdot 10^{-3}$
NV2+3-Ia*	VMC	$-(4.18 + 0.31 \pm 0.62) \cdot 10^{-3}$	$1.06 \cdot 10^{-3}$
	GFMC	$-(4.25 + 0.31 \pm 0.66) \cdot 10^{-3}$	$1.08 \cdot 10^{-3}$
AV18+UX	VMC	$-(4.48 + 0.27 \pm 0.67) \cdot 10^{-3}$	$1.02 \cdot 10^{-3}$
	GFMC	$-(4.06 + 0.40 \pm 0.48) \cdot 10^{-3}$	$1.17 \cdot 10^{-3}$
AV18+IL7	VMC	$-(4.55 + 0.26 \pm 0.61) \cdot 10^{-3}$	$1.01 \cdot 10^{-3}$
	GFMC	$-(4.32 + 0.29 \pm 0.64) \cdot 10^{-3}$	$1.06 \cdot 10^{-3}$

Table 3.1: Summary of the results for  $\overline{\delta_{\text{NS}}}$ . For the energy-independent component,  $\delta_{\text{NS}}^{(0)}$ , the first term encodes the contribution of the magnetic and spin-orbit two-body operators. The second term is the  $\mathcal{O}(\alpha^2)$  correction arising from  $M_{F,p}^+$ . The last contribution arises from the contact interactions, with LECs set to the *arbitrary* values  $g_{V1}^{NN} \pm g_{V2}^{NN} = \pm \frac{1}{m_N} \frac{1}{(2F_\pi)^2}$ . The last column shows the energy dependent part,  $\overline{\delta_{\text{NS}}^E}$ .

### 3.4. $^{10}\text{C} \rightarrow ^{10}\text{B}$ and $^{14}\text{O} \rightarrow ^{14}\text{N}$ with Quantum Monte Carlo

Next, we report the pioneering studies of  $\delta_{\text{NS}}$  based on the EFT approach, by computing the matrix elements for the potentials defined in Section 3.2.2 with many-body methods. Recently, such evaluations have been performed using quantum Monte Carlo methods; namely, VMC and GFMC for  $^{10}\text{C}$  [20], and VMC and AFDMC for  $^{14}\text{O}$  [19]. As an example, the VMC calculation of the nuclear matrix elements of various potentials is shown in Fig.3.5.

To make connections with experimental data, for  $\beta^+$  decay, one combines the matrix elements of the potentials to give both the energy-independent part (see Eq.(3.21), including the  $\mathcal{O}(\alpha^2)$  contribution not displayed),

$$\delta_{\text{NS}}^{(0)} = \frac{2}{g_V(\mu_\pi) M_F^{(0)}} \sum_{N=n,p} \left[ \alpha \left( M_{\text{GT},N}^{\text{mag}} + M_{\text{T},N}^{\text{mag}} + M_{\text{GT},N}^{\text{CT}} + M_{\text{LS},N} \right) + \alpha^2 M_{F,N}^+ \right], \quad (3.32)$$

and the energy-dependent part (see Eq.(3.16)),

$$\overline{\delta_{\text{NS}}^E} = -\frac{2}{g_V(\mu_\pi) M_F^{(0)}} \left[ M_E^0 E_0 + \frac{m_e^2}{E_e} M_{m_e} \right], \quad (3.33)$$

where the vector coupling constant  $g_V$  is evaluated at a scale  $\mu_\pi = m_\pi$  giving  $g_V(m_\pi) = 1.01494(12)$  [88], and the electron

energy  $E_e$  is averaged over phase-space. The matrix element  $M_{i,N}^X$  denotes

$$M_{i,N}^X = \langle f | V_{i,N}^X | i \rangle \quad (3.34)$$

for a given potential  $V_{i,N}^X$  defined in Ref. [19]. These potentials are obtained by Fourier-transforming the momentum-space potentials  $\mathcal{V}(\mathbf{q}, \mathbf{P})$  in Section 3.2.2 into coordinate space, and scaling out appropriate powers of  $\alpha$ . The nuclear initial and final states are denoted as  $|i\rangle$  and  $|f\rangle$ , respectively. The values of these contributions sum to give the overall correction,

$$\overline{\delta_{\text{NS}}} = \delta_{\text{NS}}^{(0)} + \overline{\delta_{\text{NS}}^E} . \quad (3.35)$$

For  $^{10}\text{C}$ , the GFMC results were obtained for four different models of the nuclear interaction. Namely, two phenomenological models— the Argonne  $v_{18}$  [120] plus either the Illinois-7 (IL7) [121] or Urbana X (UX) [122] three nucleon forces— and two Norfolk chiral potential models [70, 71, 123]. Norfolk potential models are denoted as NV2+3-Ia and NV2+3-Ia\* in the literature. The main results are summarized for VMC and GFMC calculations in  $^{10}\text{C}$  in Table 3.1. For VMC calculations of  $^{14}\text{O}$  using the interaction of Refs. [124, 125], the results are <sup>4</sup>:

$$\delta_{\text{NS}}^{(0)} = -2.84(88) \cdot 10^{-3} , \quad \overline{\delta_{\text{NS}}^E} = 2.06(41) \cdot 10^{-3} . \quad (3.36)$$

The comparison with traditional approach (i.e. Ref.[96]) is most conveniently done in terms of the full  $V_{ud}$  [126]. The GFMC values of  $|V_{ud}(^{10}\text{C})|$  are compared with the traditional extraction below,

$$\text{NV2+3-Ia} \quad V_{ud}|_{^{10}\text{C}} = 0.97355(66)_{\text{exp}}(12)_{g_V}(17)_{\mu}(9)_{\delta_C}(38)_{g_V^{\text{NN}}}, \quad (3.37)$$

$$\text{NV2+3-Ia*} \quad V_{ud}|_{^{10}\text{C}} = 0.97345(66)_{\text{exp}}(12)_{g_V}(17)_{\mu}(9)_{\delta_C}(32)_{g_V^{\text{NN}}}, \quad (3.38)$$

$$\text{AV18+UX} \quad V_{ud}|_{^{10}\text{C}} = 0.97336(66)_{\text{exp}}(12)_{g_V}(17)_{\mu}(9)_{\delta_C}(23)_{g_V^{\text{NN}}}, \quad (3.39)$$

$$\text{AV18+IL7} \quad V_{ud}|_{^{10}\text{C}} = 0.97349(66)_{\text{exp}}(12)_{g_V}(17)_{\mu}(9)_{\delta_C}(31)_{g_V^{\text{NN}}}, \quad (3.40)$$

$$\text{Traditional} \quad V_{ud}|_{^{10}\text{C}} = 0.97318(66)_{\text{exp}}(9)_{\Delta_R^V}(24)_{\delta_{\text{NS}}}(9)_{\delta_C} . \quad (3.41)$$

For  $^{14}\text{O}$ , the comparison gives,

$$\text{EFT} \quad V_{ud}|_{^{14}\text{O}} = 0.97411(10)_{\text{exp}}(12)_{g_V}(22)_{\mu}(12)_{\delta_C}(43)_{g_V^{\text{NN}}}(20)_{\delta_{\text{NS}}^E}, \quad (3.42)$$

$$\text{Traditional} \quad V_{ud}|_{^{14}\text{O}} = 0.97405(13)_{\text{exp}}(9)_{\Delta_R^V}(31)_{\delta_{\text{NS}}}(12)_{\delta_C} . \quad (3.43)$$

The main theoretical uncertainty in the EFT approach is due to two undetermined LECs, namely,  $g_{V1}^{NN}$  and  $g_{V2}^{NN}$ . The magnitudes of these two LECs can only be estimated using chiral power counting. Reducing this uncertainty in the future may involve lattice calculations of two-nucleon matrix elements, which can be quite challenging in practice. An alternative approach suggested in Ref. [19] is to take these LECs as free fitting parameters, and perform a global fit, together with  $V_{ud}$  to different superallowed transition rates. In this review we point out the possibility to pin down the LECs through the matching procedure outlined in Section 2. Other uncertainties include variations in the matching scales of the EFT ( $\mu$ ), the value of the coupling  $g_V(\mu)$  at the matching scales, the uncertainty in the isospin breaking corrections taken from [126] ( $\delta_C$ ), and missing higher order energy-dependent terms in the chiral expansion denoted by  $\delta_{\text{NS}}^E$ . In comparison, the traditional extraction has uncertainties from its approach to computing  $\delta_{\text{NS}}$ , as well as for the transition independent radiative corrections  $\Delta_R^V$ ; the latter is included in  $g_V(\mu)$  in the EFT approach.

<sup>4</sup>Results for  $\delta_{\text{NS}}^{(0)}$  and  $V_{ud}$  were corrected for the re-evaluation of  $\mathcal{V}_0^{\text{rec}}$  matrix element. Private communication with Emanuele Mereghetti and Wouter Dekens.

## 4. Recoil-order corrections to allowed beta decays

In-depth investigations of angular correlations in nuclear  $\beta$  decay have historically been instrumental in uncovering the “vector-minus-axial vector” (V-A) nature of the charged current in the electroweak interaction [127, 128]. Presently, research in nuclear  $\beta$  decay continues to be at the forefront of probing for potential deviations from the Standard Model, particularly in the search for additional scalar (S) and tensor (T) Lorentz-invariant interactions that can naturally emerge in extensions beyond the Standard Model. Precise measurements of the  $\beta$ - $\nu$  angular correlation, the  $\beta$  asymmetry, and the Fierz interference term serve as critical tests constraining possible new physics. Ongoing and upcoming experiments aim to enhance the precision of these measurements further [12, 5].

Recoil-order terms are generally omitted in  $\beta$ -decay theory because they are proportional to  $q/m_N$  or higher, where  $q$  represents the momentum transfer—typically a few MeV/c—and  $m_N$  is the nucleon mass [129]. Consequently, in most  $\beta$  decays, recoil effects contribute less than one percent of the dominant Fermi and Gamow-Teller (GT) amplitudes. Nonetheless, when measurements reach very high precision, these recoil-order terms become significant and must be incorporated into the analyses of the experiments, particularly in cases where the primary contributions are suppressed or the recoil effects are unexpectedly large.

The study of recoil-order corrections in allowed  $\beta$  decays provides a sensitive theoretical handle on sub-percent effects that can obscure or imitate signatures of BSM interactions. These corrections arise from higher-order terms in the nuclear weak current—such as weak magnetism, induced tensor, and higher-multipole axial components—which modify the  $\beta$  spectrum shape and angular correlations at the  $10^{-3}$  level. Quantifying these effects within *ab initio* many-body approaches is therefore essential to distinguish genuine BSM contributions from Standard-Model nuclear structure effects. In this section, we review three complementary calculations that address this challenge: (i) the  ${}^6\text{He} \rightarrow {}^6\text{Li}$  decay computed with the NCSM, providing the first consistent evaluation of recoil and shape corrections with quantified uncertainties; (ii) the same transition studied using GFMC, incorporating explicit two-body weak currents and full spectral reconstruction; and (iii) the  ${}^8\text{Li}$  and  ${}^8\text{B}$   $\beta$  decays analyzed with the SA-NCSM, where correlations between recoil-order form factors and nuclear deformation help reduce uncertainties on the *ab initio* predictions.

### 4.1. ${}^6\text{He} \rightarrow {}^6\text{Li}$ beta decay corrections with NCSM

The  $\beta$ -decay of  ${}^6\text{He}$  offers a particularly clean probe of BSM tensor currents thanks to its pure GT character, and its light nuclear mass which makes it computationally tractable within *ab initio* many-body frameworks, allowing high-precision theoretical predictions. Several experimental programs are currently pursuing precision studies of this decay. At the Laboratoire de Physique Corpusculaire de CAEN [130], and the University of Washington CENPA through the He6-CRES Collaboration [131], efforts focus on measuring the  $\beta$ -electron energy spectrum, while at SARAF, SNRC [132] the emphasis is on the angular correlation between the emitted  $\beta$  particle and neutrino. As these measurements strive for per-mil level accuracy, precise Standard Model calculations are essential to fully exploit their potential for constraining new physics.

For a pure GT transition, the differential decay rate can be written as  $d\Gamma \propto 1 + a\vec{\beta} \cdot \hat{\nu} + b\frac{m_e}{E_e}$ , where  $\vec{\beta} = \frac{\vec{k}}{E_e}$  is the emitted electron direction,  $\vec{k}_e$ ,  $E_e$  and  $m_e$  are its momentum, energy, and mass, respectively,  $\hat{\nu}$  is the unit vector in the direction of the neutrino momentum  $\vec{\nu}$ . The coefficients  $a$  and  $b$  encode the leading angular correlation and spectral observables and are particularly sensitive to BSM tensor interactions. Specifically, the  $\beta$ - $\nu$  angular-correlation coefficient  $a$  is quadratically sensitive to the tensor coupling  $\epsilon_T$ , while the Fierz interference term  $b$  depends linearly on  $\epsilon_T$  [133, 4].

In the Standard Model limit, one has  $a = -1/3$  and  $b = 0$ , and current experiments aim to detect per-mil-level deviations from these values as possible signatures of BSM physics.

However, at the same level of experimental precision, nuclear-structure small effects become relevant. Recoil and shape corrections arise at next-to-leading order (NLO) in several small expansion parameters, namely the non-relativistic  $p_F/m_N \approx 0.2$  ( $P_{\text{Fermi}}$  is Fermi momentum and  $m_N$  is the nucleon mass), the momentum transfer  $qr \approx 0.05$  ( $\vec{q} = \vec{\nu} + \vec{k}_e$  and  $r$  is the nuclear radius), and the nucleon recoil  $q/m_N \approx 0.004$ . These Standard-Model corrections modify the effective values of  $a$  and  $b$  and, if not properly accounted for, can mimic the effects of BSM tensor couplings.

Following Ref. [134], the fully differential decay rate including these recoil and shape corrections can be written as,

$$\frac{d\Gamma}{dE_e d\Omega_e d\Omega_\nu} \propto (E_0 - E_e)^2 k_e E_e F^-(Z_f, E_e) C_{\text{corr}} 3 (1 + \delta_1) \left[ 1 - \frac{1}{3} (1 + \tilde{\delta}_a) \vec{\beta} \cdot \hat{\nu} + \delta_b \frac{m_e}{E_e} \right] \left| \langle \|\hat{L}_1^A\| \rangle \right|^2, \quad (4.1)$$

where  $E_0$  is the maximum electron energy,  $F^-(Z_f, E_e)$  is the Fermi function accounting for Coulomb distortion of the electron wave function, and  $C_{\text{corr}}$  represents other corrections which do not affect the observables. Lastly,  $\langle \|\hat{L}_1^A\| \rangle$  corresponds to the reduced matrix element of the leading GT multipole operator between the initial and final wave functions, while  $\delta_1$ ,  $\tilde{\delta}_a$ , and  $\delta_b$  parameterize recoil and shape corrections arising from subleading multipole contributions.

These corrections depend on reduced matrix elements of rank-1 multipole operators of the weak current and can be expressed as

$$\begin{aligned} \delta_1 &\equiv \frac{2}{3} \Re \left[ -E_0 \frac{\langle \|\hat{C}_1^A/q\| \rangle}{\langle \|\hat{L}_1^A\| \rangle} + \sqrt{2} (E_0 - 2E_e) \frac{\langle \|\hat{M}_1^V/q\| \rangle}{\langle \|\hat{L}_1^A\| \rangle} \right], \\ \tilde{\delta}_a &\equiv \frac{4}{3} \Re \left[ 2E_0 \frac{\langle \|\hat{C}_1^A/q\| \rangle}{\langle \|\hat{L}_1^A\| \rangle} + \sqrt{2} (E_0 - 2E_e) \frac{\langle \|\hat{M}_1^V/q\| \rangle}{\langle \|\hat{L}_1^A\| \rangle} \right], \\ \delta_b &\equiv \frac{2}{3} m_e \Re \left[ \frac{\langle \|\hat{C}_1^A/q\| \rangle}{\langle \|\hat{L}_1^A\| \rangle} + \sqrt{2} \frac{\langle \|\hat{M}_1^V/q\| \rangle}{\langle \|\hat{L}_1^A\| \rangle} \right], \end{aligned} \quad (4.2)$$

where  $\hat{C}_1^A$ ,  $\hat{M}_1^V$ , and  $\hat{L}_1^A$  denote the axial-charge, vector-magnetic, and axial-longitudinal multipole operators, respectively.

Ref. [13] carried out the first fully consistent *ab initio* calculation of recoil and shape corrections including uncertainty quantification essential for precision searches. Nuclear wave functions were obtained using the NCSM with  $\chi$ EFT interactions [135, 136, 137, 138]. Two Hamiltonians were employed: NNLO<sub>opt</sub> (two-nucleon forces only) and NNLO<sub>sat</sub> (including three-nucleon forces) [139, 140]. Matrix elements were computed in the impulse approximation, with one-body axial and vector operators constructed as in Ref. [141]:

$$\begin{aligned} \hat{L}_{JM_J}^A &= \sum_{j=1}^A i \left( g_A + \frac{\tilde{g}_P}{(2m_N)^2} q^2 \right) \hat{\Sigma}_{JM_J}''(q\vec{r}_j) \tau_j^+, \\ \hat{C}_{JM_J}^A &= \sum_{j=1}^A \frac{iq}{m_N} \left[ g_A \hat{\Omega}'_{JM_J}(q\vec{r}_j) - \frac{1}{2} \frac{\tilde{g}_P}{2m_N} (E_0 + \Delta E_c) \hat{\Sigma}_{JM_J}''(q\vec{r}_j) \right] \tau_j^+, \\ \hat{M}_{JM_J}^V &= \sum_{j=1}^A \frac{-iq}{m_N} \left[ g_V \hat{\Delta}_{JM_J}(q\vec{r}_j) - \frac{1}{2} \mu \hat{\Sigma}'_{JM_J}(q\vec{r}_j) \right] \tau_j^+, \end{aligned} \quad (4.3)$$

with additional electromagnetic contributions from Coulomb energy shift  $\Delta E_c \approx 0.85$  MeV following Refs. [142, 134] and evaluated using Refs. [143, 144], as well as from Coulomb relevant order corrections from Refs. [145, 146]. Translational invariance was ensured by using one-body densities in Jacobi coordinates [147], thus eliminating spurious center-of-mass motion. The NCSM calculations were performed using model spaces up to  $N_{\text{max}} = 12$  and with varying HO parameter  $\hbar\Omega = 16\text{--}24$  MeV to assess convergence. Method and parametric uncertainties from the many-body solver were quantified

by varying model spaces and comparing the two chiral interactions. Uncertainties due to the omission of two-body weak currents were estimated from EFT power counting ( $\epsilon_{\text{EFT}} \lesssim 0.15$ ) and from comparisons with experimental observables such as the  ${}^6\text{Li}$  magnetic moment and  $B(M1)$  transition, and the  ${}^6\text{He}$  half-life [148, 149, 150]. The subleading multipoles and higher-order terms omitted from the nonrelativistic expansion were estimated following the controlled formalism of Ref. [134].

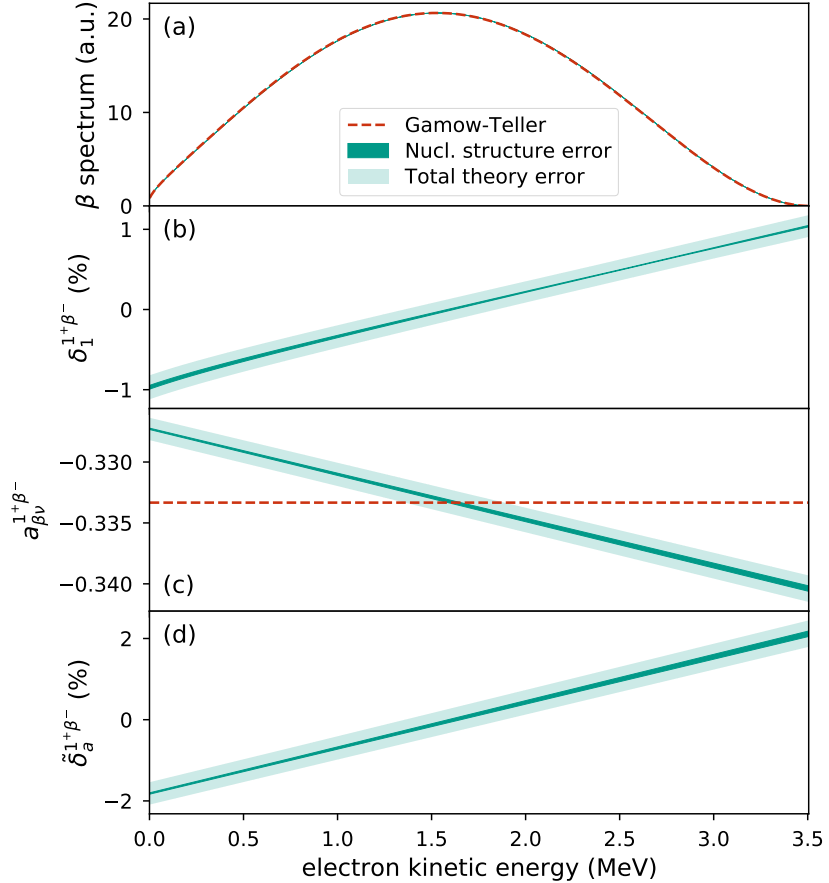


Figure 4.1: (a) Calculated energy dependence of the spectrum of  ${}^6\text{He}$   $\beta$ -decay, in arbitrary units. Dashed line is the pure GT spectrum, while the filled bands include nuclear-structure dependent corrections. (b) The residual nuclear structure correction  $\delta_1$  compared to the pure GT spectrum (Eq. (4.2)). (c) Energy dependence of the angular correlation  $a_{\beta\nu}$ . Dashed line corresponds to the SM value,  $a_{\beta\nu} = -1/3$ . (d) Relative size of the  $\tilde{\delta}_a$  correction from (4.2). The width of the dark filled bands shows the variation with the employed nuclear Hamiltonian and NCSM model space parameters for HO frequency  $\hbar\Omega = 16, 20, 24$  MeV,  $N_{\text{max}} = 8, 10, 12$  (10, 12, 14) using the NNLO<sub>sat</sub> (NNLO<sub>opt</sub>) interaction, using translationally-invariant one-body densities. The width of the light filled band shows the total estimated theory error. Reprinted figure from [13].

The resulted calculations, presented in Fig. 4.1 and summarized in Table 4.1, revealed that nuclear-structure corrections produce measurable modifications to the GT observables. After averaging over the  $\beta$ -energy spectrum, the correction to the angular correlation was found to be  $\langle \tilde{\delta}_a \rangle = -2.54(68) \cdot 10^{-3}$ , which corresponds to a 0.7% modification of the GT angular correlation  $a = -1/3$ . The extracted angular-correlation coefficient from available experimental data [152], after including radiative, atomic, and the newly calculated structure effects, becomes  $a = -0.3331(32)$ , slightly shifted from the naive GT value but consistent with the standard model. Additionally, a nonzero Fierz-like contribution  $\delta_b = -1.52(18) \cdot 10^{-3}$  arises entirely due to nuclear structure effects. These value implies an energy-dependent distortion of the spectrum at the  $10^{-3}$  level, comparable to the target precision of current experiments.

Table 4.1: Calculated nuclear-structure corrections for the  ${}^6\text{He} \rightarrow {}^6\text{Li}$   $\beta$  decay obtained in Ref. [13] using the *ab initio* NCSM with chiral EFT interactions. Quoted NCSM uncertainties include methodological and parametric uncertainties of the many-body solver, as well as contributions from omitted two-body weak currents (EFT truncation), subleading multipoles, and higher-order terms. Angle brackets  $\langle \cdot \rangle$  denote averaging over the  $\beta$ -energy spectrum.

Observable	Symbol	Value	Uncertainty	
Fierz-like term	$\delta_b$	$-1.52 \times 10^{-3}$	$1.8 \times 10^{-4}$	
Angular-correlation correction	$\langle \tilde{\delta}_a \rangle$	$-2.54 \times 10^{-3}$	$6.8 \times 10^{-4}$	
Total extracted angular-correlation	$a$	-0.3331	0.0032	
Multipole Operator	Symbol	Value	Uncertainty	
Longitudinal	$\langle \hat{L}_1^A / i \rangle$	0.464	0.016	
Electric	$\langle \hat{E}_1^A / i \rangle$	0.657	0.023	
Magnetic	$\langle \hat{M}_1^V / iq \rangle$	$-1.36 \times 10^{-3}$	$1.5 \times 10^{-4}$	
Coulomb	$\langle \hat{C}_1^A / iq \rangle$	$-1.39 \times 10^{-4}$	$1.8 \times 10^{-5}$	
Holstein's Form Factor	Symbol	Shell Model [151]	NCSM [13]	Extracted from Exp. [151]
Gamow–Teller	$ c $		2.85(14)	2.75(3)
Weak magnetism	$ b_{\text{WM}} $		66.7(8.3)	69.0(1.0)
Induced tensor	$ d^I $	2.4	7.73(59)	
Induced tensor to GT ratio	$ d^I/(Ac) $	0.12	0.45(4)	2.0(1.5)

The results were also benchmarked against the 1975 calculation by Calaprice [151], which expressed the transition in terms of the Gamow–Teller ( $c$ ), weak magnetism ( $b_{\text{WM}}$ ), and induced tensor ( $d$ ) form factors. The NCSM values for the Gamow–Teller and weak-magnetism form factors,  $c = 2.85(14)$  and  $b_{\text{WM}} = 66.7(8.3)$ , agree well with Calaprice’s values ( $c = 2.75(3)$ ,  $b_{\text{WM}} = 69.0(1.0)$ ) extracted from measurements of half-life and M1 transition, respectively. For the induced tensor component, however, the NCSM result  $d^I \approx 7.73(59)$  is significantly larger than the value obtained in the shell-model calculation reported by Calaprice ( $d^I \approx 2.4$ ). Nonetheless, when expressed as a ratio  $d^I/(Ac) \approx 0.45(4)$ , the NCSM prediction lies closer to the value 2.0(1.5) inferred from the angular-correlation measurements analysis, which assumes all other recoil corrections and other effects are well known (which, of course, is not the case).

A key outcome of these calculations is their quantified theoretical uncertainties, achieved for the first time. The resulting accuracy of order  $10^{-4}$  places future measurements within the discovery window for BSM physics, as illustrated in Fig. 4.2. Experiments observing additional per-mil deviations from these SM predictions would imply nonzero BSM tensor couplings. Furthermore, the indirect dependence of the measured angular correlation on the Fierz term  $b$  transforms its naive quadratic sensitivity to  $\epsilon_T$  into an effective linear one, significantly enhancing experimental reach for tensor interactions within angular correlation measurements. Overall, these NCSM results establish a high-precision Standard Model benchmark for the  ${}^6\text{He} \rightarrow {}^6\text{Li}$  decay.

## 4.2. ${}^6\text{He} \rightarrow {}^6\text{Li}$ beta decay spectrum with QMC

Interference between BSM currents with the  $V - A$  structure of the SM would induce a distinctive dependence in the  $\beta$ -decay spectrum on the ratio of the electron mass to the outgoing electron energy,  $m_e/E_e$ . This term, known as the Fierz interference term [154], is usually denoted by  $b$ . The first constraint on its value  $-0.018 < b < 0.052$  came from direct

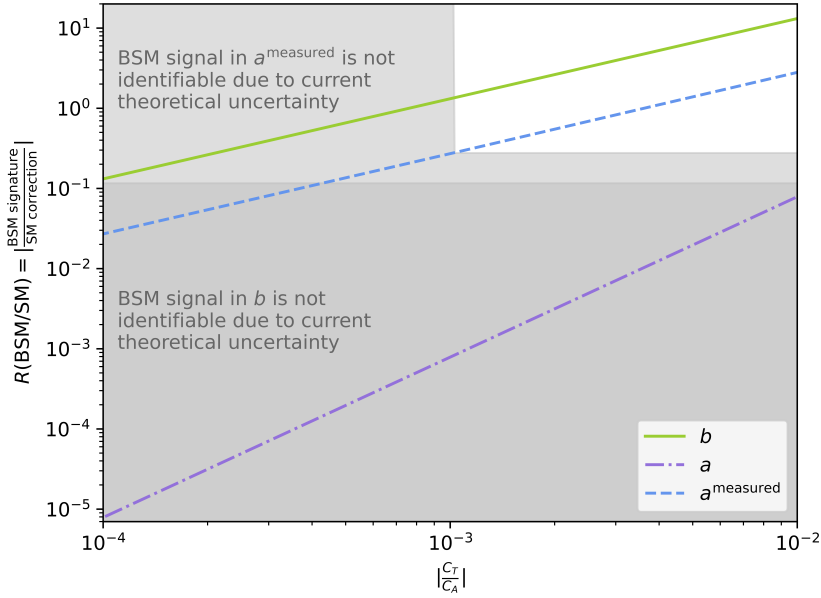


Figure 4.2: Ratio of possible BSM-induced signals to SM nuclear-structure corrections for the  ${}^6\text{He}$   $\beta$  decay [13]. The solid green, dash-dotted purple, and dashed blue lines correspond to the Fierz term  $b$ , angular correlation  $a$ , and experimentally measured  $a^{\text{measured}}$ , respectively. If the ratio is of the order of 1, the corrections should be calculated explicitly. The limit of theoretical uncertainty consequently occurs when the ratio is about the size of the theoretical uncertainty in calculating the SM corrections. The white region indicates where the theoretical uncertainty of the SM corrections (below  $10^{-4}$ ) allows clean separation between SM and BSM effects. In the other domains, separation is limited by theoretical uncertainties. Reprinted figure with permission from [153]. Copyright 2023 by the American Physical Society.

neutron measurements [155, 156], and measurements of super-allowed  $0^+ \rightarrow 0^+$   $\beta$ -decays constrain the Fierz interference term induced by scalar currents to  $b < 3.3 \cdot 10^{-3}$  at the 90% confidence level [96]. Measuring purely GT  $\beta$ -decay spectra can place constraints on tensor and pseudoscalar contributions to  $b$ . On-going measurements of the purely GT  ${}^6\text{He}$   $\beta$ -decay spectrum [157, 158, 159] are aiming for  $a < 0.1\%$  precision. This would provide a rather clear signature of  $b$ , as the shape of the spectrum for this specific decay would be [154],

$$\frac{d\Gamma}{dE_e} = \frac{d\Gamma_0}{dE_e} \left[ 1 + b \frac{m_e}{E_e} \right], \quad (4.4)$$

where  $d\Gamma_0/dE_e$  is the SM spectrum. This level of precision would allow for constraints on new physics up to the level of 10 TeV [160]; however, this simple picture in Eq. 4.4 is complicated by the fact that it is also possible to generate a non-zero value of  $b$  by accounting for recoil corrections that come from the small momentum transferred to the nucleus in the decay [161, 162]. Thus, in order to connect with on-going experimental analyses, it is important to have equally precise theoretical calculations.

The  ${}^6\text{He}$   $\beta$  decay can be written down in terms of the standard multipole decomposition [163] as follows,

$$\begin{aligned} d\Gamma = & (2\pi)\delta(E_i - E_f - E_\nu - E_e)G_F^2 V_{ud}^2 \frac{4\pi}{2J_i + 1} \\ & \left[ (1 + \hat{\mathbf{k}}_\nu \cdot \hat{\mathbf{k}}_e) |C_1(q)|^2 + (1 - \hat{\mathbf{k}}_\nu \cdot \hat{\mathbf{k}}_e + 2(\hat{\mathbf{k}}_\nu \cdot \hat{\mathbf{q}})(\hat{\mathbf{q}} \cdot \hat{\mathbf{k}}_e)) |L_1(q; A)|^2 \right. \\ & \left. - \hat{\mathbf{q}} \cdot (\hat{\mathbf{k}}_\nu + \hat{\mathbf{k}}_e) 2\text{Re}(L_1(q; A)C_1^*(q; a)) \right] + \left[ (1 - (\hat{\mathbf{k}}_\nu \cdot \hat{\mathbf{q}})(\hat{\mathbf{q}} \cdot \hat{\mathbf{k}}_e)) (|M_1(q; V)|^2 \right. \\ & \left. + |E_1(q; A)|^2) + \hat{\mathbf{q}} \cdot (\hat{\mathbf{k}}_\nu - \hat{\mathbf{k}}_e) 2\text{Re}(M_1(q; V)E_1^*(q; A)) \right], \end{aligned} \quad (4.5)$$

where the value  $V_{ud} = 0.97373(31)$  [96] was adopted,  $G_F$  is the Fermi coupling constant,  $\mathbf{q}$  is the momentum transferred to the nucleus,  $\mathbf{k}_{e(\nu)}$  and  $E_{e(\nu)}$  indicate the electron (neutrino) momentum and energy, respectively,  $E_{i(f)}$  is the energy

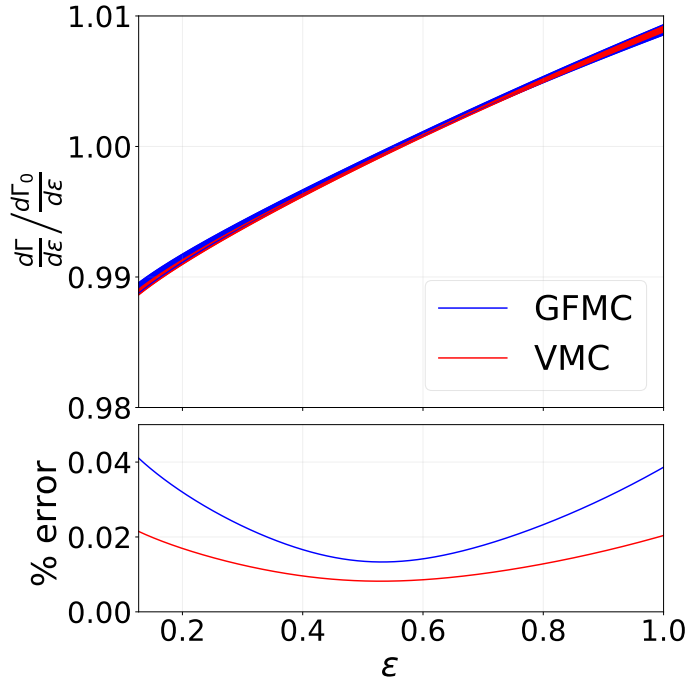


Figure 4.3: The Standard Model (SM) spectrum for  ${}^6\text{He}$   $\beta$  decay relative to the zero recoil approximation computed with GFMC (blue band), compared to results including BSM tensor (red band) and pseudoscalar (green band) contributions. The width of the band represents variations in the model Hamiltonian. Figure reprinted with permission from Ref. [15].

of the initial (final) state nucleus, and  $J_i$  is the angular momentum of the initial state. The four multipoles entering the rate can be recast as matrix elements which one can compute using QMC techniques [164],

$$C_1(q; A) = \frac{i}{\sqrt{4\pi}} \langle {}^6\text{Li}, 10 | \rho_+^\dagger(q\hat{\mathbf{z}}; A) | {}^6\text{He}, 00 \rangle \quad (4.6)$$

$$L_1(q; A) = \frac{i}{\sqrt{4\pi}} \langle {}^6\text{Li}, 10 | \hat{\mathbf{z}} \cdot \mathbf{j}_+^\dagger(q\hat{\mathbf{z}}; A) | {}^6\text{He}, 00 \rangle \quad (4.7)$$

$$E_1(q; A) = -\frac{i}{\sqrt{2\pi}} \langle {}^6\text{Li}, 10 | \hat{\mathbf{z}} \cdot \mathbf{j}_+^\dagger(q\hat{\mathbf{x}}; A) | {}^6\text{He}, 00 \rangle \quad (4.8)$$

$$M_1(q; V) = -\frac{1}{\sqrt{2\pi}} \langle {}^6\text{Li}, 10 | \hat{\mathbf{y}} \cdot \mathbf{j}_+^\dagger(q\hat{\mathbf{x}}; V) | {}^6\text{He}, 00 \rangle, \quad (4.9)$$

where  $\mathbf{j}_+^\dagger = \mathbf{j}_x^\dagger + i\mathbf{j}_y^\dagger$  with the subscripts  $x$  and  $y$  indicating isospin components— and  $\rho_+^\dagger$  is similarly defined. The operators  $\rho$  and  $\mathbf{j}$  are the charge changing weak charge and current operators, and the letters  $A$  and  $V$  indicate either the axial or vector component of the current. The bras and kets denote the initial and final state nuclei, as well as their  $JT$  quantum numbers. Because the  $Q$ -value of the decay,  $Q \approx 3.5$  MeV, limits the momentum transfer to the nucleus  $q$  such that  $q/m_\pi = qr_\pi \lesssim 0.03$ , it was noted in Ref. [15] that one can perform an expansion of the multipoles in  $qr_\pi$ . Noting also that the multipoles are either purely even or odd polynomials in  $q$ , one obtains the following expressions,

$$C_1(q; A) = -i \frac{qr_\pi}{3} \left( C_1^{(1)}(A) - \frac{(qr_\pi)^2}{10} C_1^{(3)}(A) + \mathcal{O}[(qr_\pi)^4] \right), \quad (4.10)$$

$$L_1(q; A) = -i \frac{1}{3} \left( L_1^{(0)}(A) - \frac{(qr_\pi)^2}{10} L_1^{(2)}(A) + \mathcal{O}[(qr_\pi)^4] \right), \quad (4.11)$$

$$M_1(q; V) = -i \frac{qr_\pi}{3} \left( M_1^{(1)}(V) - \frac{(qr_\pi)^2}{10} M_1^{(3)}(V) + \mathcal{O}[(qr_\pi)^4] \right), \quad (4.12)$$

$$E_1(q; A) = -i \frac{1}{3} \left( E_1^{(0)}(A) - \frac{(qr_\pi)^2}{10} E_1^{(2)}(A) + \mathcal{O}[(qr_\pi)^4] \right). \quad (4.13)$$

Expanding in this way, combined with using current operators that admit an expansion in  $m_\pi/\Lambda_\chi$ , means that one can obtain a spectrum retaining terms up to the desired precision  $q/\Lambda_\chi$ . In the case of  ${}^6\text{He}$   $\beta$  decay, one needs only up to the quadratic term in  $q$  to achieve a below 0.1% accuracy for a given model. Working to this order, the expression of the spectrum in terms of the multipole coefficients is,

$$\begin{aligned}
\frac{d\Gamma}{d\varepsilon} = & (1 + \Delta_R^V)(1 + \delta_R(Z, \varepsilon)) \frac{G_F^2 W_0^5 V_{ud}^2}{2\pi^3} \sqrt{1 - \frac{\mu_e^2}{\varepsilon^2}} \varepsilon^2 (1 - \varepsilon)^2 F_0(Z, \varepsilon) L_0(Z, \varepsilon) S(Z, \varepsilon) R_N(\varepsilon) \\
& \frac{4\pi}{2J_i + 1} \frac{1}{9} \left\{ 3 \left| L_1^{(0)} \right|^2 \left[ 1 + \alpha Z W_0 R \left( \frac{2}{35} - \frac{233}{630} \frac{\alpha Z}{W_0 R} - \frac{1}{70} \frac{\mu_e^2}{\varepsilon} - \frac{4}{7} \varepsilon \right) \right] \right. \\
& + 2 W_0 r_\pi \left[ \left( 1 - 2\varepsilon + \frac{\mu_e^2}{\varepsilon} \right) \text{Re}(E_1^{(0)} M_1^{(1)*}) - \left( 1 - \frac{\mu_e^2}{\varepsilon} \right) \text{Re}(L_1^{(0)} C_1^{(1)*}) \right] \\
& + \frac{(W_0 r_\pi)^2}{3} \left[ \left( 3 - 4\varepsilon(1 - \varepsilon) - \mu_e^2 \frac{2 + \varepsilon}{\varepsilon} \right) |C_1^{(1)}|^2 - \frac{3}{5} \left( 1 - \frac{\mu_e^2}{\varepsilon} (2 - \varepsilon) \right) \text{Re} \left( L_1^{(0)} L_1^{(2)*} \right) \right. \\
& \left. \left. + \left( 3 - 10\varepsilon(1 - \varepsilon) + \mu_e^2 \frac{4 - 7\varepsilon}{\varepsilon} \right) \left( |M_1^{(1)}|^2 - \frac{1}{5} \text{Re} \left( E_1^{(0)} E_1^{(2)*} \right) \right) \right] \right. \\
& \left. - \frac{4}{7} \frac{\alpha Z W_0 r_\pi^2}{R} (1 - \varepsilon) \left( \frac{E_1^{(0)} E_1^{(2)}}{2} - L_1^{(0)} L_1^{(2)} \right) \right\}, \tag{4.14}
\end{aligned}$$

where the scaled variables  $E_e = W_0 \varepsilon$  and  $m_e = W_0 \mu_e$  have been introduced, with  $W_0 = M_i - M_f = 4.016$  MeV in the case of the  ${}^6\text{He} \rightarrow {}^6\text{Li}$  transition.  $M_i$  and  $M_f$  are the masses of the initial and final state nuclei. The effects of nuclear recoil are retained to leading order in  $W_0/M_f$ , and nuclear recoil makes it so that the electron endpoint energy shifts from  $E_e = W_0$  to  $E_e = W_0 - \frac{W_0^2 - m_e^2}{2M_f}$ . The above spectrum has also incorporated Coulomb corrections, which depend on the nuclear charge  $Z$ , the fine structure constant alpha  $\alpha$ , and the nuclear radius  $R$ . There are additionally corrections from the distortion of the outgoing electron wave function  $F_0(Z, \varepsilon) L_0(Z, \varepsilon)$ , higher order electromagnetic corrections  $\Delta_R^V$  and  $\delta_R$ , the effects of atomic shielding  $S$ , and recoil kinematic corrections  $R_N$ , which are defined in Ref. [15]

While the resultant spectrum would naively give the required precision to connect with experiment, one has not taken into account the effects of using different models on the uncertainty. The goal of Ref. [15] was to perform the calculation with various models of the nuclear interaction in order to estimate the model dependence. In particular, four models the Norfolk two- and three-nucleon interactions [70, 71, 123] were employed in the computation of the nuclear matrix elements. The upper panel of Fig. 4.3 shows the distortion of the  $\beta$  decay spectrum relative to  $d\Gamma_0/d\varepsilon$  as a function of  $\varepsilon$  for VMC (red) and GFMC (blue). The spectrum receives distortions of up to  $\approx 1\%$ , with the dominant correction coming from the  $M_1$  multipole. Because it was found that the isospin symmetry breaking between  $M_1$  obtained from  ${}^6\text{He}$   $\beta$  decay and the electromagnetic decay of  ${}^6\text{Li}(1^+; 0)$  to the ground state was smaller than the experimental uncertainty on the latter, the experimental value was adopted to further constrain any potential model dependence. The dominant source of uncertainty on the spectrum comes from the model dependence on the theoretical values of  $L_1^{(2)}$  and  $E_1^{(2)}$ , and the overall spectrum uncertainty seen in the lower panel of Fig. 4.3 is below the 0.1% goal needed to compare with experiment. Finally, it was found that the SM Fierz term induced by recoil is  $\delta_b = -1.47(3) \times 10^{-3}$  in the GFMC calculation, which agreed with the previous *ab initio* evaluation discussed in Section 4.1, while also greatly reducing the uncertainty because of the explicit inclusion of two-body currents.

Because of the level of precision obtained in the theoretical calculation, it was possible to incorporate BSM physics effects to see the effects on the spectrum. Including leading order tensor and pseudoscalar currents indicated that experiments would have sensitive to tensor contributions not currently excluded by other analyses. Further, it was shown

that in a minimal extension to the SM with one heavier sterile neutron with mass 1 MeV, a characteristic kink would be present in the spectrum. Thus, the GFMC prediction can help to place further constraints on BSM physics scenarios.

### 4.3. ${}^8\text{Li} \rightarrow {}^8\text{Be}$ and ${}^8\text{B} \rightarrow {}^8\text{Be}$ beta decays corrections with SA-NCSM

In the recent years, a series of high-precision angular correlations measurements have been performed using  ${}^8\text{Li}$  and  ${}^8\text{B}$  beta decays to set stringent constraints on the BSM tensor currents in the weak interactions [165, 166, 167, 16]. In these experiments, the largest source of the systematic errors on the  $\beta$ - $\nu$  correlation parameter  $a$  stem from the uncertainty in the recoil-order terms. In particular, four recoil-order terms have been determined by the simulations to contribute most to the systematic error budget, namely, the second-forbidden axial vectors ( $j_2$  and  $j_3$ ), induced tensor ( $d^I$ ), and weak magnetism ( $b_{\text{WM}}$ ), with  $j_2$  and  $j_3$  being especially large. The operators of these recoil-order terms are given in the impulse approximation (IA) by Holstein as [129]<sup>5</sup>:

$$\begin{aligned} j_K(q^2) &= -(-)^{(J'-J)} \frac{2}{3} \frac{g_A(q^2)}{\sqrt{2J+1}} \frac{(Am_Nc^2)^2}{(\hbar c)^2} \langle J' | \sum_{i=1}^A \tau_i^\pm [Q_i \times \sigma_i]^K | J \rangle, \text{ with } K = 2, 3, \\ d^I(q^2) &= (-)^{(J'-J)} A \frac{g_A(q^2)}{\sqrt{2J+1}} \langle J' | \sum_{i=1}^A \tau_i^\pm \sqrt{2} [L_i \times \sigma_i]^1 | J \rangle, \\ b_{\text{WM}}(q^2) &= A \frac{(-)^{(J'-J)}}{\sqrt{2J+1}} \left[ g_M(q^2) \langle J' | \sum_{i=1}^A \tau_i^\pm \sigma_i | J \rangle + g_V(q^2) \langle J' | \sum_{i=1}^A \tau_i^\pm L_i | J \rangle \right], \end{aligned} \quad (4.15)$$

where  $g_V(0) = 1$ ,  $g_A(0) \approx 1.27$  and  $g_M(0) \approx 4.70$  are the vector, axial and weak magnetism coupling constants,  $A$  is the mass number and  $J(J')$  is the total angular momentum of the initial (final) nucleus. The  $\tau_i/2$ ,  $\sigma_i/2$ ,  $Q_i = \sqrt{16\pi/5}r_i^2Y_{2\mu}(\hat{r}_i)$ , and  $L_i$  are the isospin, intrinsic spin, quadrupole moment and angular momentum operators, respectively, of the  $i^{\text{th}}$  particle. The matrix elements in Eq. (4.15) are computed translationally invariant in the SA-NCSM. These recoil-order form factors are usually reported as the ratios  $j_{2,3}/A^2c$ ,  $d/Ac$ , and  $b/Ac$  that enter into the expression of the  $\beta$ -decay rate for nuclei undergoing delayed  $\alpha$ -particle emission [129, 165, 168, 166], with

$$c(q^2) = (-)^{(J'-J)} \frac{g_A(q^2)}{\sqrt{2J+1}} \langle J' | \sum_{i=1}^A \tau_i^\pm \sigma_i | J \rangle = (-)^{(J'-J)} \frac{g_A(q^2)}{\sqrt{2J+1}} M_{GT}, \quad (4.16)$$

where  $M_{GT}$  is the conventional GT matrix element and  $A$  is the nuclear mass number. For the calculations of these recoil-order terms, we adopted various chiral nucleon-nucleon (NN) potentials without renormalization in nuclear medium, namely, N3LO-EM [27], NNLOopt [169], and NNLOsat [140], and in addition, the soft JISP16 phase-equivalent NN interaction [170].

${}^8\text{Li}$  and  ${}^8\text{B}$   $\beta$  decays predominantly proceeds via a nearly pure [171] Gamow-Teller transition from the  $J^\pi = 2^+$ , isospin  $T = 1$   ${}^8\text{B}$  ground state to the broad  $J^\pi = 2^+$ ,  $T = 0$  resonance in  ${}^8\text{Be}$  at 3 MeV which immediately breaks into two  $\alpha$  particles (Fig. 4.4). Since this transition to the lowest  $2^+$  state in  ${}^8\text{Be}$  accounts for most of the statistics in the experiment, it is vital to obtain the corresponding recoil-order terms with high precision. Remarkably, there appears to be a strong correlation between  $j_{2,3}/A^2c$  and the ground state quadrupole moments of  ${}^8\text{Li}$  and  ${}^8\text{B}$  based on calculations across several

<sup>5</sup>Note that in Ref. [129] the convention of angular momentum couplings is such that the final state's angular momentum is coupled to the spherical tensor to yield the initial state's angular momentum. Here, we couple the initial state to the spherical tensor to yield the final state. Hence, the expressions in Eq. (4.15) differ from Ref. [129] by a factor of  $(-1)^{(J'-J)}$ .

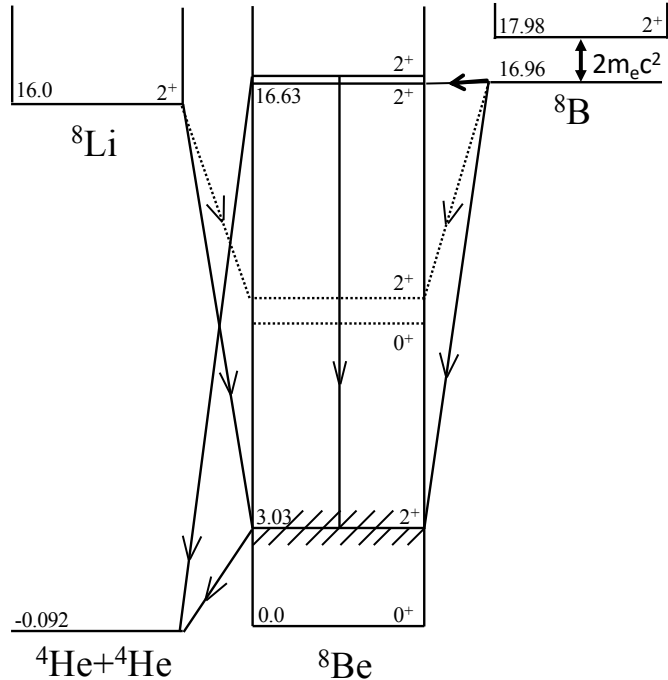


Figure 4.4: Level diagram of the  ${}^8\text{Li}$  and  ${}^8\text{B}$   $\beta$  decays to  ${}^8\text{Be}$ . All of  ${}^8\text{Be}$  states are above the  $\alpha + \alpha$  separation threshold. The dotted levels correspond to the states that have not been directly observed experimentally, but calculated in the SA-NCSM and proposed in earlier studies (see text for details).

NN interactions,  $N_{\max}$  and  $\hbar\Omega$  parameters. In Fig. 4.5, each marker corresponds to one calculation with a specific model space and harmonic oscillator spacing  $\hbar\Omega$  using a NN potential mentioned above. The values of  $j_2/A^2c$  and  $j_3/A^2c$  for the transition to the  ${}^8\text{Be}$   $2_1^+$  state were predicted by performing a linear regression and using the  ${}^8\text{Li}$  and  ${}^8\text{B}$  experimentally measured ground state quadrupole moments from Refs. [54, 172]. To accommodate large model spaces, clustering, and collectivity, the symmetry-adapted basis of SA-NCSM was used to select the model spaces of about one-third of the points in Fig. 4.5 following the prescription of Ref. [63]. The total uncertainties on the predictions from the correlation plots arise from two parts: the  ${}^8\text{Li}$  and  ${}^8\text{B}$  ground state  $Q(2^+)$  experimental uncertainty intersecting with the linear regression slope and the regression uncertainty from the Student's t-distribution at 95% confidence level (depicted as dark and light horizontal bands, respectively, in Fig. 4.5). The linear dependence between  $j_{2,3}/A^2c$  and  $Q(2_{g.s.}^+)$  persists regardless of errors that arise from many-body truncation (including SA model space choices), use of various NN interactions that have different regulators and momentum cutoffs, and two-body currents in operators for  $Q(2_{g.s.}^+)$  [173] and axial-vector beta transitions [113, 174, 65]. Therefore, thanks to the diverse range of inputs, the regression uncertainty contains the effects of the many-body truncation and these additional corrections making our predictions parameters and model (interaction) independent. We note that correlations between different observables in *ab initio* calculations have also been used in other works to reduce uncertainties on predictions for slowly converging observables (see, *e.g.*, Refs [175, 176, 177]).

The predictions for  $j_2/A^2c$  and  $j_3/A^2c$  recoil-order terms, as well as the weak magnetism  $b_{\text{WM}}/Ac$  and induced tensor  $d^I/Ac$  terms, for the lowest four  $2^+$  states in  ${}^8\text{Be}$  calculated from SA-NCSM, are summarized in Table 4.2. The  $d/Ac$  prediction for  $2_1^+$  is based on a correlation similar to the one for  $j_{2,3}/A^2c$  (Fig. 4.6). For  $b_{\text{WM}}/Ac$  to all states in  ${}^8\text{Be}$  and for the other recoil-order terms to higher-lying  $2^+$  states, the values were calculated using NNLO<sub>opt</sub> and JISP16 with uncertainties from varying  $\hbar\Omega$  from 20 MeV by 5 MeV and model-space sizes from  $N_{\max}=6\text{--}12$ . In addition to being necessary for the current measurements of BSM terms in the weak interaction,  $b_{\text{WM}}/Ac$  predictions are of interest

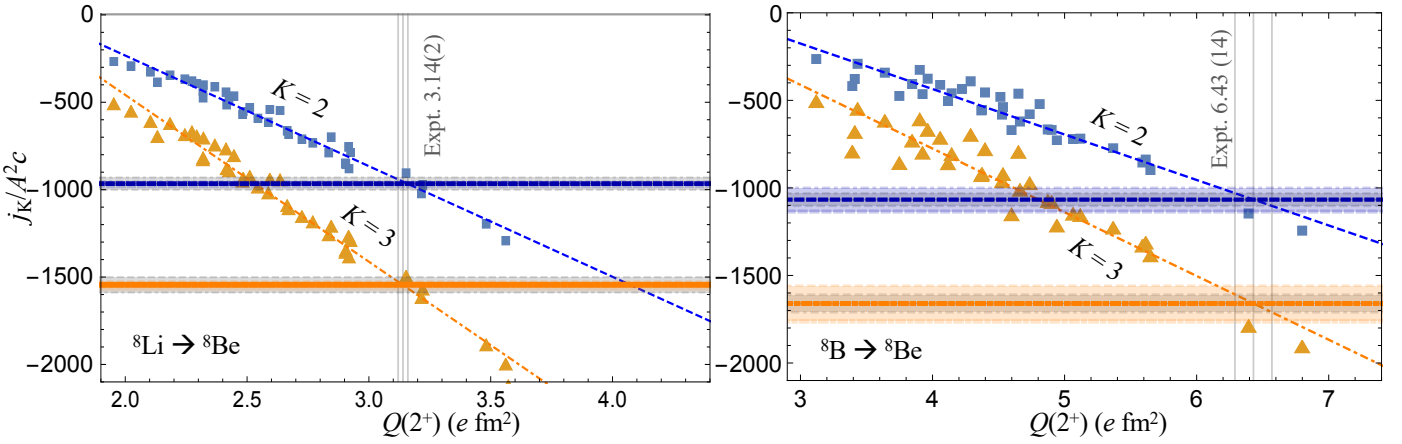


Figure 4.5: Calculated  $j_2/A^2c$  and  $j_3/A^2c$  from SA-NCSM (squares and triangles, respectively) and their predicted values (upper and lower horizontal lines, respectively) for the  ${}^8\text{Li}$   $\beta$  decay (left) and  ${}^8\text{B}$   $\beta$  decay (right) to  $2_1^+$  in  ${}^8\text{Be}$  vs. the calculated quadrupole moments [ $Q(2^+)$ ] of the initial nuclei. Calculations use the NNLO<sub>opt</sub>, NNLO<sub>sat</sub> and N<sup>3</sup>LO chiral potentials, and the JISP16 NN, in  $N_{\text{max}}=6\text{--}12$  model spaces. The vertical gray lines show the experimental values of  ${}^8\text{Li}$  and  ${}^8\text{B}$   $Q(2^+)$  with uncertainties [54, 172]. The darker horizontal bands are uncertainties solely from the  $Q(2^+)$  experimental uncertainty while the lighter bands also include the linear regression uncertainty. Figures adapted from Refs. [14, 16] with permissions.

to experiments that test the CVC hypothesis and  $d^I/Ac$  is of importance to determining the existence of second-class currents [178].

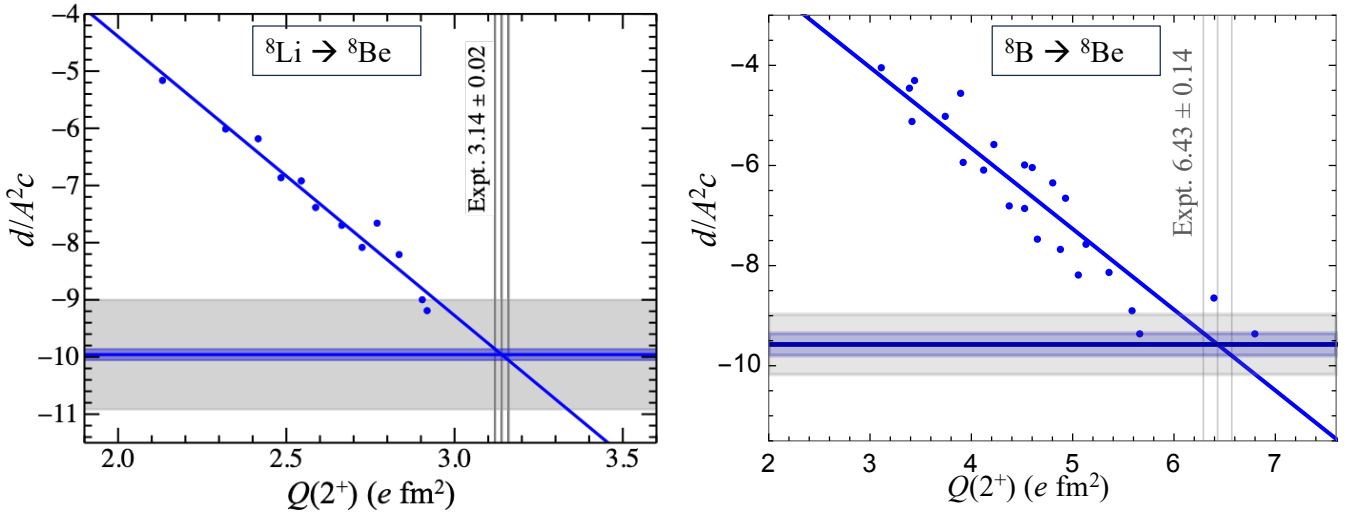


Figure 4.6: Calculated  $d/A^2c$  from SA-NCSM (blue dots) and their predicted values for the  ${}^8\text{Li}$   $\beta$  decay (left) and  ${}^8\text{B}$   $\beta$  decay (right) to  $2_1^+$  in  ${}^8\text{Be}$  vs. the calculated quadrupole moments [ $Q(2^+)$ ] of the initial nuclei. The vertical gray lines show the experimental values of  ${}^8\text{Li}$  and  ${}^8\text{B}$   $Q(2^+)$  with uncertainties [54, 172]. The horizontal blue bands are uncertainties solely from the  $Q(2^+)$  experimental uncertainty while the gray bands also include the linear regression uncertainty.

Earlier experimentally deduced values for these recoil-order terms were reported in Ref. [179] by Sumikama *et al.* These values, namely  $j_2/A^2c = -490 \pm 70$ ,  $j_3/A^2c = -980 \pm 280$ ,  $d^I/Ac = 5.5 \pm 1.7$ , and  $b_{\text{WM}}/Ac = 7.5 \pm 0.2$ , are different from our theoretical predictions, and were derived through a comprehensive fit to  $\beta$ -spin alignment data [179] and  $\beta$ - $\alpha$  angular correlation measurements [180] from  ${}^8\text{Li}$  and  ${}^8\text{B}$  beta decays. Due to the limited magnitude of higher-order effects and the relatively large statistical uncertainties, the recoil-order terms  $j_2/A^2c$ ,  $j_3/A^2c$  and  $d^I/Ac$  were assumed in Ref. [179] to be independent of the  ${}^8\text{Be}$  excitation energy. Consequently, the reported values were averaged over the entire beta

Table 4.2: The recoil-order terms from SA-NCSM. Results for the  $2_1^+$   $j_{2,3}/A^2c$  and  $d/Ac$  are based on the correlation to  $Q(2_{\text{g.s.}}^+)$ ; all other calculations use NNLO<sub>opt</sub> and JISP16 and have error bars from variations in  $\hbar\Omega$  by 5 MeV and in model-space sizes up to  $N_{\text{max}}=12$ . Table adapted from Ref. [16] with permission.

		$j_2/A^2c$	$j_3/A^2c$	$d^I/Ac$	$b_{\text{WM}}/Ac$
${}^8\text{Li} \rightarrow {}^8\text{Be}$	$2_1^+$	$-966 \pm 36$	$-1546 \pm 44$	$10.0 \pm 1.0$	$6.0 \pm 0.4$
	$2_2^+$ (intruder)	$-10 \pm 10$	$-80 \pm 30$	$-0.5 \pm 0.5$	$3.7 \pm 0.4$
	$2_3^+$ (doublet 1)	$12 \pm 5$	$-60 \pm 15$	$0.3 \pm 0.2$	$3.8 \pm 0.2$
	$2_4^+$ (doublet 2)	$11 \pm 3$	$-65 \pm 11$	$0.2 \pm 0.2$	$3.8 \pm 0.2$
${}^8\text{B} \rightarrow {}^8\text{Be}$	$2_1^+$	$-1067 \pm 68$	$-1660 \pm 102$	$9.6 \pm 0.6$	$6.1 \pm 0.5$
	$2_2^+$ (intruder)	$10 \pm 45$	$-41 \pm 75$	$-0.5 \pm 0.8$	$3.7 \pm 0.4$
	$2_3^+$ (doublet 1)	$8 \pm 4$	$-53 \pm 20$	$0.1 \pm 0.1$	$3.8 \pm 0.2$
	$2_4^+$ (doublet 2)	$7 \pm 5$	$-70 \pm 13$	$0.2 \pm 0.1$	$3.8 \pm 0.2$

decay spectrum. Conversely, the SA-NCSM wavefunctions are computed for specific states; therefore, the predictions in Table 4.2 correspond solely to the each of the  $2^+$  final states, in the  ${}^8\text{Be}$  spectrum. The SA-NCSM calculations indicate significant differences in the recoil-order terms between the lowest  $2_1^+$  state and higher-lying states, notably for the  $j_K/A^2c$  terms, where the values differ by nearly two orders of magnitude (see Table 4.2). Averaging of the calculated recoil-order terms over the entire  $\beta$  spectrum would likely yield values similar to the ones obtained by Sumikama *et al.* Accordingly, the latest angular-correlation experiment described in Refs. [166] and [16] minimize sensitivity to higher-lying states by restricting the analysis to decays associated primarily with the lowest  $2_1^+$  state in  ${}^8\text{Be}$  for which the calculated recoil-order terms are well constrained.

Since both  $j_2/A^2c$  and  $j_3/A^2c$  for the  ${}^8\text{Be}$  lowest  $2_1^+$  state are strongly correlated with the  ${}^8\text{Li}$  and  ${}^8\text{B}$  g.s. quadrupole moments (Fig. 4.5), it is expected that there is a strong correlation between  $j_2$  and  $j_3$ . Indeed, the calculated  $j_2/A^2c$  vs.  $j_3/A^2c$  for all four interactions under consideration follow an almost perfect linear trendline (Fig. 4.7). Notably, the experimentally deduced values of  $j_2/A^2c$  vs.  $j_3/A^2c$  from Sumikama *et al.* [179], which have been determined over the whole range of the  $\beta$  energy spectrum, align remarkably well with the calculated correlation. In other words the ratio  $j_3/j_2$  from experiment agrees with the ratio from all the calculations.

The comprehensive analysis of recoil-order terms in the  $\beta$  decays of  ${}^8\text{Li}$  and  ${}^8\text{B}$ , supported by SA-NCSM calculations across various nuclear interactions, reveals robust correlations that are largely independent of the chosen models and parameters. These correlations between the recoil-order form factors and the ground state quadrupole moments enhance the precision of theoretical predictions essential for constraining BSM weak tensor currents. The consistency between calculated and experimental ratios of  $j_2/j_3$  recoil-order terms underscores the reliability of the current theoretical framework and its potential to refine the interpretation of  $\beta$ -decay measurements in the search for new physics.

## 5. Summary and outlook

Recent advances in *ab initio* nuclear many-body theories have significantly enhanced our understanding of nuclear  $\beta$  decays, especially in the context of probing BSM physics. State-of-the-art many-body methods, such as NCSM, SA-NCSM and QMC, now enable precise calculations of radiative and recoil-order corrections with quantified uncertainties. These developments are vital for interpreting high-precision experimental data and for extracting fundamental parameters

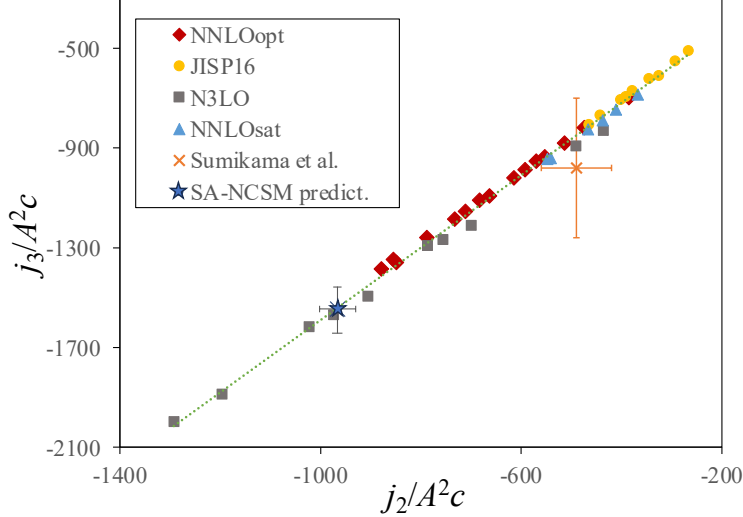


Figure 4.7: Calculated  ${}^8\text{Li}$  beta decay  $j_3/A^2c$  vs.  $j_2/A^2c$  values to the lowest  $2^+$  state in  ${}^8\text{Be}$  with  $\text{NNLO}_{\text{opt}}$ ,  $\text{NNLO}_{\text{sat}}$ ,  $\text{N3LO-EM}$  and  $\text{JISP16}$  interactions for the same model spaces as in Fig. 4.5  ${}^8\text{Li} \rightarrow {}^8\text{Be}$  plot, along with the values from Sumikama *et al.* [179] (orange cross) and the SA-NCSM prediction (blue star) from Table 4.2. The linear fit (dotted green line) is added to guide the eye. Figure adapted from Ref. [14] Supplemental Material with permissions.

like  $V_{ud}$  with unparalleled accuracy.

The integration of EFT frameworks with *ab initio* calculations has provided a robust theoretical foundation for evaluating structure-dependent radiative corrections. *Ab initio* calculations of radiative corrections, such as the  $\delta_{NS}$  term in superallowed  $\beta$  decays of  ${}^{10}\text{C} \rightarrow {}^{10}\text{B}$  and  ${}^{14}\text{O} \rightarrow {}^{14}\text{C}$  have achieved unprecedented precision. These results have significantly reduced theoretical uncertainties to the order of  $10^{-4}$ . This level of accuracy enables current and future experiments to probe BSM physics with enhanced sensitivity, as even small deviations could indicate new interactions or particles. Experiments observing deviations beyond these refined predictions could potentially reveal new physics at energy scales up to 10 TeV.

Similarly, advances in *ab initio* many-body calculations of recoil-order terms have played a crucial role in refining the limits on BSM weak interaction currents. High-precision predictions of recoil corrections for  ${}^6\text{He}$ ,  ${}^8\text{Li}$  and  ${}^8\text{B}$   $\beta$  decays have helped improve the experimental bounds on possible non-SM contributions. These calculations quantify uncertainties arising from many-body models and underlying NN interactions leading to more reliable interpretations of experimental data. As a result, they have tightened the constraints on exotic tensor couplings in the weak interaction, further restricting the level of new physics discovery.

In future studies, several key directions are poised to further advance the field:

- **Enhanced Many-body Precision:** Performing larger many-body calculations and incorporating more *ab initio* methods can reduce uncertainties in decay corrections. In cases where possible, correlations with known observables can help further reduce uncertainties on theory predictions.
- **Development of New NN Interactions:** Refinement of NN interactions and the incorporation of non-nucleonic degrees of freedom can improve the theoretical precision of *ab initio* models. Developing methods to explicitly include non-nucleonic intermediate states could address current limitations.
- **Broader Range of Nuclei:** Extending *ab initio* calculations to a wider range of nuclei will broaden the scope of

BSM searches. Experimental measurements have already been done for heavier nuclei such as  $^{22}\text{Na}$  [181],  $^{23}\text{Ne}$  [182, 183] and  $^{32}\text{Ar}$  [184], with more planned [5]. Performing theoretical calculations for these nuclei with quantified uncertainties will be vital for reducing distinguishing between BSM physics and nuclear physics effects.

- **Additional Decay Modes:** Unique forbidden  $\beta$  decays offer complementary sensitivity to BSM physics relative to allowed decays, with enhanced reach to exotic weak currents (including right-handed components inaccessible in allowed spectra), and to light new physics that modify low-energy spectra, opening up a new regime of BSM physics within precision  $\beta$ -decay searches [185, 153, 186]. With multiple experimental programs now targeting such decays [132, 187, 188], a key theoretical priority is to extend *ab initio* calculations to forbidden spectra with consistent recoil, radiative, and Coulomb corrections and quantified uncertainties. NCSM calculations of the unique first forbidden decay of  $^{16}\text{N}$ , including recoil-order and Coulomb corrections, have recently been completed [189], which will provide a benchmark in this direction and a template for similar studies in heavier systems.
- **Synergy with Experiments:** As experimental precision in  $\beta$  decay measurements continues to improve, with the aim of reaching sub-per-mil accuracy, parallel progress in theoretical predictions is essential. Close collaboration between theorists and experimentalists will be vital for interpreting results and constraining or discovering BSM physics. [5, 190].
- **Complementarity with High-Energy Searches:** Nuclear  $\beta$  decay studies offer a complementary approach to collider experiments, probing energy scales beyond direct reach. Integrating findings from low-energy precision measurements with collider data will provide a comprehensive strategy for uncovering new physics.

The input that *ab initio* nuclear theory has provided to high-precision experiments is rapidly advancing our capacity to test the Standard Model and explore potential new physics. Continued efforts in theoretical developments, coupled with innovative experimental techniques, promise to keep nuclear  $\beta$  decays at the forefront of fundamental physics research in the coming decades.

## Acknowledgments

The work of CYS is supported in part by the U.S. Department of Energy (DOE), Office of Science, Office of Nuclear Physics, under award DE-FG02-97ER41014, by the FRIB Theory Alliance award DE-SC0013617, by the DOE Topical Collaboration "Nuclear Theory for New Physics", award No. DE-SC0023663, and by University of Tennessee, Knoxville. The work of AGM is supported in part by the Hebrew University of Jerusalem through the Dalia and Dan Maydan Post-Doctoral Fellowship. The work of GBK is supported by Los Alamos National Laboratory's Laboratory Directed Research and Development program under project 20240742PRD1 (G. B. K.). The work of GHS is supported by the U.S. Department of Energy, Office of Science, Office of Nuclear Physics, under the FRIB Theory Alliance award DE-SC0013617. This work benefited from high performance computational resources provided by the National Energy Research Scientific Computing Center (NERSC), a U.S. Department of Energy Office of Science User Facility at Lawrence Berkeley National Laboratory operated under Contract No. DE-AC02-05CH11231, as well as the Frontera computing project at the Texas Advanced Computing Center. Frontera is made possible by National Science Foundation award OAC-1818253.

## Author's contributions (*optional section*)

Detailing here the contributions of the authors of the review.

## References

- [1] V. Cirigliano, S. Gardner, B. Holstein, Beta Decays and Non-Standard Interactions in the LHC Era, *Prog. Part. Nucl. Phys.* 71 (2013) 93–118. [doi:10.1016/j.ppnp.2013.03.005](https://doi.org/10.1016/j.ppnp.2013.03.005).
- [2] O. Naviliat-Cuncic, M. González-Alonso, Prospects for precision measurements in nuclear decay in the lhc era, *Annalen der Physik* 525 (8-9) (2013) 600–619.
- [3] K. K. Vos, H. W. Wilschut, R. G. E. Timmermans, *Symmetry violations in nuclear and neutron  $\beta$  decay*, *Rev. Mod. Phys.* 87 (2015) 1483–1516. [doi:10.1103/RevModPhys.87.1483](https://doi.org/10.1103/RevModPhys.87.1483).  
URL <https://link.aps.org/doi/10.1103/RevModPhys.87.1483>
- [4] A. Falkowski, M. González-Alonso, O. Naviliat-Cuncic, Comprehensive analysis of beta decays within and beyond the standard model, *Journal of High Energy Physics* 2021 (4) (2021) 126. [doi:10.1007/JHEP04\(2021\)126](https://doi.org/10.1007/JHEP04(2021)126).
- [5] M. Brodeur, N. Buzinsky, M. Caprio, V. Cirigliano, J. Clark, P. Fasano, J. Formaggio, A. Gallant, A. Garcia, S. Gандolfi, et al., Nuclear  $\beta$  decay as a probe for physics beyond the standard model, arXiv preprint arXiv:2301.03975 (2023).
- [6] N. Cabibbo, Unitary Symmetry and Leptonic Decays, *Phys. Rev. Lett.* 10 (1963) 531–533. [doi:10.1103/PhysRevLett.10.531](https://doi.org/10.1103/PhysRevLett.10.531).
- [7] M. Kobayashi, T. Maskawa, CP Violation in the Renormalizable Theory of Weak Interaction, *Prog. Theor. Phys.* 49 (1973) 652–657. [doi:10.1143/PTP.49.652](https://doi.org/10.1143/PTP.49.652).
- [8] P. D. Group, P. A. Zyla, R. M. Barnett, J. Beringer, O. Dahl, D. A. Dwyer, D. E. Groom, C. J. Lin, K. S. Lugovsky, E. Pianori, D. J. Robinson, C. G. Wohl, W. M. Yao, K. Agashe, G. Aielli, B. C. Allanach, C. Amsler, M. Antonelli,

E. C. Aschenauer, D. M. Asner, H. Baer, S. Banerjee, L. Baudis, C. W. Bauer, J. J. Beatty, V. I. Belousov, S. Bethke, A. Bettini, O. Biebel, K. M. Black, E. Blucher, O. Buchmuller, V. Burkert, M. A. Bychkov, R. N. Cahn, M. Carena, A. Ceccucci, A. Cerri, D. Chakraborty, R. S. Chivukula, G. Cowan, G. D'Ambrosio, T. Damour, D. de Florian, A. de Gouvêa, T. DeGrand, P. de Jong, G. Dissertori, B. A. Dobrescu, M. D'Onofrio, M. Doser, M. Drees, H. K. Dreiner, P. Eerola, U. Egede, S. Eidelman, J. Ellis, J. Erler, V. V. Ezhela, W. Fettscher, B. D. Fields, B. Foster, A. Freitas, H. Gallagher, L. Garren, H. J. Gerber, G. Gerbier, T. Gershon, Y. Gershtein, T. Gherghetta, A. A. Godizov, M. C. Gonzalez-Garcia, M. Goodman, C. Grab, A. V. Gritsan, C. Grojean, M. Grünewald, A. Gurtu, T. Gutsche, H. E. Haber, C. Hanhart, S. Hashimoto, Y. Hayato, A. Hebecker, S. Heinemeyer, B. Heltsley, J. J. Hernández-Rey, K. Hikasa, J. Hisano, A. Höcker, J. Holder, A. Holtkamp, J. Huston, T. Hyodo, K. F. Johnson, M. Kado, M. Karliner, U. F. Katz, M. Kenzie, V. A. Khoze, S. R. Klein, E. Klempt, R. V. Kowalewski, F. Krauss, M. Kreps, B. Krusche, Y. Kwon, O. Lahav, J. Laiho, L. P. Lellouch, J. Lesgourgues, A. R. Liddle, Z. Ligeti, C. Lippmann, T. M. Liss, L. Littenberg, C. Lourengo, S. B. Lugovsky, A. Lusiani, Y. Makida, F. Maltoni, T. Mannel, A. V. Manohar, W. J. Marciano, A. Masoni, J. Matthews, U. G. Meißner, M. Mikhasenko, D. J. Miller, D. Milstead, R. E. Mitchell, K. Mönig, P. Molaro, F. Moortgat, M. Moskovic, K. Nakamura, M. Narain, P. Nason, S. Navas, M. Neubert, P. Nevski, Y. Nir, K. A. Olive, C. Patrignani, J. A. Peacock, S. T. Petcov, V. A. Petrov, A. Pich, A. Piepke, A. Pomarol, S. Profumo, A. Quadt, K. Rabbertz, J. Rademacker, G. Raffelt, H. Ramani, M. Ramsey-Musolf, B. N. Ratcliff, P. Richardson, A. Ringwald, S. Roesler, S. Rolli, A. Romaniouk, L. J. Rosenberg, J. L. Rosner, G. Rybka, M. Ryskin, R. A. Ryutin, Y. Sakai, G. P. Salam, S. Sarkar, F. Sauli, O. Schneider, K. Scholberg, A. J. Schwartz, J. Schwiening, D. Scott, V. Sharma, S. R. Sharpe, T. Shutt, M. Silari, T. Sjöstrand, P. Skands, T. Skwarnicki, G. F. Smoot, A. Soffer, M. S. Sozzi, S. Spanier, C. Spiering, A. Stahl, S. L. Stone, Y. Sumino, T. Sumiyoshi, M. J. Syphers, F. Takahashi, M. Tanabashi, J. Tanaka, M. Taševský, K. Terashi, J. Terning, U. Thoma, R. S. Thorne, L. Tiator, M. Titov, N. P. Tkachenko, D. R. Tovey, K. Trabelsi, P. Urquijo, G. Valencia, R. Van de Water, N. Varelas, G. Venanzoni, L. Verde, M. G. Vincter, P. Vogel, W. Vogelsang, A. Vogt, V. Vorobyev, S. P. Wakely, W. Walkowiak, C. W. Walter, D. Wands, M. O. Wascko, D. H. Weinberg, E. J. Weinberg, M. White, L. R. Wiencke, S. Willocq, C. L. Woody, R. L. Workman, M. Yokoyama, R. Yoshida, G. Zanderighi, G. P. Zeller, O. V. Zenin, R. Y. Zhu, S. L. Zhu, F. Zimmermann, J. Anderson, T. Basaglia, V. S. Lugovsky, P. Schaffner, W. Zheng, Review of Particle Physics, Progress of Theoretical and Experimental Physics 2020 (8), 083C01 (08 2020). [doi:10.1093/ptep/ptaa104](https://doi.org/10.1093/ptep/ptaa104).

- [9] V. Cirigliano, A. Crivellin, M. Hoferichter, M. Moulson, Scrutinizing ckm unitarity with a new measurement of the  $k\mu 3/k\mu 2$  branching fraction, Physics Letters B 838 (2023) 137748.
- [10] V. Cirigliano, W. Dekens, J. de Vries, E. Mereghetti, T. Tong, Anomalies in global SMEFT analyses. A case study of first-row CKM unitarity, JHEP 03 (2024) 033. [doi:10.1007/JHEP03\(2024\)033](https://doi.org/10.1007/JHEP03(2024)033).
- [11] N. Severijns, M. Beck, O. Naviliat-Cuncic, Tests of the standard electroweak model in nuclear beta decay, Rev. Mod. Phys. 78 (3) (2006) 991.
- [12] M. González-Alonso, O. Naviliat-Cuncic, N. Severijns, New physics searches in nuclear and neutron  $\beta$  decay, Prog. Part. Nucl. Phys. 104 (2019) 165–223. [doi:https://doi.org/10.1016/j.ppnp.2018.08.002](https://doi.org/10.1016/j.ppnp.2018.08.002).
- [13] A. Glick-Magid, C. Forssén, D. Gazda, D. Gazit, P. Gysbers, P. Navrátil, Nuclear ab initio calculations of  ${}^6\text{He}$   $\beta$ -decay for beyond the standard model studies, Phys. Lett. B 832 (2022) 137259. [doi:https://doi.org/10.1016/](https://doi.org/10.1016/)

- [14] G. H. Sargsyan, K. D. Launey, M. T. Burkey, A. T. Gallant, N. D. Scielzo, G. Savard, A. Mercenne, T. Dytrych, D. Langr, L. Varriano, B. Longfellow, T. Y. Hirsh, J. P. Draayer, *Impact of clustering on the  ${}^8\text{Li}$   $\beta$  decay and recoil form factors*, Phys. Rev. Lett. 128 (2022) 202503. [doi:10.1103/PhysRevLett.128.202503](https://doi.org/10.1103/PhysRevLett.128.202503).  
URL <https://link.aps.org/doi/10.1103/PhysRevLett.128.202503>
- [15] G. B. King, A. Baroni, V. Cirigliano, S. Gandolfi, L. Hayen, E. Mereghetti, S. Pastore, M. Piarulli, *Ab initio calculation of the  $\beta$ -decay spectrum of  $\text{He6}$* , Phys. Rev. C 107 (1) (2023) 015503. [doi:10.1103/PhysRevC.107.015503](https://doi.org/10.1103/PhysRevC.107.015503).
- [16] B. Longfellow, A. T. Gallant, G. H. Sargsyan, M. T. Burkey, T. Y. Hirsh, G. Savard, N. D. Scielzo, L. Varriano, M. Brodeur, D. P. Burdette, J. A. Clark, D. Lascar, K. D. Launey, P. Mueller, D. Ray, K. S. Sharma, A. A. Valverde, G. L. Wilson, X. L. Yan, *Improved tensor current limit from  ${}^8\text{B}$   $\beta$  decay including new recoil-order calculations*, Phys. Rev. Lett. 132 (2024) 142502. [doi:10.1103/PhysRevLett.132.142502](https://doi.org/10.1103/PhysRevLett.132.142502).  
URL <https://link.aps.org/doi/10.1103/PhysRevLett.132.142502>
- [17] M. Gennari, M. Drissi, M. Gorchtein, P. Navratil, C.-Y. Seng, *Ab Initio Strategy for Taming the Nuclear-Structure Dependence of Vud Extractions: The  $\text{C10} \rightarrow \text{B10}$  Superallowed Transition*, Phys. Rev. Lett. 134 (1) (2025) 012501. [doi:10.1103/PhysRevLett.134.012501](https://doi.org/10.1103/PhysRevLett.134.012501).
- [18] V. Cirigliano, W. Dekens, J. de Vries, S. Gandolfi, M. Hoferichter, E. Mereghetti, *Radiative Corrections to Superallowed  $\beta$  Decays in Effective Field Theory*, Phys. Rev. Lett. 133 (21) (2024) 211801. [doi:10.1103/PhysRevLett.133.211801](https://doi.org/10.1103/PhysRevLett.133.211801).
- [19] V. Cirigliano, W. Dekens, J. de Vries, S. Gandolfi, M. Hoferichter, E. Mereghetti, *Ab initio electroweak corrections to superallowed  $\beta$  decays and their impact on Vud*, Phys. Rev. C 110 (5) (2024) 055502. [doi:10.1103/PhysRevC.110.055502](https://doi.org/10.1103/PhysRevC.110.055502).
- [20] G. B. King, J. Carlson, A. R. Flores, S. Gandolfi, E. Mereghetti, S. Pastore, M. Piarulli, R. B. Wiringa, *Quantum Monte Carlo calculation of  $\delta_{\text{NS}}$  in  ${}^{10}\text{C}$  using an effective field theory approach*, arXiv preprint arXiv:2509.07310 (9 2025).
- [21] H. Hergert, *A Guided Tour of *ab initio* Nuclear Many-Body Theory*, Front. in Phys. 8 (2020) 379. [doi:10.3389/fphy.2020.00379](https://doi.org/10.3389/fphy.2020.00379).
- [22] A. Ekström, C. Forssén, G. Hagen, G. R. Jansen, W. Jiang, T. Papenbrock, *What is ab initio in nuclear theory?*, Front. Phys. 11 (2023) 1129094. [doi:10.3389/fphy.2023.1129094](https://doi.org/10.3389/fphy.2023.1129094).
- [23] S. R. Beane, W. Detmold, K. Orginos, M. J. Savage, *Nuclear Physics from Lattice QCD*, Prog. Part. Nucl. Phys. 66 (2011) 1–40. [doi:10.1016/j.ppnp.2010.08.002](https://doi.org/10.1016/j.ppnp.2010.08.002).
- [24] R. B. Wiringa, V. G. J. Stoks, R. Schiavilla, *Phys. Rev. C* 51 (1995) 38.
- [25] R. Machleidt, *Phys. Rev. C* 63 (2001) 024001.

- [26] P. F. Bedaque, U. van Kolck, Effective field theory for few-nucleon systems, *Annu. Rev. Nucl. Part. Sci.* 52 (1) (2002) 339–396. [doi:10.1146/annurev.nucl.52.050102.090637](https://doi.org/10.1146/annurev.nucl.52.050102.090637).
- [27] D. R. Entem, R. Machleidt, *Phys. Rev. C* 68 (2003) 041001(R).
- [28] E. Epelbaum, H. Krebs, U. G. Meißner, Precision nucleon-nucleon potential at fifth order in the chiral expansion, *Phys. Rev. Lett.* 115 (12) (2015) 122301. [doi:10.1103/PhysRevLett.115.122301](https://doi.org/10.1103/PhysRevLett.115.122301).
- [29] H.-W. Hammer, S. König, U. van Kolck, [Nuclear effective field theory: Status and perspectives](#), *Rev. Mod. Phys.* 92 (2020) 025004. [doi:10.1103/RevModPhys.92.025004](https://doi.org/10.1103/RevModPhys.92.025004)  
URL <https://link.aps.org/doi/10.1103/RevModPhys.92.025004>
- [30] D. B. Kaplan, M. J. Savage, M. B. Wise, A New expansion for nucleon-nucleon interactions, *Phys. Lett. B* 424 (1998) 390–396. [doi:10.1016/S0370-2693\(98\)00210-X](https://doi.org/10.1016/S0370-2693(98)00210-X).
- [31] U. van Kolck, Naturalness in nuclear effective field theories, *Eur. Phys. J. A* 56 (3) (2020) 97. [doi:10.1140/epja/s10050-020-00092-1](https://doi.org/10.1140/epja/s10050-020-00092-1).
- [32] B. Barrett, P. Navrátil, J. Vary, *Prog. Part. Nucl. Phys.* 69 (2013) 131.
- [33] B. Verhaar, A method for the elimination of spurious states in the nuclear harmonic oscillator shell model, *Nucl. Phys.* 21 (1960) 508–525. [doi:10.1016/0029-5582\(60\)90073-0](https://doi.org/10.1016/0029-5582(60)90073-0).
- [34] K. Kravvaris, P. Navrátil, S. Quaglioni, C. Hebborn, G. Hupin, Ab initio informed evaluation of the radiative capture of protons on  $^{7}\text{Be}$ , *Phys. Lett. B* 845 (2023) 138156. [doi:10.1016/j.physletb.2023.138156](https://doi.org/10.1016/j.physletb.2023.138156).
- [35] L. Jokiniemi, P. Navrátil, J. Kotila, K. Kravvaris, [Muon capture on  \$^{6}\text{Li}\$ ,  \$^{12}\text{C}\$ , and  \$^{16}\text{O}\$  from ab initio nuclear theory](#), *Phys. Rev. C* 109 (2024) 065501. [doi:10.1103/PhysRevC.109.065501](https://doi.org/10.1103/PhysRevC.109.065501)  
URL <https://link.aps.org/doi/10.1103/PhysRevC.109.065501>
- [36] R. J. Furnstahl, G. Hagen, T. Papenbrock, Corrections to nuclear energies and radii in finite oscillator spaces, *Phys. Rev. C* 86 (2012) 031301(R).
- [37] S. A. Coon, M. I. Avetian, M. K. G. Kruse, U. van Kolck, P. Maris, J. P. Vary, [Convergence properties of ab initio calculations of light nuclei in a harmonic oscillator basis](#), *Phys. Rev. C* 86 (2012) 054002. [doi:10.1103/PhysRevC.86.054002](https://doi.org/10.1103/PhysRevC.86.054002)  
URL <https://link.aps.org/doi/10.1103/PhysRevC.86.054002>
- [38] K. A. Wendt, C. Forssén, T. Papenbrock, D. Sääf, Infrared length scale and extrapolations for the no-core shell model, *Phys. Rev. C* 91 (2015) 061301.
- [39] P. Maris, J. P. Vary, A. M. Shirokov, [Ab initio no-core full configuration calculations of light nuclei](#), *Phys. Rev. C* 79 (2009) 014308. [doi:10.1103/PhysRevC.79.014308](https://doi.org/10.1103/PhysRevC.79.014308)  
URL <https://link.aps.org/doi/10.1103/PhysRevC.79.014308>
- [40] D. Shanks, Non-linear transformations of divergent and slowly convergent sequences, *Journal of Mathematics and Physics* 34 (1-4) (1955) 1–42. [doi:10.1002/sapm19553411](https://doi.org/10.1002/sapm19553411).

- [41] A. Bohr, B. R. Mottelson, Nuclear Structure, Vol. 1, Benjamin, New York, 1969.
- [42] J. P. Elliott, Collective Motion in the Nuclear Shell Model. I. Classification Schemes for States of Mixed Configurations, Proc. Roy. Soc. A 245 (1958) 128.
- [43] J. P. Elliott, Collective Motion in the Nuclear Shell Model. II. The Introduction of Intrinsic Wave-Functions, Proc. Roy. Soc. A 245 (1958) 562.
- [44] J. P. Elliott, M. Harvey, Collective Motion in the Nuclear Shell Model. III. The Calculation of Spectra, Proc. Roy. Soc. A 272 (1962) 557.
- [45] G. Rosensteel, D. J. Rowe, Nuclear  $Sp(3, R)$  Model, Phys. Rev. Lett. 38 (1977) 10.
- [46] D. J. Rowe, Microscopic theory of the nuclear collective model, Reports on Progr. in Phys. 48 (1985) 1419.
- [47] O. Castaños, J. P. Draayer, Y. Leschber, Z. Phys. A 329 (1988) 33.
- [48] Y. Leschber, J. P. Draayer, Phys. Letts. B 190 (1987) 1.
- [49] K. D. Launey, T. Dytrych, J. P. Draayer, Symmetry-guided large-scale shell-model theory, Prog. Part. Nucl. Phys. 89 (2016) 101 (review). [doi:10.1016/j.ppnp.2016.02.001](https://doi.org/10.1016/j.ppnp.2016.02.001).
- [50] T. Dytrych, K. D. Launey, J. P. Draayer, D. J. Rowe, J. L. Wood, G. Rosensteel, C. Bahri, D. Langr, R. B. Baker, [Physics of nuclei: Key role of an emergent symmetry](#), Phys. Rev. Lett. 124 (2020) 042501. [doi:10.1103/PhysRevLett.124.042501](https://doi.org/10.1103/PhysRevLett.124.042501)  
URL <https://link.aps.org/doi/10.1103/PhysRevLett.124.042501>
- [51] K. T. Hecht, The use of  $SU(3)$  in the elimination of spurious center of mass states, Nucl. Phys. A 170 (1) (1971) 34–54. [doi:10.1016/0375-9474\(71\)90681-6](https://doi.org/10.1016/0375-9474(71)90681-6).
- [52] D. Millener, in: J. Draayer, J. Janecke (Eds.), Group Theory and Special Symmetries in Nuclear Physics, World Scientific, Singapore, 1992, p. 276.
- [53] D. Langr, T. Dytrych, J. P. Draayer, K. D. Launey, P. Tvrđík, Efficient algorithm for representations of  $u(3)$  in  $u(n)$ , Computer Physics Communications 244 (2019) 442. [doi:10.1016/j.cpc.2019.05.018](https://doi.org/10.1016/j.cpc.2019.05.018).
- [54] D. Borremans, D. L. Balabanski, K. Blaum, W. Geithner, S. Gheysen, P. Himpe, M. Kowalska, J. Lassen, P. Lievens, S. Mallion, R. Neugart, G. Neyens, N. Vermeulen, D. Yordanov, [New measurement and reevaluation of the nuclear magnetic and quadrupole moments of  \${}^8Li\$  and  \${}^9Li\$](#) , Phys. Rev. C 72 (2005) 044309. [doi:10.1103/PhysRevC.72.044309](https://doi.org/10.1103/PhysRevC.72.044309)  
URL <https://link.aps.org/doi/10.1103/PhysRevC.72.044309>
- [55] N. Stone, [Table of nuclear electric quadrupole moments](#), Atomic Data and Nuclear Data Tables 111-112 (2016) 1–28. [doi:https://doi.org/10.1016/j.adt.2015.12.002](https://doi.org/10.1016/j.adt.2015.12.002).  
URL <https://www.sciencedirect.com/science/article/pii/S0092640X16000024>
- [56] A. C. Dreyfuss, K. D. Launey, J. E. Escher, G. H. Sargsyan, R. B. Baker, T. Dytrych, J. P. Draayer, [Clustering and  \$\alpha\$ -capture reaction rate from ab initio symmetry-adapted descriptions of  \${}^{20}Ne\$](#) , Phys. Rev. C 102 (2020) 044608.

doi:10.1103/PhysRevC.102.044608.

URL <https://link.aps.org/doi/10.1103/PhysRevC.102.044608>

- [57] P. Ruotsalainen, J. Henderson, G. Hackman, G. H. Sargsyan, K. D. Launey, A. Saxena, P. C. Srivastava, S. R. Stroberg, T. Grahn, J. Pakarinen, G. C. Ball, R. Julin, P. T. Greenlees, J. Smallcombe, C. Andreoiu, N. Bernier, M. Bowry, M. Buckner, R. Caballero-Folch, A. Chester, S. Cruz, L. J. Evitts, R. Frederick, A. B. Garnsworthy, M. Holl, A. Kurkjian, D. Kisliuk, K. G. Leach, E. McGee, J. Measures, D. Mücher, J. Park, F. Sarazin, J. K. Smith, D. Southall, K. Starosta, C. E. Svensson, K. Whitmore, M. Williams, C. Y. Wu, *Isospin symmetry in  $b(e2)$  values: Coulomb excitation study of  $^{21}\text{Mg}$* , Phys. Rev. C 99 (2019) 051301. doi:10.1103/PhysRevC.99.051301.  
URL <https://link.aps.org/doi/10.1103/PhysRevC.99.051301>
- [58] J. Williams, G. C. Ball, A. Chester, T. Domingo, A. B. Garnsworthy, G. Hackman, J. Henderson, R. Henderson, R. Krücken, A. Kumar, K. D. Launey, J. Measures, O. Paetkau, J. Park, G. H. Sargsyan, J. Smallcombe, P. C. Srivastava, K. Starosta, C. E. Svensson, K. Whitmore, M. Williams, *Structure of  $^{28}\text{Mg}$  and influence of the neutron  $pf$  shell*, Phys. Rev. C 100 (2019) 014322. doi:10.1103/PhysRevC.100.014322.  
URL <https://link.aps.org/doi/10.1103/PhysRevC.100.014322>
- [59] K. D. Launey, A. Mercenne, G. H. Sargsyan, H. Shows, R. B. Baker, M. E. Miora, T. Dytrych, J. P. Draayer, Emergent clustering phenomena in the framework of the *ab initio* symmetry-adapted no-core shell model, in: Proceedings of the 4th International Workshop on 'State of the Art in Nuclear Cluster Physics' (SOTANCP4), May 2018, Galveston, Texas, Vol. 2038, AIP Conference Proceedings, 2018.
- [60] K. D. Launey, A. Mercenne, T. Dytrych, Nuclear dynamics and reactions in the *ab initio* symmetry-adapted framework, Annu. Rev. Nucl. Part. Sci. 71 (2021) 253. doi:10.1146/annurev-nucl-102419-033316.
- [61] R. B. Baker, C. Elster, T. Dytrych, K. D. Launey, *Ab initio* leading order effective potential for elastic proton scattering based on the symmetry-adapted no-core shell model, Phys. Rev. C 110 (2024) 034605. doi:10.1103/PhysRevC.110.034605.
- [62] M. Burrows, R. B. Baker, S. Bacca, K. D. Launey, T. Dytrych, D. Langr, Response functions and giant monopole resonances for light to medium-mass nuclei from the *ab initio* symmetry-adapted no-core–shell model, J. of Phys. G 52 (3) (2025) 035107. doi:10.1088/1361-6471/adb901.
- [63] K. D. Launey, T. Dytrych, G. H. Sargsyan, R. B. Baker, J. P. Draayer, Emergent symplectic symmetry in atomic nuclei: *Ab initio* symmetry-adapted no-core shell model, Eur. Phys. J. Spec. Top. 229 (2020) 2429. doi:10.1140/epjst/e2020-000178-3.
- [64] K. D. Launey, G. H. Sargsyan, A. Mercenne, J. E. Escher, D. C. Mumma, Ab initio symmetry-adapted approaches to nuclear reactions, arXiv preprint arXiv:2510.15171 (2025).
- [65] G. B. King, L. Andreoli, S. Pastore, M. Piarulli, R. Schiavilla, R. B. Wiringa, J. Carlson, S. Gandolfi, *Chiral effective field theory calculations of weak transitions in light nuclei*, Phys. Rev. C 102 (2020) 025501. doi:10.1103/PhysRevC.102.025501.  
URL <https://link.aps.org/doi/10.1103/PhysRevC.102.025501>

- [66] J. Carlson, S. Gandolfi, F. Pederiva, S. C. Pieper, R. Schiavilla, K. E. Schmidt, R. B. Wiringa, Quantum Monte Carlo methods for nuclear physics, *Rev. Mod. Phys.* 87 (2015) 1067. [doi:10.1103/RevModPhys.87.1067](https://doi.org/10.1103/RevModPhys.87.1067).
- [67] S. Gandolfi, D. Lonardoni, A. Lovato, M. Piarulli, Atomic nuclei from quantum monte carlo calculations with chiral eft interactions, *Frontiers in Physics* 8 (2020) 117.
- [68] G. B. King, S. Pastore, Recent Progress in the Electroweak Structure of Light Nuclei Using Quantum Monte Carlo Methods, *Ann. Rev. Nucl. Part. Sci.* 74 (1) (2024) 343–368. [doi:10.1146/annurev-nucl-101920-021401](https://doi.org/10.1146/annurev-nucl-101920-021401).
- [69] R. B. Wiringa, Variational calculations of few-body nuclei, *Phys. Rev. C*43 (1991) 1585–1598. [doi:10.1103/PhysRevC.43.1585](https://doi.org/10.1103/PhysRevC.43.1585).
- [70] M. Piarulli, L. Girlanda, R. Schiavilla, A. Kievsky, A. Lovato, L. E. Marcucci, S. C. Pieper, M. Viviani, R. B. Wiringa, Local chiral potentials with  $\Delta$ -intermediate states and the structure of light nuclei, *Phys. Rev. C*94 (5) (2016) 054007. [doi:10.1103/PhysRevC.94.054007](https://doi.org/10.1103/PhysRevC.94.054007).
- [71] M. Piarulli, et al., Light-nuclei spectra from chiral dynamics, *Phys. Rev. Lett.* 120 (5) (2018) 052503. [doi:10.1103/PhysRevLett.120.052503](https://doi.org/10.1103/PhysRevLett.120.052503).
- [72] R. B. Wiringa, S. C. Pieper, J. Carlson, V. R. Pandharipande, Quantum Monte Carlo calculations of  $A = 8$  nuclei, *Phys. Rev. C*62 (2000) 014001. [doi:10.1103/PhysRevC.62.014001](https://doi.org/10.1103/PhysRevC.62.014001).
- [73] B. S. Pudliner, V. R. Pandharipande, J. Carlson, S. C. Pieper, R. B. Wiringa, Quantum Monte Carlo calculations of nuclei with  $A \leq 7$ , *Phys. Rev. C*56 (1997) 1720–1750. [doi:10.1103/PhysRevC.56.1720](https://doi.org/10.1103/PhysRevC.56.1720).
- [74] K. E. Schmidt, S. Fantoni, A quantum Monte Carlo method for nucleon systems, *Phys. Lett. B*446 (1999) 99–103. [doi:10.1016/S0370-2693\(98\)01522-6](https://doi.org/10.1016/S0370-2693(98)01522-6).
- [75] D. Lonardoni, S. Gandolfi, J. E. Lynn, C. Petrie, J. Carlson, K. E. Schmidt, A. Schwenk, Auxiliary field diffusion Monte Carlo calculations of light and medium-mass nuclei with local chiral interactions, *Phys. Rev. C* 97 (4) (2018) 044318. [doi:10.1103/PhysRevC.97.044318](https://doi.org/10.1103/PhysRevC.97.044318).
- [76] M. Pervin, S. C. Pieper, R. B. Wiringa, Quantum Monte Carlo calculations of electroweak transition matrix elements in  $A = 6,7$  nuclei, *Phys. Rev. C*76 (2007) 064319. [doi:10.1103/PhysRevC.76.064319](https://doi.org/10.1103/PhysRevC.76.064319).
- [77] X. Feng, M. Gorchtein, L.-C. Jin, P.-X. Ma, C.-Y. Seng, First-principles calculation of electroweak box diagrams from lattice QCD, *Phys. Rev. Lett.* 124 (19) (2020) 192002. [doi:10.1103/PhysRevLett.124.192002](https://doi.org/10.1103/PhysRevLett.124.192002).
- [78] J.-S. Yoo, T. Bhattacharya, R. Gupta, S. Mondal, B. Yoon, Electroweak box diagram contribution for pion and kaon decay from lattice QCD, *Phys. Rev. D* 108 (3) (2023) 034508. [doi:10.1103/PhysRevD.108.034508](https://doi.org/10.1103/PhysRevD.108.034508).
- [79] D. Pocanic, et al., Precise measurement of the  $\pi^+ \rightarrow \pi^0 e^+ \nu$  branching ratio, *Phys. Rev. Lett.* 93 (2004) 181803. [doi:10.1103/PhysRevLett.93.181803](https://doi.org/10.1103/PhysRevLett.93.181803).
- [80] W. Altmannshofer, et al., PIONEER: Studies of Rare Pion Decays (3 2022).
- [81] C.-Y. Seng, M. Gorchtein, H. H. Patel, M. J. Ramsey-Musolf, Reduced Hadronic Uncertainty in the Determination of  $V_{ud}$ , *Phys. Rev. Lett.* 121 (24) (2018) 241804. [doi:10.1103/PhysRevLett.121.241804](https://doi.org/10.1103/PhysRevLett.121.241804).

- [82] C. Y. Seng, M. Gorchtein, M. J. Ramsey-Musolf, Dispersive evaluation of the inner radiative correction in neutron and nuclear  $\beta$  decay, Phys. Rev. D 100 (1) (2019) 013001. [doi:10.1103/PhysRevD.100.013001](https://doi.org/10.1103/PhysRevD.100.013001).
- [83] C.-Y. Seng, X. Feng, M. Gorchtein, L.-C. Jin, Joint lattice QCD–dispersion theory analysis confirms the quark-mixing top-row unitarity deficit, Phys. Rev. D 101 (11) (2020) 111301. [doi:10.1103/PhysRevD.101.111301](https://doi.org/10.1103/PhysRevD.101.111301).
- [84] A. Czarnecki, W. J. Marciano, A. Sirlin, Radiative Corrections to Neutron and Nuclear Beta Decays Revisited, Phys. Rev. D 100 (7) (2019) 073008. [doi:10.1103/PhysRevD.100.073008](https://doi.org/10.1103/PhysRevD.100.073008).
- [85] K. Shiells, P. G. Blunden, W. Melnitchouk, Electroweak axial structure functions and improved extraction of the  $V_{ud}$  CKM matrix element, Phys. Rev. D 104 (3) (2021) 033003. [doi:10.1103/PhysRevD.104.033003](https://doi.org/10.1103/PhysRevD.104.033003).
- [86] L. Hayen, Standard model  $\mathcal{O}(\alpha)$  renormalization of  $g_A$  and its impact on new physics searches, Phys. Rev. D 103 (11) (2021) 113001. [doi:10.1103/PhysRevD.103.113001](https://doi.org/10.1103/PhysRevD.103.113001).
- [87] P.-X. Ma, X. Feng, M. Gorchtein, L.-C. Jin, K.-F. Liu, C.-Y. Seng, B.-G. Wang, Z.-L. Zhang, Lattice QCD Calculation of Electroweak Box Contributions to Superallowed Nuclear and Neutron Beta Decays, Phys. Rev. Lett. 132 (19) (2024) 191901. [doi:10.1103/PhysRevLett.132.191901](https://doi.org/10.1103/PhysRevLett.132.191901).
- [88] V. Cirigliano, W. Dekens, E. Mereghetti, O. Tomalak, Effective field theory for radiative corrections to charged-current processes: Vector coupling, Phys. Rev. D 108 (5) (2023) 053003. [doi:10.1103/PhysRevD.108.053003](https://doi.org/10.1103/PhysRevD.108.053003).
- [89] P. Vander Griend, Z. Cao, R. J. Hill, R. Plestid, The Fermi function and the neutron’s lifetime, Phys. Lett. B 868 (2025) 139678. [doi:10.1016/j.physletb.2025.139678](https://doi.org/10.1016/j.physletb.2025.139678).
- [90] Z. Cao, R. J. Hill, R. Plestid, P. Vander Griend, Factorization and resummation of qed radiative corrections for neutron beta decay, Phys. Rev. D 112 (2025) 113006. [doi:10.1103/639y-63wk](https://doi.org/10.1103/639y-63wk)  
URL <https://link.aps.org/doi/10.1103/639y-63wk>
- [91] F. Moretti, M. Gorbahn, S. Jäger, Beyond Leading Logarithms in  $g_V$ : The Semileptonic Weak Hamiltonian at  $\mathcal{O}(\alpha \alpha_s^2)$ , arXiv preprint arXiv:2510.27648 (10 2025).
- [92] Y. Fuwa, et al., Improved measurements of neutron lifetime with cold neutron beam at J-PARC, arXiv preprint arXiv:2412.19519 (12 2024).
- [93] M. Beck, et al., Improved determination of the  $\beta-\bar{\nu}_e$  angular correlation coefficient  $a$  in free neutron decay with the aSPECT spectrometer, Phys. Rev. C 101 (5) (2020) 055506. [doi:10.1103/PhysRevC.101.055506](https://doi.org/10.1103/PhysRevC.101.055506).
- [94] M. Beck, W. Heil, C. Schmidt, S. Baefslér, F. Glück, G. Konrad, U. Schmidt, Reanalysis of the  $\beta-\bar{\nu}^-e$  Angular Correlation Measurement from the aSPECT Experiment with New Constraints on Fierz Interference, Phys. Rev. Lett. 132 (10) (2024) 102501. [doi:10.1103/PhysRevLett.132.102501](https://doi.org/10.1103/PhysRevLett.132.102501).
- [95] B. Märkisch, et al., Measurement of the Weak Axial-Vector Coupling Constant in the Decay of Free Neutrons Using a Pulsed Cold Neutron Beam, Phys. Rev. Lett. 122 (24) (2019) 242501. [doi:10.1103/PhysRevLett.122.242501](https://doi.org/10.1103/PhysRevLett.122.242501).
- [96] J. C. Hardy, I. S. Towner, Superallowed  $0^+ \rightarrow 0^+$  nuclear  $\beta$  decays: 2020 critical survey, with implications for  $V_{ud}$  and CKM unitarity, Phys. Rev. C 102 (4) (2020) 045501. [doi:10.1103/PhysRevC.102.045501](https://doi.org/10.1103/PhysRevC.102.045501).

- [97] W. Jaus, G. Rasche, Nuclear Structure Dependence of  $O(\alpha)$  Corrections to Fermi Decays and the Value of the Kobayashi-Maskawa Matrix Element  $V$  ( $U D$ ), *Phys. Rev. D* 41 (1990) 166–176. [doi:10.1103/PhysRevD.41.166](https://doi.org/10.1103/PhysRevD.41.166).
- [98] F. C. Barker, B. A. Brown, W. Jaus, G. Rasche, Determination of  $V$  ( $ud$ ) from Fermi decays and the unitarity of the KM mixing matrix, *Nucl. Phys. A* 540 (1992) 501–519. [doi:10.1016/0375-9474\(92\)90171-F](https://doi.org/10.1016/0375-9474(92)90171-F).
- [99] I. S. Towner, The Nuclear structure dependence of radiative corrections in superallowed Fermi beta decay, *Nucl. Phys. A* 540 (1992) 478–500. [doi:10.1016/0375-9474\(92\)90170-0](https://doi.org/10.1016/0375-9474(92)90170-0).
- [100] I. S. Towner, Quenching of spin operators in the calculation of radiative corrections for nuclear beta decay, *Phys. Lett. B* 333 (1994) 13–16. [doi:10.1016/0370-2693\(94\)91000-6](https://doi.org/10.1016/0370-2693(94)91000-6).
- [101] C.-Y. Seng, M. Gorchtein, Dispersive formalism for the nuclear structure correction  $\delta NS$  to the  $\beta$  decay rate, *Phys. Rev. C* 107 (3) (2023) 035503. [doi:10.1103/PhysRevC.107.035503](https://doi.org/10.1103/PhysRevC.107.035503).
- [102] M. Gorchtein, C. Y. Seng, Superallowed Nuclear Beta Decays and Precision Tests of the Standard Model, *Ann. Rev. Nucl. Part. Sci.* 74 (1) (2024) 23–47. [doi:10.1146/annurev-nucl-102622-020726](https://doi.org/10.1146/annurev-nucl-102622-020726).
- [103] A. Sirlin, Current Algebra Formulation of Radiative Corrections in Gauge Theories and the Universality of the Weak Interactions, *Rev. Mod. Phys.* 50 (1978) 573, [Erratum: *Rev.Mod.Phys.* 50, 905 (1978)]. [doi:10.1103/RevModPhys.50.573](https://doi.org/10.1103/RevModPhys.50.573).
- [104] V. Cirigliano, W. Dekens, E. Mereghetti, O. Tomalak, Effective field theory for radiative corrections to charged-current processes. II. Axial-vector coupling, *Phys. Rev. D* 111 (5) (2025) 053005. [doi:10.1103/PhysRevD.111.053005](https://doi.org/10.1103/PhysRevD.111.053005).
- [105] V. Cirigliano, W. Dekens, J. De Vries, M. L. Graesser, E. Mereghetti, S. Pastore, U. Van Kolck, New Leading Contribution to Neutrinoless Double- $\beta$  Decay, *Phys. Rev. Lett.* 120 (20) (2018) 202001. [doi:10.1103/PhysRevLett.120.202001](https://doi.org/10.1103/PhysRevLett.120.202001).
- [106] V. Cirigliano, W. Dekens, J. De Vries, M. L. Graesser, E. Mereghetti, S. Pastore, M. Piarulli, U. Van Kolck, R. B. Wiringa, Renormalized approach to neutrinoless double- $\beta$  decay, *Phys. Rev. C* 100 (5) (2019) 055504. [doi:10.1103/PhysRevC.100.055504](https://doi.org/10.1103/PhysRevC.100.055504).
- [107] C.-Y. Seng, High-precision determination of radiative corrections to superallowed nuclear beta decays, 2025.
- [108] R. Haydock, The inverse of a linear operator, *Journal of Physics A: Mathematical, Nuclear and General* 7 (17) (1974) 2120.
- [109] E. Dagotto, Correlated electrons in high-temperature superconductors, *Rev. Mod. Phys.* 66 (1994) 763–840. [doi:10.1103/RevModPhys.66.763](https://doi.org/10.1103/RevModPhys.66.763).
- [110] M. A. Marchisio, N. Barnea, W. Leidemann, G. Orlandini, Lorentz integral transform for inclusive and exclusive cross-sections with the Lanczos method, *Few Body Syst.* 33 (2003) 259–276. [doi:10.1007/s00601-003-0017-z](https://doi.org/10.1007/s00601-003-0017-z).
- [111] T. W. Donnelly, J. D. Walecka, Electron Scattering and Nuclear Structure, *Ann. Rev. Nucl. Part. Sci.* 25 (1975) 329–405. [doi:10.1146/annurev.ns.25.120175.001553](https://doi.org/10.1146/annurev.ns.25.120175.001553).

- [112] T. W. Donnelly, J. A. Formaggio, B. R. Holstein, R. G. Milner, B. Surrow, Foundations of Nuclear and Particle Physics, Cambridge University Press, 2017.
- [113] P. Gysbers, et al., Discrepancy between experimental and theoretical  $\beta$ -decay rates resolved from first principles, *Nature Phys.* 15 (5) (2019) 428–431. [doi:10.1038/s41567-019-0450-7](https://doi.org/10.1038/s41567-019-0450-7).
- [114] N. Armesto, Nuclear shadowing, *J. Phys. G* 32 (2006) R367–R394. [doi:10.1088/0954-3899/32/11/R01](https://doi.org/10.1088/0954-3899/32/11/R01).
- [115] B. Z. Kopeliovich, J. G. Morfin, I. Schmidt, Nuclear Shadowing in Electro-Weak Interactions, *Prog. Part. Nucl. Phys.* 68 (2013) 314–372. [doi:10.1016/j.ppnp.2012.09.004](https://doi.org/10.1016/j.ppnp.2012.09.004).
- [116] D. J. Gross, C. H. Llewellyn Smith, High-energy neutrino - nucleon scattering, current algebra and partons, *Nucl. Phys. B* 14 (1969) 337–347. [doi:10.1016/0550-3213\(69\)90213-2](https://doi.org/10.1016/0550-3213(69)90213-2).
- [117] W. C. Leung, et al., A Measurement of the Gross-Llewellyn-Smith Sum Rule from the CCFR  $xF_3$  Structure Function, *Phys. Lett. B* 317 (1993) 655–659. [doi:10.1016/0370-2693\(93\)91386-2](https://doi.org/10.1016/0370-2693(93)91386-2).
- [118] C. Kim, S. Mintz, Muon-capture rate in 6li and the pcac hypothesis, *Physics Letters B* 31 (8) (1970) 503–505.
- [119] M. Gorchtein,  $\gamma$ W Box Inside Out: Nuclear Polarizabilities Distort the Beta Decay Spectrum, *Phys. Rev. Lett.* 123 (4) (2019) 042503. [doi:10.1103/PhysRevLett.123.042503](https://doi.org/10.1103/PhysRevLett.123.042503).
- [120] R. B. Wiringa, V. G. J. Stoks, R. Schiavilla, An Accurate nucleon-nucleon potential with charge independence breaking, *Phys. Rev. C* 51 (1995) 38–51. [doi:10.1103/PhysRevC.51.38](https://doi.org/10.1103/PhysRevC.51.38).
- [121] S. C. Pieper, V. R. Pandharipande, R. B. Wiringa, J. Carlson, Realistic models of pion exchange three nucleon interactions, *Phys. Rev. C* 64 (2001) 014001. [doi:10.1103/PhysRevC.64.014001](https://doi.org/10.1103/PhysRevC.64.014001).
- [122] R. B. Wiringa, R. Schiavilla, S. C. Pieper, J. Carlson, Nucleon and nucleon-pair momentum distributions in  $A \leq 12$  nuclei, *Phys. Rev. C* 89 (2) (2014) 024305. [doi:10.1103/PhysRevC.89.024305](https://doi.org/10.1103/PhysRevC.89.024305).
- [123] A. Baroni, et al., Local chiral interactions, the tritium Gamow-Teller matrix element, and the three-nucleon contact term, *Phys. Rev. C* 98 (4) (2018) 044003. [doi:10.1103/PhysRevC.98.044003](https://doi.org/10.1103/PhysRevC.98.044003).
- [124] A. Gezerlis, I. Tews, E. Epelbaum, M. Freunek, S. Gandolfi, K. Hebeler, A. Nogga, A. Schwenk, Local chiral effective field theory interactions and quantum Monte Carlo applications, *Phys. Rev. C* 90 (5) (2014) 054323. [doi:10.1103/PhysRevC.90.054323](https://doi.org/10.1103/PhysRevC.90.054323).
- [125] J. E. Lynn, I. Tews, J. Carlson, S. Gandolfi, A. Gezerlis, K. E. Schmidt, A. Schwenk, Chiral Three-Nucleon Interactions in Light Nuclei, Neutron- $\alpha$  Scattering, and Neutron Matter, *Phys. Rev. Lett.* 116 (6) (2016) 062501. [doi:10.1103/PhysRevLett.116.062501](https://doi.org/10.1103/PhysRevLett.116.062501).
- [126] J. C. Hardy, I. S. Towner, Superallowed  $0^+ \rightarrow 0^+$  nuclear  $\beta$  decays: 2014 critical survey, with precise results for  $V_{ud}$  and CKM unitarity, *Phys. Rev. C* 91 (2) (2015) 025501. [doi:10.1103/PhysRevC.91.025501](https://doi.org/10.1103/PhysRevC.91.025501).
- [127] T.-D. Lee, C.-N. Yang, Question of parity conservation in weak interactions, *Phys. Rev.* 104 (1) (1956) 254.
- [128] J. D. Jackson, S. B. Treiman, H. W. Wyld, Possible tests of time reversal invariance in beta decay, *Phys. Rev.* 106 (1957) 517–521. [doi:10.1103/PhysRev.106.517](https://doi.org/10.1103/PhysRev.106.517).

- [129] B. R. Holstein, [Recoil effects in allowed beta decay: The elementary particle approach](#), Rev. Mod. Phys. 46 (1974) 789–814. [doi:10.1103/RevModPhys.46.789](https://doi.org/10.1103/RevModPhys.46.789).  
 URL <https://link.aps.org/doi/10.1103/RevModPhys.46.789>
- [130] V. Cirigliano, A. Garcia, D. Gazit, O. Naviliat-Cuncic, G. Savard, A. Young, Precision beta decay as a probe of new physics (2019). [doi:10.48550/ARXIV.1907.02164](https://doi.org/10.48550/ARXIV.1907.02164).
- [131] D. M. Asner, R. F. Bradley, L. de Viveiros, P. J. Doe, J. L. Fernandes, M. Fertl, E. C. Finn, J. A. Formaggio, D. Furse, A. M. Jones, J. N. Kofron, B. H. LaRoque, M. Leber, E. L. McBride, M. L. Miller, P. Mohanmurthy, B. Monreal, N. S. Oblath, R. G. H. Robertson, L. J. Rosenberg, G. Rybka, D. Rysewyk, M. G. Sternberg, J. R. Tedeschi, T. Thümmler, B. A. VanDevender, N. L. Woods, Single-electron detection and spectroscopy via relativistic cyclotron radiation, Phys. Rev. Lett. 114 (2015) 162501. [doi:10.1103/PhysRevLett.114.162501](https://doi.org/10.1103/PhysRevLett.114.162501).
- [132] B. Ohayon, J. Chocron, T. Hirsh, A. Glick-Magid, Y. Mishnayot, I. Mukul, H. Rahangdale, S. Vaintraub, O. Heber, D. Gazit, G. Ron, Weak interaction studies at saraf, Hyperfine Interact. 239 (1) (2018) 57. [doi:10.1007/s10751-018-1535-x](https://doi.org/10.1007/s10751-018-1535-x).
- [133] B. R. Holstein, [Limit on fierz interference in nuclear beta decay](#), Phys. Rev. C 16 (1977) 753–756. [doi:10.1103/PhysRevC.16.753](https://doi.org/10.1103/PhysRevC.16.753).  
 URL <https://link.aps.org/doi/10.1103/PhysRevC.16.753>
- [134] A. Glick-Magid, D. Gazit, A formalism to assess the accuracy of nuclear-structure weak interaction effects in precision  $\beta$ -decay studies, J. Phys. G 49 (10) (2022) 105105. [doi:10.1088/1361-6471/ac7edc](https://doi.org/10.1088/1361-6471/ac7edc).
- [135] E. Epelbaum, H.-W. Hammer, U.-G. Meißner, Modern theory of nuclear forces, Rev. Mod. Phys. 81 (2009) 1773–1825. [doi:10.1103/RevModPhys.81.1773](https://doi.org/10.1103/RevModPhys.81.1773).
- [136] R. Machleidt, D. Entem, Chiral effective field theory and nuclear forces, Phys. Rep. 503 (1) (2011) 1 – 75. [doi:10.1016/j.physrep.2011.02.001](https://doi.org/10.1016/j.physrep.2011.02.001).
- [137] P. Navrátil, J. P. Vary, B. R. Barrett, Properties of  $^{12}\text{C}$  in the ab initio nuclear shell model, Phys. Rev. Lett. 84 (2000) 5728–5731. [doi:10.1103/PhysRevLett.84.5728](https://doi.org/10.1103/PhysRevLett.84.5728).
- [138] B. R. Barrett, P. Navrátil, J. P. Vary, Ab initio no core shell model, Prog. Part. Nucl. Phys. 69 (Supplement C) (2013) 131 – 181. [doi:https://doi.org/10.1016/j.ppnp.2012.10.003](https://doi.org/10.1016/j.ppnp.2012.10.003).
- [139] A. Ekström, G. Baardsen, C. Forssén, G. Hagen, M. Hjorth-Jensen, G. R. Jansen, R. Machleidt, W. Nazarewicz, T. Papenbrock, J. Sarich, S. M. Wild, Optimized chiral nucleon-nucleon interaction at next-to-next-to-leading order, Phys. Rev. Lett. 110 (2013) 192502. [doi:10.1103/PhysRevLett.110.192502](https://doi.org/10.1103/PhysRevLett.110.192502).
- [140] A. Ekström, G. R. Jansen, K. A. Wendt, G. Hagen, T. Papenbrock, B. D. Carlsson, C. Forssén, M. Hjorth-Jensen, P. Navrátil, W. Nazarewicz, [Accurate nuclear radii and binding energies from a chiral interaction](#), Phys. Rev. C 91 (2015) 051301. [doi:10.1103/PhysRevC.91.051301](https://doi.org/10.1103/PhysRevC.91.051301).  
 URL <https://link.aps.org/doi/10.1103/PhysRevC.91.051301>
- [141] T. Donnelly, W. Haxton, Multipole operators in semileptonic weak and electromagnetic interactions with nuclei, Atom. Data Nucl. Data Tabl. 23 (1979) 103–176. [doi:10.1016/0092-640X\(79\)90003-2](https://doi.org/10.1016/0092-640X(79)90003-2).

- [142] H. Behrens, W. Bühring, Electron radial wave functions and nuclear beta-decay, no. 67, Oxford University Press, USA, 1982.
- [143] B. S. Pudliner, V. R. Pandharipande, J. Carlson, S. C. Pieper, R. B. Wiringa, Quantum monte carlo calculations of nuclei with  $a \leq 7$ , Phys. Rev. C 56 (1997) 1720–1750. [doi:10.1103/PhysRevC.56.1720](https://doi.org/10.1103/PhysRevC.56.1720).
- [144] M. Antony, A. Pape, J. Britz, Coulomb displacement energies between analog levels for  $3 \leq a \leq 239$ , At. Data Nucl. Data Tables 66 (1) (1997) 1–63. [doi:https://doi.org/10.1006/adnd.1997.0740](https://doi.org/10.1006/adnd.1997.0740).
- [145] L. Hayen, N. Severijns, K. Bodek, D. Rozpedzik, X. Mousseot, High precision analytical description of the allowed  $\beta$  spectrum shape, Rev. Mod. Phys. 90 (2018) 015008. [doi:10.1103/RevModPhys.90.015008](https://doi.org/10.1103/RevModPhys.90.015008).
- [146] L. Hayen, A. R. Young, Consistent description of angular correlations in  $\beta$  decay for beyond standard model physics searches (2020).
- [147] P. Navrátil, Translationally invariant density, Phys. Rev. C 70 (2004) 014317. [doi:10.1103/PhysRevC.70.014317](https://doi.org/10.1103/PhysRevC.70.014317).
- [148] S. Pastore, S. C. Pieper, R. Schiavilla, R. B. Wiringa, Quantum monte carlo calculations of electromagnetic moments and transitions in  $a \leq 9$  nuclei with meson-exchange currents derived from chiral effective field theory, Phys. Rev. C 87 (2013) 035503. [doi:10.1103/PhysRevC.87.035503](https://doi.org/10.1103/PhysRevC.87.035503).
- [149] U. Friman-Gayer, C. Romig, T. Hüther, K. Albe, S. Bacca, T. Beck, M. Berger, J. Birkhan, K. Hebeler, O. J. Hernandez, J. Isaak, S. König, N. Pietralla, P. C. Ries, J. Rohrer, R. Roth, D. Savran, M. Scheck, A. Schwenk, R. Seutin, V. Werner, Role of chiral two-body currents in  ${}^6\text{Li}$  magnetic properties in light of a new precision measurement with the relative self-absorption technique, Phys. Rev. Lett. 126 (2021) 102501. [doi:10.1103/PhysRevLett.126.102501](https://doi.org/10.1103/PhysRevLett.126.102501).
- [150] S. Vaintraub, N. Barnea, D. Gazit,  ${}^6\text{He}\beta$ -decay rate and the suppression of the axial constant in nuclear matter, Phys. Rev. C 79 (2009) 065501. [doi:10.1103/PhysRevC.79.065501](https://doi.org/10.1103/PhysRevC.79.065501).
- [151] F. P. Calaprice, Second class interactions and the electron-neutrino correlation in nuclear beta decay, Phys. Rev. C 12 (1975) 2016–2021. [doi:10.1103/PhysRevC.12.2016](https://doi.org/10.1103/PhysRevC.12.2016).
- [152] C. H. Johnson, F. Pleasonton, T. A. Carlson, Precision measurement of the recoil energy spectrum from the decay of  $\text{he}^6$ , Phys. Rev. 132 (1963) 1149–1165. [doi:10.1103/PhysRev.132.1149](https://doi.org/10.1103/PhysRev.132.1149).
- [153] A. Glick-Magid, D. Gazit, Multipole decomposition of tensor interactions of fermionic probes with composite particles and BSM signatures in nuclear reactions, Phys. Rev. D 107 (7) (2023) 075031. [doi:10.1103/PhysRevD.107.075031](https://doi.org/10.1103/PhysRevD.107.075031).
- [154] J. D. Jackson, S. B. Treiman, H. W. Wyld, Possible tests of time reversal invariance in Beta decay, Phys. Rev. 106 (1957) 517–521. [doi:10.1103/PhysRev.106.517](https://doi.org/10.1103/PhysRev.106.517).
- [155] H. Saul, C. Roick, H. Abele, H. Mest, M. Klopff, A. Petukhov, T. Soldner, X. Wang, D. Werder, B. Märkisch, Limit on the Fierz Interference Term b from a Measurement of the Beta Asymmetry in Neutron Decay, Phys. Rev. Lett. 125 (11) (2020) 112501. [doi:10.1103/PhysRevLett.125.112501](https://doi.org/10.1103/PhysRevLett.125.112501).
- [156] X. Sun, et al., Improved limits on Fierz interference using asymmetry measurements from the Ultracold Neutron Asymmetry (UCNA) experiment, Phys. Rev. C 101 (3) (2020) 035503. [doi:10.1103/PhysRevC.101.035503](https://doi.org/10.1103/PhysRevC.101.035503).

- [157] A. Garcia, et al., <http://faculty.washington.edu/agarcia3/Chirality-flipping/>.
- [158] W. Byron, H. Harrington, R. J. Taylor, W. DeGraw, N. Buzinsky, B. Dodson, M. Fertl, A. García, G. Garvey, B. Graner, M. Guigue, L. Hayen, X. Huyan, K. S. Khaw, K. Knutsen, D. McClain, D. Melconian, P. Müller, E. Novitski, N. S. Oblath, R. G. H. Robertson, G. Rybka, G. Savard, E. Smith, D. D. Stancil, M. Sternberg, D. W. Storm, H. E. Swanson, J. R. Tedeschi, B. A. VanDevender, F. E. Wietfeldt, A. R. Young, X. Zhu, [First observation of cyclotron radiation from mev-scale  \$e^\pm\$  following nuclear  \$\beta\$  decay](#), Phys. Rev. Lett. 131 (2023) 082502. [doi:10.1103/PhysRevLett.131.082502](https://doi.org/10.1103/PhysRevLett.131.082502).  
 URL <https://link.aps.org/doi/10.1103/PhysRevLett.131.082502>
- [159] M. Kanafani, X. Fléchard, O. Naviliat-Cuncic, G. D. Chung, S. Leblond, E. Liénard, X. Mougeot, G. Quéméner, A. S. D. Filippo, J.-C. Thomas, Precision measurements in the beta decay of  ${}^6\text{He}$ , EPJ Web Conf. 282 (2023) 01010. [doi:10.1051/epjconf/202328201010](https://doi.org/10.1051/epjconf/202328201010).
- [160] V. Cirigliano, A. Garcia, D. Gazit, O. Naviliat-Cuncic, G. Savard, A. Young, Precision Beta Decay as a Probe of New Physics (7 2019).
- [161] F. P. Calaprice, Second class interactions and the electron-neutrino correlation in nuclear beta decay, Physical Review C 12 (6) (1975) 2016–2021. [doi:10.1103/PhysRevC.12.2016](https://doi.org/10.1103/PhysRevC.12.2016).
- [162] B. R. Holstein, Recoil Effects in Allowed beta Decay: The Elementary Particle Approach, Rev. Mod. Phys. 46 (1974) 789, [Erratum: Rev.Mod.Phys. 48, 673–673 (1976)]. [doi:10.1103/RevModPhys.46.789](https://doi.org/10.1103/RevModPhys.46.789).
- [163] J. D. Walecka, Theoretical Nuclear and Subnuclear Physics, Oxford University Press, New York, 1995.
- [164] J. Carlson, R. Schiavilla, Structure and dynamics of few nucleon systems, Rev. Mod. Phys. 70 (1998) 743–842. [doi:10.1103/RevModPhys.70.743](https://doi.org/10.1103/RevModPhys.70.743).
- [165] M. Sternberg, R. Segel, N. Scielzo, G. Savard, J. Clark, P. Bertone, F. Buchinger, M. Burkey, S. Caldwell, A. Chaudhuri, et al., Limit on tensor currents from  $\text{Li}^8 \beta$  decay, Phys. Rev. Lett. 115 (18) (2015) 182501.
- [166] M. T. Burkey, G. Savard, A. T. Gallant, N. D. Scielzo, J. A. Clark, T. Y. Hirsh, L. Varriano, G. H. Sargsyan, K. D. Launey, M. Brodeur, D. P. Burdette, E. Heckmaier, K. Joerres, J. W. Klimes, K. Kolos, A. Laminack, K. G. Leach, A. F. Levand, B. Longfellow, B. Maaß, S. T. Marley, G. E. Morgan, P. Mueller, R. Orford, S. W. Padgett, A. Pérez Galván, J. R. Pierce, D. Ray, R. Segel, K. Siegl, K. S. Sharma, B. S. Wang, [Improved limit on tensor currents in the weak interaction from  \${}^8\text{Li} \beta\$  decay](#), Phys. Rev. Lett. 128 (2022) 202502. [doi:10.1103/PhysRevLett.128.202502](https://doi.org/10.1103/PhysRevLett.128.202502).  
 URL <https://link.aps.org/doi/10.1103/PhysRevLett.128.202502>
- [167] A. T. Gallant, N. D. Scielzo, G. Savard, J. A. Clark, M. Brodeur, F. Buchinger, D. P. Burdette, M. T. Burkey, S. Caldwell, J. E. Crawford, A. Czeszumska, C. M. Deibel, J. Greene, D. Heslop, T. Y. Hirsh, A. F. Levand, B. Longfellow, G. E. Morgan, P. Mueller, R. Orford, S. Padgett, N. Paul, A. P. Galván, A. Reimer, R. Segel, K. S. Sharma, K. Siegl, L. Varriano, B. J. Zabransky, [Angular correlations in the  \$\beta\$  decay of  \${}^8\text{B}\$ : First tensor-current limits from a mirror-nucleus pair](#), Phys. Rev. Lett. 130 (2023) 192502. [doi:10.1103/PhysRevLett.130.192502](https://doi.org/10.1103/PhysRevLett.130.192502).  
 URL <https://link.aps.org/doi/10.1103/PhysRevLett.130.192502>

- [168] M. T. Burkey, Searching for tensor currents in the weak interaction using lithium-8  $\beta$  decay, Ph.D. thesis, Chicago U. (2019). [doi:10.6082/uchicago.1697](https://doi.org/10.6082/uchicago.1697).
- [169] A. Ekström, G. Baardsen, C. Forssén, G. Hagen, M. Hjorth-Jensen, G. R. Jansen, R. Machleidt, W. Nazarewicz, et al., An optimized chiral nucleon-nucleon interaction at next-to-next-to-leading order, Phys. Rev. Lett. 110 (2013) 192502.
- [170] A. Shirokov, V. Kulikov, P. Maris, A. Mazur, E. Mazur, J. Vary, Nn interaction jisp16: Current status and prospect, in: EPJ Web of Conferences, Vol. 3, EDP Sciences, 2010, p. 05015.
- [171] R. B. Wiringa, S. Pastore, S. C. Pieper, G. A. Miller, Charge-symmetry breaking forces and isospin mixing in  ${}^8\text{Be}$ , Phys. Rev. C 88 (2013) 044333. [doi:10.1103/PhysRevC.88.044333](https://doi.org/10.1103/PhysRevC.88.044333)  
URL <https://link.aps.org/doi/10.1103/PhysRevC.88.044333>
- [172] T. Sumikama, T. Nagatomo, M. Ogura, T. Iwakoshi, Y. Nakashima, H. Fujiwara, K. Matsuta, T. Minamisono, M. Fukuda, M. Mihara, Electric quadrupole moment of the proton halo nucleus  ${}^8\text{B}$ , Phys. Rev. C 74 (2006) 024327. [doi:10.1103/PhysRevC.74.024327](https://doi.org/10.1103/PhysRevC.74.024327)  
URL <https://link.aps.org/doi/10.1103/PhysRevC.74.024327>
- [173] A. A. Filin, D. Möller, V. Baru, E. Epelbaum, H. Krebs, P. Reinert, High-accuracy calculation of the deuteron charge and quadrupole form factors in chiral effective field theory, Phys. Rev. C 103 (2021) 024313. [doi:10.1103/PhysRevC.103.024313](https://doi.org/10.1103/PhysRevC.103.024313)  
URL <https://link.aps.org/doi/10.1103/PhysRevC.103.024313>
- [174] P. Maris, E. Epelbaum, R. J. Furnstahl, J. Golak, K. Hebeler, T. Hüther, H. Kamada, H. Krebs, U.-G. Meißner, J. A. Melendez, A. Nogga, P. Reinert, R. Roth, R. Skibiński, V. Soloviov, K. Topolnicki, J. P. Vary, Y. Volkotrub, H. Witała, T. Wolfgruber, Light nuclei with semilocal momentum-space regularized chiral interactions up to third order, Phys. Rev. C 103 (2021) 054001. [doi:10.1103/PhysRevC.103.054001](https://doi.org/10.1103/PhysRevC.103.054001)  
URL <https://link.aps.org/doi/10.1103/PhysRevC.103.054001>
- [175] A. Calci, R. Roth, Sensitivities and correlations of nuclear structure observables emerging from chiral interactions, Phys. Rev. C 94 (2016) 014322. [doi:10.1103/PhysRevC.94.014322](https://doi.org/10.1103/PhysRevC.94.014322)  
URL <https://link.aps.org/doi/10.1103/PhysRevC.94.014322>
- [176] M. A. Caprio, P. Maris, P. J. Fasano, Robust ab initio predictions for dimensionless ratios of  $e2$  and radius observables. i. electric quadrupole moments and deformation, Phys. Rev. C 112 (2025) 044318. [doi:10.1103/6zk6-1sy6](https://doi.org/10.1103/6zk6-1sy6)  
URL <https://link.aps.org/doi/10.1103/6zk6-1sy6>
- [177] M. A. Caprio, P. J. Fasano, P. Maris, Robust ab initio predictions for dimensionless ratios of  $e2$  and radius observables. ii. estimation of  $e2$  transition strengths by calibration to the charge radius, Phys. Rev. C 112 (2025) 044319. [doi:10.1103/mxqf-bbp9](https://doi.org/10.1103/mxqf-bbp9)  
URL <https://link.aps.org/doi/10.1103/mxqf-bbp9>
- [178] L. De Braeckeleer, E. G. Adelberger, J. H. Gundlach, M. Kaplan, D. Markoff, A. M. Nathan, W. Schieff, K. A. Snover, D. W. Storm, K. B. Swartz, D. Wright, B. A. Brown, Radiative decays of the 16.6 and 16.9 mev states in

<sup>8</sup>Be and tests of the conservation of the vector current in the a=8 multiplet, Phys. Rev. C 51 (1995) 2778–2788.

doi:[10.1103/PhysRevC.51.2778](https://doi.org/10.1103/PhysRevC.51.2778).

URL <https://link.aps.org/doi/10.1103/PhysRevC.51.2778>

- [179] T. Sumikama, K. Matsuta, T. Nagatomo, M. Ogura, T. Iwakoshi, Y. Nakashima, H. Fujiwara, M. Fukuda, M. Mihara, K. Minamisono, T. Yamaguchi, T. Minamisono, **Test of the conserved vector current hypothesis by a  $\beta$ -ray angular distribution measurement in the mass-8 system**, Phys. Rev. C 83 (2011) 065501. doi:[10.1103/PhysRevC.83.065501](https://doi.org/10.1103/PhysRevC.83.065501).
- URL <https://link.aps.org/doi/10.1103/PhysRevC.83.065501>
- [180] R. D. McKeown, G. T. Garvey, C. A. Gagliardi, **Beta-alpha angular correlations in mass 8**, Phys. Rev. C 22 (1980) 738–749. doi:[10.1103/PhysRevC.22.738](https://doi.org/10.1103/PhysRevC.22.738).
- URL <https://link.aps.org/doi/10.1103/PhysRevC.22.738>
- [181] S. Triambak, L. Phuthu, A. García, G. C. Harper, J. N. Orce, D. A. Short, S. P. R. Steininger, A. Diaz Varela, R. Dunlop, D. S. Jamieson, W. A. Richter, G. C. Ball, P. E. Garrett, C. E. Svensson, C. Wrede,  **$2_1^+$  to  $3_1^+$   $\gamma$  width in  $^{22}\text{Na}$  and second class currents**, Phys. Rev. C 95 (2017) 035501. doi:[10.1103/PhysRevC.95.035501](https://doi.org/10.1103/PhysRevC.95.035501).
- URL <https://link.aps.org/doi/10.1103/PhysRevC.95.035501>
- [182] H. Rahangdale, Y. Mishnayot, B. Ohayon, T. Hirsh, S. Vaintraub, A. Glick-Magid, D. Gazit, G. Ron, **Branching ratio measurement in  $^{23}\text{Ne}$  beta decay**, HNPS Advances in Nuclear Physics 26 (2019) 31–36. doi:[10.12681/hnps.1792](https://doi.org/10.12681/hnps.1792).
- URL <https://eproceedings.epublishing.ekt.gr/index.php/hnps/article/view/1792>
- [183] Y. Mishnayot, A. Glick-Magid, H. Rahangdale, G. Ron, D. Gazit, J. T. Harke, M. Hass, B. Ohayon, A. Gallant, N. D. Scielzo, S. Vaintraub, R. O. Hughes, T. Hirsch, C. Forssén, D. Gazda, P. Gysbers, J. Menéndez, P. Navrátil, L. Weissman, A. Kreisel, B. Kaizer, H. Daphna, M. Buzaglo, **Constraining new physics with a novel measurement of the  $^{23}\text{Ne}$   $\beta$ -decay branching ratio** (2021).
- [184] D. Atanasov, F. Cresto, L. Nies, M. Pomorski, M. Versteegen, P. Alfaurt, V. Araujo-Escalona, P. Ascher, B. Blank, L. Daudin, et al., **Experimental setup for weak interaction studies with radioactive ion-beams wisard**, Nuclear Instruments and Methods in Physics Research Section A: Accelerators, Spectrometers, Detectors and Associated Equipment 1050 (2023) 168159.
- [185] A. Glick-Magid, Y. Mishnayot, I. Mukul, M. Hass, S. Vaintraub, G. Ron, D. Gazit, **Beta spectrum of unique first-forbidden decays as a novel test for fundamental symmetries**, Phys. Lett. B 767 (2017) 285 – 288. doi:<https://doi.org/10.1016/j.physletb.2017.02.023>.
- URL <http://www.sciencedirect.com/science/article/pii/S0370269317301132>
- [186] C.-Y. Seng, A. Glick-Magid, V. Cirigliano, **Unique forbidden beta decays at zero momentum transfer**, Phys. Rev. Lett. 134 (2025) 081805. doi:[10.1103/PhysRevLett.134.081805](https://doi.org/10.1103/PhysRevLett.134.081805).
- URL <https://link.aps.org/doi/10.1103/PhysRevLett.134.081805>
- [187] I. Mardor, O. Aviv, M. Avrigeanu, D. Berkovits, A. Dahan, T. Dickel, I. Eliyahu, M. Gai, I. Gavish-Segev, S. Halfon, M. Hass, T. Hirsh, B. Kaiser, D. Kijel, A. Kreisel, Y. Mishnayot, I. Mukul, B. Ohayon, M. Paul, A. Perry, H. Rahangdale, J. Rodnizki, G. Ron, R. Sasson-Zukran, A. Shor, I. Silverman, M. Tessler, S. Vaintraub, L.

Weissman, The Soreq applied research accelerator facility (SARAF): Overview, research programs and future plans, Eur. Phys. J. A 54 (5) (2018) 91. [doi:10.1140/epja/i2018-12526-2](https://doi.org/10.1140/epja/i2018-12526-2).

- [188] P. Shuai, B. C. Rasco, K. P. Rykaczewski, A. Fijałkowska, M. Karny, M. Wolińska Cichocka, R. K. Grzywacz, C. J. Gross, D. W. Stracener, E. F. Zganjar, J. C. Batchelder, J. C. Blackmon, N. T. Brewer, S. Go, M. Cooper, K. C. Goetz, J. W. Johnson, C. U. Jost, T. T. King, J. T. Matta, J. H. Hamilton, A. Laminack, K. Miernik, M. Madurga, D. Miller, C. D. Nesaraja, S. Padgett, S. V. Paulauskas, M. M. Rajabali, T. Ruland, M. Stepaniuk, E. H. Wang, J. A. Winger, Determination of  $\beta$ -decay feeding patterns of  $^{88}\text{Rb}$  and  $^{88}\text{Kr}$  using the Modular Total Absorption Spectrometer at ORNL HRIBF, Phys. Rev. C 105 (2022) 054312. [doi:10.1103/PhysRevC.105.054312](https://doi.org/10.1103/PhysRevC.105.054312).
- [189] A. Glick-Magid, C. Forssén, D. Gazda, D. Gazit, L. Jokiniemi, K. Kravvaris, P. Navrátil, Spectrum peak asymmetry of the unique first-forbidden  $\beta$ -decay of  $^{16}\text{N}$  as a new-physics probe, in prep. (2026).
- [190] G. B. King, et al., Future directions in nuclear  $\beta$  decay at FRIB and beyond, in prep. (2026).

## A. Appendices, if necessary